Doctoral Dissertation

Analysis and Design of Active Cobalt Species on MFI Zeolite for Catalytic Methylation of Benzene with Methane

メタンによるベンゼンのメチル化反応に活性な

MFI ゼオライト上の Co 種の解析と設計

January 2022

Hitoshi Matsubara

Department of Chemistry and Biotechnology

Graduated School of Engineering

Tottori University

Preface

The studies presented in this thesis were carried out under the direction of Professor Naonobu Katada, Associate Professor Etsushi Tsuji, and Associate Professor Satoshi Suganuma, Course of Applied Chemistry, Department of Chemistry and Biotechnology, Graduated School of Engineering, Tottori University, during 2019-2022.

The object of this thesis is to analyze and design of active cobalt species on zeolite for catalytic methylation of benzene with methane. The author wishes that knowledges from this thesis would be new guidelines for the design of catalysts for methane conversion reactions.

Hitoshi Matsubara

Department of Chemistry and Biotechnology

Graduate School of Engineering, Tottori University

4-101 Minami, Koyama-cho, Tottori 680-8552, Japan

January 2022

Contents

Chapter 1　General Introduction

1-1 Zeolite

Zeolites have three-dimensional frameworks constructed by covalent bonds between Si and O with the basic composition of SiO_2, where a part of Si atoms is isomorphously substituted by an Al atom. Here, an isomorphously substituting Al atom produces a negative charge, and a cation is bonded to compensate for it. The site where this cation is held is called an ion exchange site, and it can hold cations such as H^+, NH_4^+,

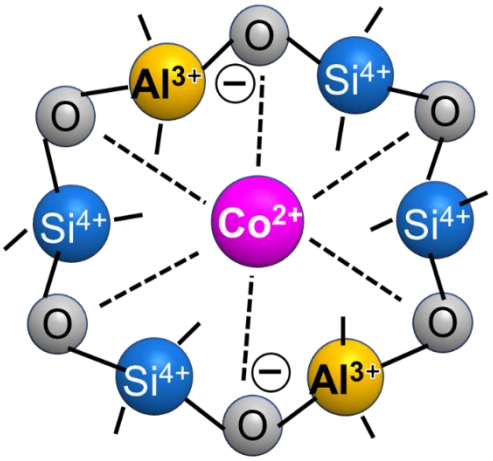

Figure 1-1. Schematic structure of ion exchange site in zeolite.

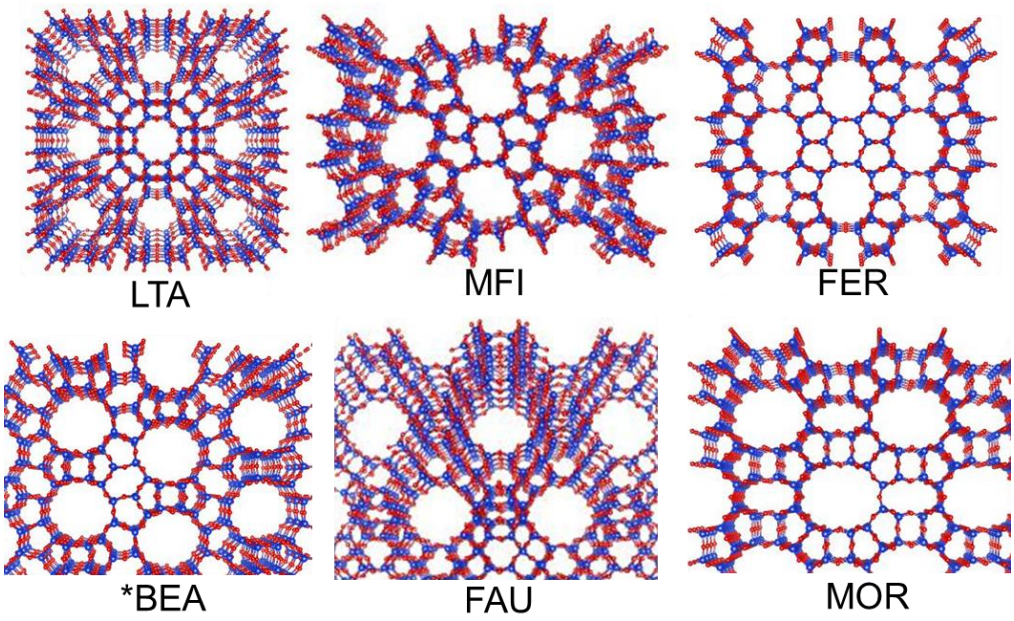

Figure 1-2. Framework structures of various zeolites.

and Co^{2+} as shown in Figure 1-1. The zeolites have a variety of framework topologies, each with a different pore size (Figure 1-2). The framework topologies are distinguished by a three-letter code called framework type code, such as MFI, FER, and MOR. The pores have a high area of walls with several hundred square meters per gram. A zeolite is principally identified with the framework topology, framework composition (Al concentration in the framework) and the counter cation species.

1-2 Applications of zeolite materials

Na-LTA zeolite, a type of zeolite traditionally called Na-A type zeolite or molecular sieve 4A, is contained by detergents and works to soften the water used to wash clothes

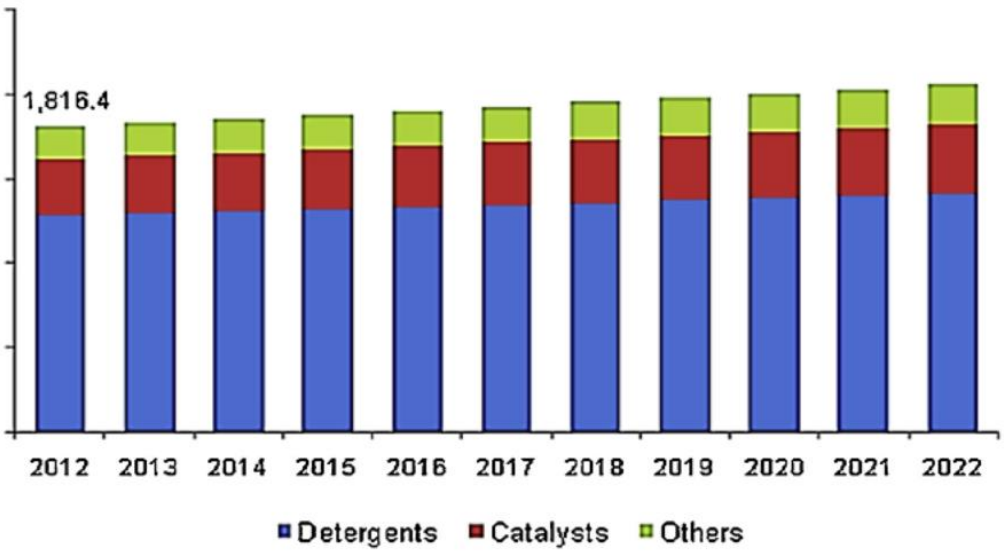

Figure 1-3. Global market of zeolite molecular sieves associated with application, 2012 - 2022 (Kilo Tons) [1].

[1-3]. Global market of zeolite associated with their applications is shown in Figure 1-3. As it is obvious, detergents possess the largest portion of the all markets [1]. As shown in Figure 1-1, zeolites are capable of holding cations in their ion exchange sites. When LTA zeolites holding Na^+ are added to hard water, the Na^+ held in the LTA is replaced by Ca^{2+} and Mg^{2+} in the hard water. As Ca^{2+} and Mg^{2+} are retained in the LTA and Na^+ is released into the water, hard water is converted into soft water, which helps detergent dissolution more easily in water and enhances the cleaning effect [1]. LTA zeolite and FAU (X-type) zeolite are also used as dehydrating agents. Alkaline-forms of zeolites with high concentration of ion exchange sites are used to dehydrate organic solvents because of the high hydrophilicity due to the high density of cation-ion exchange site pair with high electric field gradient, and in the cases of a zeolite with very small pores such as K-LTA (molecular sieve 3A), shape selective penetration of a small molecule such as water enhances the dehydration performance [4-6]. This shape-selective ability to adsorb only water molecules or small organic molecules is attractive.

As shown in Figure 1-3, the application of zeolite as a catalyst is also important. Zeolites are used as solid acid catalysts because they can hold H^+ (Brønsted acid site) in their ion exchange sites [7-9]. The reaction can be carried out in the pores of the zeolite to give shape selectivity to the product [7, 10, 11]. In addition, the structure of zeolites is

stable even at temperatures as high as 773 K, so it can be used at high reaction temperatures. FAU zeolite is the solid acid catalyst for the fluid catalytic cracking (FCC) process, which cracks heavy oil at ca. 873 K into useful gasoline-range hydrocarbons [12-15]. This has already been put to practical use for more than 50 years and is an indispensable technology in oil refining. The methanol to gasoline (MTG) reaction proceeds at around 673 K using MFI zeolite as a solid acid catalyst [16-19]. This process has also been demonstrated as a practical technology, and open a promising way for production of liquid fuels and chemicals from C1 compounds like CO_2 and CO instead of petroleum. Since metal ions on zeolites serve as active sites for various reactions, zeolites are also attractive materials as catalyst supports. In this field, zeolites modified with Cu and Fe are used as catalysts for decomposition (reduction) of NO_x in diesel exhaust [20-23].

1-3 Positions of Co on zeolites

The zeolite-supported cobalt shows catalytic activity for selective catalytic reduction (SCR) of NO_x with methane or ethane [24-28], and the activity has been known to be sensitive to the support zeolite and the location of ion-exchange site. The difference in the local structure of Co species is analysed by the ultraviolet-visible (UV-vis)

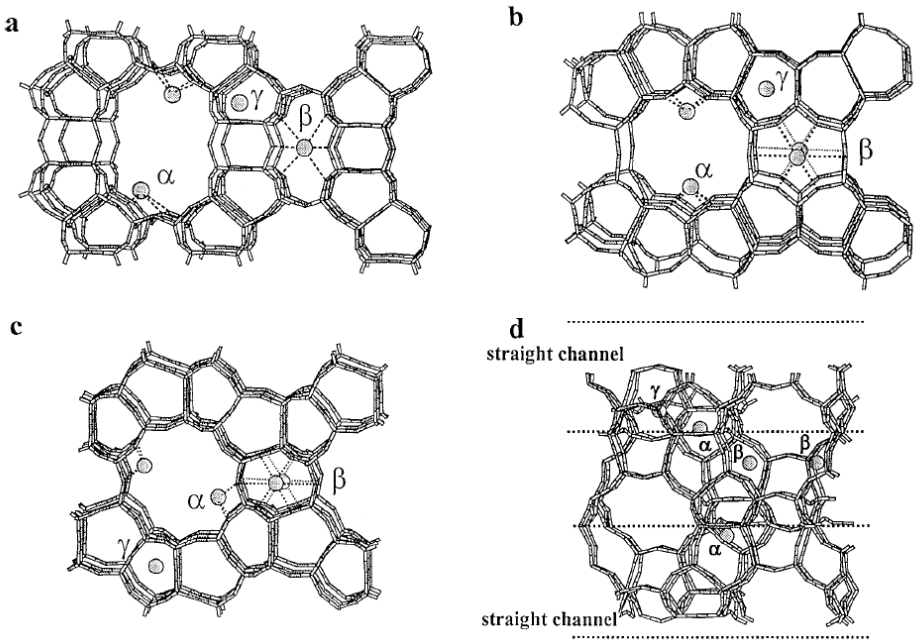

Figure 1-4. Suggested cationic sites of the α-, β-, and γ-type Co ions in (a)MOR, (b) FER, and (c) and (d) MFI structures; (c) view through the straight channel and (d) view through the sinusoidal channel, straight channel indicated by dashed lines. [28].

spectroscopy. According to Kaucký et al. [28], ion exchange sites for divalent cations on a zeolite are classified into three types (α, β and γ sites) based on the coordination environment as shown in Figure 1-4. In the case of MFI, it is proposed that the α site is located on the wall of 10-ring straight channel, the β site is located in 6-ring close to the intersection of straight and sinusoidal 10-ring channels, and the γ site is located on the pocket-like wall of sinusoidal channel. Kaucký reported that the cobalt ions bound to framework oxygens at the main channel i.e. α site were most active among the cobalt ions in MOR and FER, whereas, in MFI, that coordinated to β site possessed the highest activity for selective catalytic reduction of NO with methane [28].

1-4 Design of zeolite catalysts

As shown in Table 1-1, it has already been reported that relative concentrations of the types of the Co ions on MFI were changed by addition of Ba or Ca as secondary metal. The addition of Ca and Ba increased Co at α and decreased Co at β and γ [29]. Boix investigated the effect of platinum additive on the catalytic activity for the SCR of NO_x with methane on Co/MFI [30]. They concluded that the mono-atomic cobalt species were preferentially dispersed on the main channel walls of MFI (α site), while they moved to lattice sites with higher coordination number with addition of platinum ions. In addition, it has been found that Cu, Ni, Co, and Zn ions had different preferred positions on MOR, and these tendencies affected the catalytic activity for carbonylation of dimethyl ether into methyl acetate [31]. Moreover, Zhang et al. have studied design of catalyst with Co and In/MOR. It has been reported that Co was stably located at β-site by combining ion exchange of Co and In on MOR and calcination step as shown in Figure 1-5 [32].

Table 1-1. Relative concentrations of the individual types of the Co ions in dehydrated CoMe–MFI (ZSM-5) samples [29].

Zeolite	Co/Al	α (%)	β (%)	γ (%)
CoNa–ZSM-5	0.10	15	70	15
CoBa–ZSM-5	0.12	50	45	5
CoNa–ZSM-5	0.15	10	75	15
CoCa–ZSM-5	0.15	45	50	5

On the other hand, the ion strength of ion exchange site and pore size are supposed to affect the Lewis acidic nature of supported cation. The latter has experimentally and theoretically been clarified [33]. From results of IR spectra, it was suggested that the electron accepting abilities of Ag ion on FAU type zeolite were differed by the position of that [34]. It seems that the density of zeolite framework oxygen with lone pair around metal ions affected electron accepting abilities.

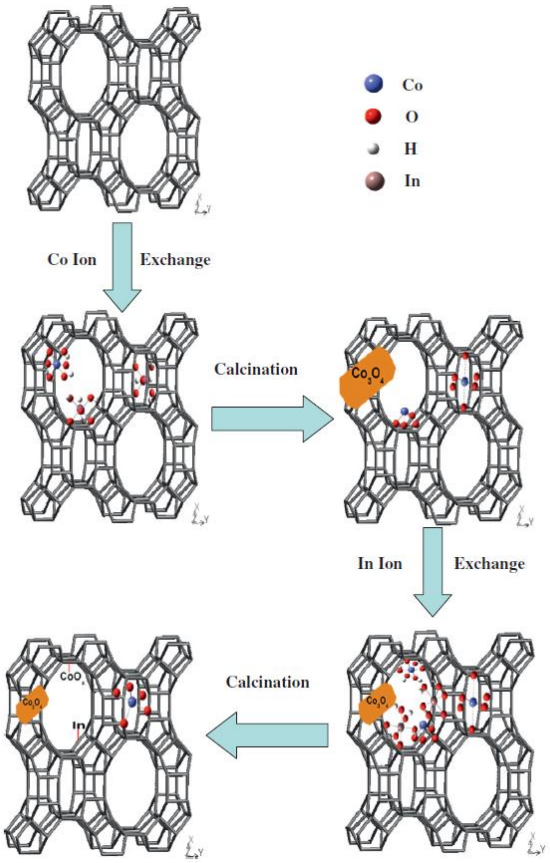

Figure 1-5. Illustration of transformation of Co^{2+} and In ions in MOR cavities [32].

For design of catalyst, not only the position of metal ions but also the concentration and distribution of Al on zeolite are important. The zeolites with high Al concentration tended to form paired Al sites ($Al{-}O{-}(Si{-}O)_2{-}Al$ sequences, Al_{pair} in Figure 1-6), so they were retained as divalent Co^{2+} (Figure 1-4). On the other hand, in single Al site ($Al{-}O{-}(Si{-}O)_{>2}{-}Al$ sequences with far distant Al atoms located in different rings, Al_{single} in Figure 1-6), one Co might be compensated for one Al, so it can be considered that it was held the Co species like $Co(OH)^+$. Therefore, it is presumed that changing the Al concentration in MFI differs the coordination environment of metal ions that affect electron acceptability.

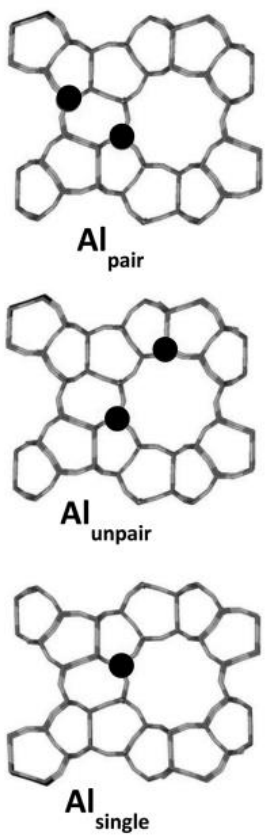

Figure 1-6. Schematic arrangement of Al atoms in Al pairs (Al_{pair}), close Al atoms in different rings (Al_{unpair}), and single Al atoms. ● shows Al in zeolite framework [35].

1-5 Natural gas

The production of natural gas is increasing year by year. In particular, the amount of natural gas has been increasing by the shale gas revolution in North America in recent years as shown in Figure 1-7 [36], and it is expected that it will increase further in the

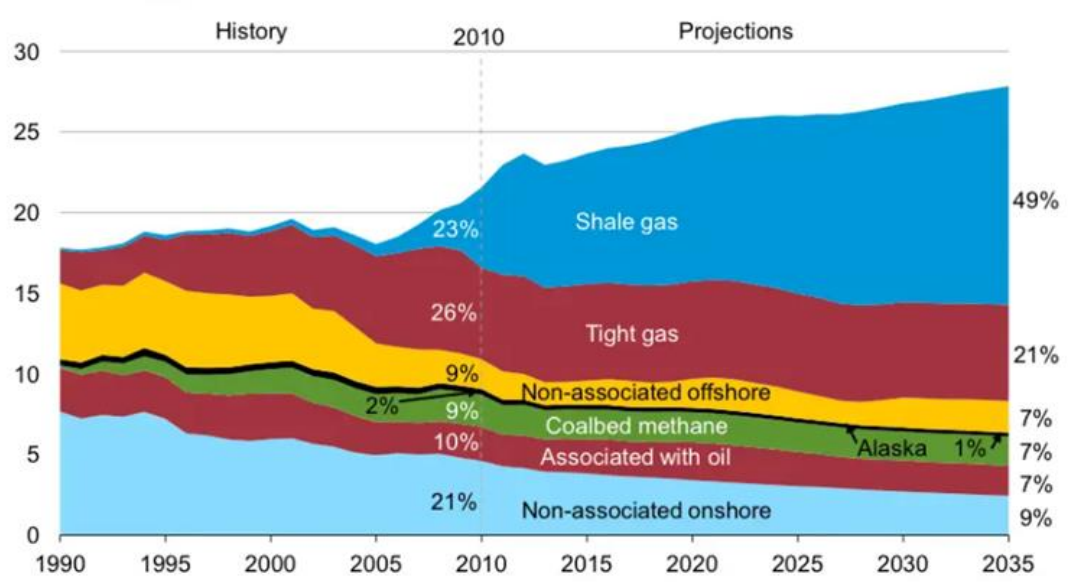

Figure 1-7. U.S. dry gas production trillion cubic feet per year [37].

future. On the other hand, petroleum is in danger of being depleted, and the situation in producing countries is unstable, so there is not always a stable supply. Therefore, conventional natural gas and shale gas are attracting attention as petroleum alternative resources. More than 88% of the components of the conventional natural gas and more than 90% of the components of shale gas are methane [38, 39].

Currently, methane can be used as a fuel or as a hydrogen source by steam reforming [40-44], both of which are costly. The problem with using it as fuel is transportation costs. The pipelines are required to transport in the gas state, and pressure must be applied at a low temperature of 111 K to transport in the liquid state. In addition, it is necessary to have equipment for freezing because it is stored in a liquefied state. On the other hand, steam reforming is a reaction at a high temperature of 823-1373 K, and it is a reaction

with a large energy loss such that CO is not selectively formed, and CO_2 is produced as a by-product [45]. Therefore, methane cannot be used effectively.

For the effective use of methane, attention is being paid to using it as a carbon resource. At present, the depletion of petroleum is in danger, so it would be very useful if methane could be used as a raw material for chemical products instead of petroleum. However, the C-H bond dissociation energy of methane is 434 kJ mol^{-1}, which is the highest among hydrocarbons [46]. For this reason, it is extremely difficult to react methane, and the development of catalysts that can effectively utilize methane is required.

1-6 Methane conversion processes

Many researchers have studied about chemical processes using methane. Steam reforming of methane is the most developed process for the production of H_2 from methane as mentioned above [47]. In this process, CH_4 and H_2O are converted to CO and H_2 (Eq. (1)), and accompanied by water gas shift reaction (Eq. (2)), CO and H_2O are converted to CO_2 and H_2.

$$CH_4 + H_2O \rightarrow CO + 3H_2 \quad (1)$$

$$CO + H_2O \leftrightarrow CO_2 + H_2 \quad (2)$$

Ni-based catalysts are the most commonly used industrially because of their high activity

for the activation of the C-H bond of CH_4, and low cost [47, 48]. At temperatures above 823 K, the rate limiting step in methane steam reforming on Ni catalysts has been reported to be the activation of the C-H bond of CH_4 [49-52]. The main problems in the steam reforming of methane on Ni catalysts are catalyst deactivation due to coke formation, and reduction of the active surface area due to sintering of Ni particles at high temperatures [47]. Deactivation of Ni due to coke has been extensively studied [53-62].

Dry reforming of CH_4 to produce CO and H_2 from CH_4 and CO_2, as shown in equation (3), has also been studied.

$$CH_4 + CO_2 \rightarrow 2CO + 2H_2 \qquad (3)$$

This reaction has attracted much attention from both industrial and environmental aspects [63]. From the environmental point of view, it is an efficient way to consume CO_2, since both CO_2 and CH_4 are recognized as greenhouse gases. From the industrial aspect, it is a useful process because it can convert CH_4 and CO_2, the cheapest and most abundant hydrocarbons, into syngas with a lower H_2 / CO ratio than steam reforming [64, 65]. It has been reported in the past that many supported metal catalysts, including noble metal and Ni-based catalysts, are used in this process [66-74]. The problem for this process is the rapid deactivation of the catalyst. This is mainly due to coke deposition and sintering of both the support and the active metal particles. It has been reported that inexpensive

Ni-based catalysts form coke more readily than expensive noble metal-based ones [63].

Oxidative coupling of methane (OCM) is a reaction that directly converts methane to ethylene and ethane (C2 hydrocarbons) as shown in Eq. (4) and (5).

$$2CH_4 + O_2 \rightarrow C_2H_4 + 2H_2O \quad (4)$$

$$4CH_4 + O_2 \rightarrow 2C_2H_6 + 2H_2O \quad (5)$$

Since ethylene is an important hydrocarbon for the production of various compounds and polymers, OCM is a useful process [75-78]. This process shows high methane conversion at lower temperatures, with a reported methane conversion of 29.7% at 693 K on nanorod $La_2O_2CO_3$ catalyst [79]. In addition, 35.3% methane conversion at 773 K was reported over La_2O_3 catalyst [80]. Various other catalysts such as La_2O_3-CeO_2 [81], Li-TbO_x/MgO [82], and Zr-Sm_2O_3 [83] have been used for this reaction. Although this process has attracted attention as a technology to minimize feedstock supply and crude oil dependency for the chemical industry [75], the industrial deployment of OCM remains limited [84, 85]. This is due to the low reaction selectivity (S_{C2} = c.a. 50% at 773K). The undesirable deep oxidation compounds (CO_x) formed in side reactions are thermodynamically more stable and produce faster than C2 hydrocarbons [75, 86].

Direct partial oxidation of methane to methanol (Eq. 6) is a "dream reaction" for heterogeneous catalysis, but despite decades of research, it remains even further away

from practical application than OCM [87].

$$2CH_4 + O_2 \rightarrow 2CH_3OH \quad (6)$$

This reaction directly converts methane into high-valued methanol at low temperatures, avoiding the production of syngas ($CO + H_2$). With reference to methanotrophic bacteria to convert methane under mild reaction conditions on methane monooxygenase enzymes (MMO) [88-90], metal-exchange zeolites, which have active site similar to that of MMO, have been studied as catalysts to activate the C-H bond of methane at low temperatures (< 523 K) [47, 91, 92]. The methane oxidation active sites of these enzymes have been reported as bis(μ-oxo)diiron and bis(μ-oxo)dicopper complexes [47, 93, 94]. Although this reaction have been carried out using various types of zeolites [95-98], copper-exchanged mordenite (Cu-MOR) catalysts have shown the most interesting catalytic performance. This is due to high methanol yield and the ease of product desorption from the active site due to the large pores [99, 100]. Although the structure of the active site is still under consideration, it has been reported that the active site of bis(μ-oxo)dicopper is the only one responsible for catalysis. However, other studies have suggested that mononuclear copper-oxo clusters and trinuclear copper-oxo clusters are also active sites [101]. The oxygen at the active site reacts with methane to produce methoxy species. At low reaction temperatures, these species adsorp strongly on the active site, preventing the

adsorption of other methane molecules and stopping the reaction. When the temperature is raised to promote desorption and methanol formation, undesirable overoxidation occurs [102, 103]. The difficulty in desorption the products and the overoxidation of CH_4 are the main problems for this process.

Non-oxidative dehydroaromatization of methane is a reaction that produces benzene directly from methane as shown in equation (7).

$$6CH_4 \rightarrow C_6H_6 + 9H_2 \qquad (7)$$

It has been found Mo/MFI [104-109], Mo/MEL [109], Zn/MFI [104], Fe/MFI [105] showed high activity at c.a. 973 K for this process. Studies of Mo/MFI catalysts for this reaction have been in progress, and Mo_2C species formed by the flowing of CH_4 to Mo species on MFI have been considered to be the active species [107, 110]. However, selectivity has not been high, leading to production of carbonaceous polymers and deactivation of catalysts [111-113]. For Mo/MFI, it has been reported that the methane conversion of 12% and 6% results in benzene selectivity of about 35% and 80%, respectively [107, 114].

Figure 1-8 summarizes the scheme for the production of high value-added compounds from methane. The methanol to olefin (MTO) and methanol to gasoline (MTG) reactions shown in Figure 1-8 are practical technologies. Olefins such as ethylene

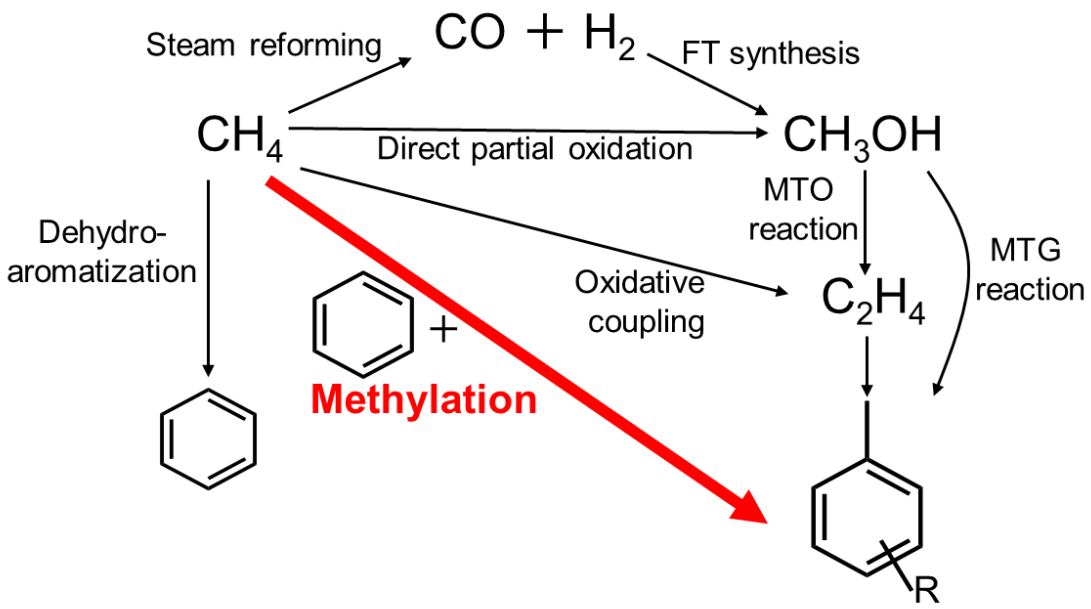

Figure 1-8. Scheme for the generation of high value-added compounds from methane.

and propylene are produced from methanol over MFI or SAPO-34 zeolite catalysts, and gasoline such as benzene and xylene are produced from methanol over MFI catalysts [115-118]. Therefore, as long as methanol can be produced from methane, high-valued olefins and gasoline can be produced from methane as sown in Figure 1-8. However, as mentioned above, the steam reforming and direct partial oxidation of methane both show low reaction selectivity and form CO_2 as a byproduct. The oxidative coupling reaction, which can generate ethylene from methane, is also a reaction with still low C2 selectivity, as discussed above. The non-oxidative dehydroaromatization reaction, which produces benzene directly from methane, is also difficult to control coke formation, and catalyst degradation has become a serious problem. Therefore, from the viewpoint of more

effective use of methane, we have been studying the use of methane as a methylating agent for benzene ring.

1-4 Catalytic methylation of benzene with methane

The methylation of benzene ring with methane as shown in Eq. (8) can be an option for effective conversion of methane into valued compounds.

$$CH_4 + C_6H_6 \rightarrow CH_3\text{-}C_6H_5 + H_2 \qquad (8)$$

For example, combining the methylation of benzene into toluene and the shape selective disproportionation of toluene into a pair of benzene and para-xylene [119, 120] should convert toluene and methane into para-xylene, whose demand as a raw material of polyethylene terephthalate is large. The preceding studies showed the activities for this reaction of some zeolite-based catalysts as H-*BEA, Cu/*BEA [121], Ag/MFI [122], Pt/MFI [123] and In/MFI [124]. He et al. reported that the batch reaction at 673 K and 6.9 MPa resulted in a benzene conversion of 12.3%, toluene selectivity of 58.8%, and xylene selectivity of 33.3% on H-BEA zeolite [121]. Baba et al. reported the results of a continuous flow reaction ($P_{CH4} = P_{C6H6} = 33.8$ kPa, $W / F = 3.6$ g h mol^{-1}) at 673 K and atmospheric pressure. According to their paper [122], the reaction proceeded on Ag/H-MFI zeolite catalyst, and the conversion of methane and that of benzene were 2.2%, and

1.6%, respectively. The reaction products were toluene and xylenes, whose yields were 0.02% and 1.1%, respectively, at a running time of 1 h. They proposed that the Ag species on MFI cleaved methane to form CH_3^+ species, which led to the methylation of benzene. Lukyanov et al. reported the conversion of methane and that of benzene were c.a. 0.5%, and about 4%, respectively, on Pt/H-MFI catalyst at atmospheric pressure in a continuous flow reactor at 643 K (CH_4 / C_6H_6 molar ratio = 9, WHSV = 1.76 h^{-1}). The toluene selectivity was 96%. They also reported that the catalyst activity was relatively stable even after 24 h [123]. In addition, it has been known that a similar reaction, oxidative methylation of benzene with methane (Eq. 9).

$$2CH_4 + 2C_6H_6 + O_2 \rightarrow 2H_3C\text{-}C_6H_5 + 2H_2O \quad (9)$$

Adebajo et al. reported that this reaction proceeded on MFI loaded various cation (H, Co, Mn, Cu, and Na) [125]. Based on these findings, metal/MFI catalysts are expected to be active in the methylation of benzene with methane.

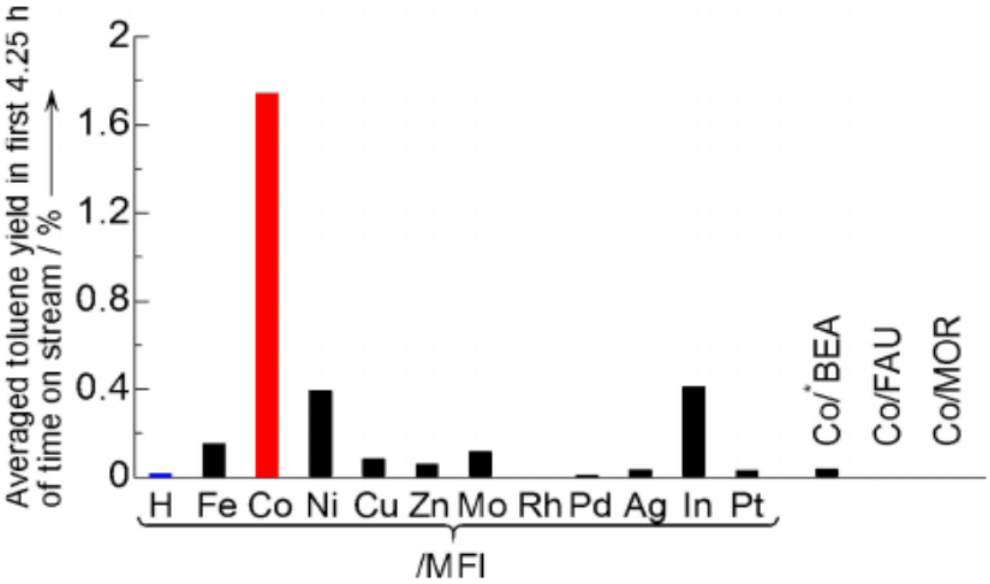

Figure 1-9. Catalytic activity for methylation of benzene with methane at 773 K over zeolite-supported metal species [126].

We recently found that the catalytic activity of Co/MFI for the reaction (eq. 8) was remarkable among the zeolite-supported transition metals as shown in Figure 1-9 [126, 127]. The activity was found in the limited cobalt loading region as shown in Figure 1-10. On a support MFI ([Al] = 1.3 mol kg^{1}, SiO_2/Al_2O_3 molar ratio = 22), the toluene yield was mainly increased with increasing Co in the region of Co/Al = 0.3-0.4 and showed the maximum at Co/Al = 0.6. Further loading reduced the activity. The cobalt species was mono-atomically held by the ion-exchange site at Co/Al < 0.6, as supported by the maximum Lewis acidity at Co/Al = 0.6, whereas Co/Al > 0.6 resulted in the aggregation of CoO particles. The activity was negligible in the region of Co/Al < 0.2, and it was generated mainly in the region of Co/Al = 0.2 to 0.6; the activity was significantly

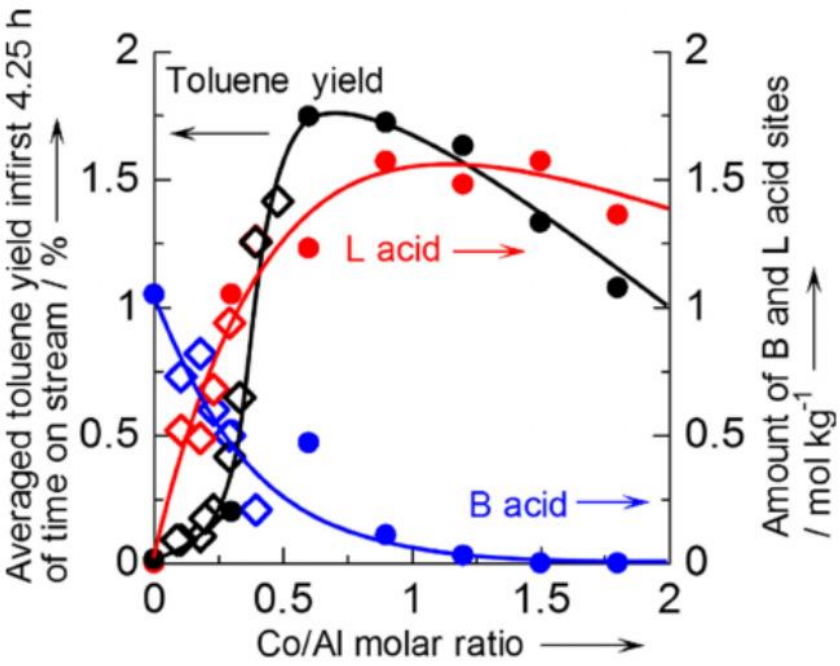

Figure 1-10. Catalytic activity for methylation of benzene with methane at 773 K (● and ◇), and amounts of Brønsted (● and ◇) and Lewis (● and ◇) acid sites on Co/MFI prepared by impregnation (●) and ion exchange (◇) methods plotted against Co/Al molar ratio [126].

increased at Co/Al = 0.3-0.4. The XAS (X-ray absorption spectroscopy) revealed that the oxidation state was approximately +II at Co/Al < 0.6. Therefore, the presence of at least two types of cobalt species with difference in the activity is speculated, even though the dispersion and oxidation state are similar; the active one probably formed at Co/Al > 0.3 and the inactive one formed at Co/Al < 0.2.

1-7 Outline of this study

Based on these backgrounds, the author focused on (i) the positions and (ii) Lewis

acidic properties of active Co species on MFI zeolite, (iii) the Al concentrations in Co/MFI catalysts and (iv) the reaction mechanism for methylation of benzene with methane. The characteristics of active Co species on MFI were analyzed. The active Co/MFI catalysts were designed from the conditions for formation of active Co species.

In the chapter 2, the effects of second metal additives on Co/MFI catalysts for the methylation of benzene ring with methane are described. The catalytic activity for methylation of benzene was found on Co/MFI zeolite; the activity was generated by loading of Co in the region of Co/Al molar ratio in the final solid = 0.2-0.6 (significantly increased at 0.25-0.4) on a support MFI with [Al] = 1.3 mol kg^{1}. It has been found that the low activity at Co/Al > 0.6 was ascribed to the cobalt oxide aggregate formation, but even in the region of Co/Al < 0.6 where cobalt was mono-atomically dispersed, the presence of at least two types of cobalt species, active and inactive ones formed at Co/Al > 0.2 and Co/Al < 0.2, respectively, is suggested. Even in the low Co/Al region, addition of typical divalent elements such as Mg, Zn, Pb and Ca during the Co loading process was found to generate the catalytic activity. It is speculated that the active cobalt species were selectively formed.

In the chapter 3, reaction mechanism for methylation of benzene with methane was elucidated by flowing methane or benzene on Co/MFI catalysts and measuring in situ IR

spectra. The IR spectrum of benzene adsorbed on Co species on MFI shifted to lower wavenumber than that of gas phase species. It means that the electronic environment of benzene was changed by adsorption to Co species on MFI. In the experiments in which C_6H_6 was flowed, followed by flowing of CH_4 or N_2, the desorption rate of C_6H_6 adsorbed on Co species was faster with CH_4 than with N_2. This indicates that the C_6H_6 previously adsorbed on the Co species in MFI reacted with CH_4, and the methylation of C_6H_6 proceeded.

In the chapter 4, crystallographic position and acidic properties of the Co species in MFI zeolite ([Al] = 1.3 mol kg^{-1}) which was catalytically active for methylation of benzene with methane were investigated with UV-vis spectroscopy and an ammonia IRMS-TPD method. Among the divalent cation sites in MFI classified into α, β and γ, loading of Co^{2+} at the α site on the wall of straight channel proceeded mainly in the relatively high Co concentration region (Co /Al > 0.25) without additive or in the low Co concentration region in the co-presence of Mg and Pb. On the other hand, Co^{2+} on MFI were classified from the view of Lewis acidity into four types (L1S, L1W, L2S and L2W). The L1S type possessing strong base-stabilizing and electron-withdrawing nature showed similar dependency on the Co content to the Co^{2+} at the α site as well as the catalytic activity for direct methylation of benzene with methane. These observations indicate that

the Co^{2+} at the α site with L1S nature was active for the methylation of benzene with methane.

In the chapter 5, effect of Al concentrations in Co/MFI catalysts for selective methylation of benzene with methane is described. The $[Al]_{Framework}$ of MFI affected the catalytic performance at 813 K. The Co species loaded on MFI with high $[Al]_{Framework}$ ($[Al]_{Framework} > 0.7$ mol kg^{-1}) tended to be deactivated by the side reaction (simple dehydrogenation of methane ($CH_4 \rightarrow C + 2H_2$)). The Co species impregnated on MFI with $[Al]_{Framework}$ of about 0.3 mol kg^{-1} showed high toluene yield and methylation selectivity. Furthermore, the decreasing in [Co] on the MFI with $[Al]_{Framework}$ = c. a. 0.3 mol kg^{-1} tended to increase the methylation selectivity.

References

[1] E. Koohsaryan, M. Anbia, M. Maghsoodlu, *J. Environ. Chem. Eng*., **8**, 104287 (2020)

[2] A. Rozhkovskaya, J. Rajapakse, G. J. Millar, *J. Water Process Eng*., **43**, 102177 (2021)

[3] K. S. Hui, C. Y. H. Chao, *J. Hazard. Mater*., **137**, 401-409 (2006)

[4] D. E. Chasan, L. L. Pytlewski, Robert O. Hutchins, N. M. Karayannis, C. Owens, *Inorg. Nucl. Chem. Lett*., **11**, 41-45 (1975)

[5] Q. Wang, R. Huang, *Tetrahedron Lett*., **41**, 3153-3155 (2000)

[6] D. J. Faria, L. M. dos Santos, F. L. Bernard, I. S. Pinto, M. A. C. D. Resende, S. Einloft, *RSC Adv*., **10**, 34895-34902 (2020)

[7] W. Vermeiren, J.-P. Gilson, *Top. Catal*., **52**, 1131-1161 (2009)

[8] E. T. C. Vogt, B. M. Weckhuysen, *Chem. Soc. Rev*., **44**, 7342-7370 (2015)

[9] J. Shi, Y. Wang, W. Yang, Y. Tang, Z. Xie, *Chem. Soc. Rev*., **44**, 8877-8903 (2015)

[10] B. Smit, T. L. M. Maesen, *Chem. Rev*., **108**, 4125-4184 (2008)

[11] J. Jae, G. A. Tompsett, A. J. Foster, K. D. Hammond, S. M. Auerbach, R. F. Lobo, G. W. Huber, *J. Catal*., **279**, 257-268 (2011)

[12] J. García-Martínez, M. Johnson, J. Valla, K. Li, J. Y. Ying, *Catal. Sci. Technol*., **2**, 987-994 (2012)

[13] J. García-Martínez, K. Li, G. Krishnaiah, *Chem. Commun*., **48**, 11841-11843 (2012)

[14] S. C. Cardona, A. Corma, *Appl. Catal. B: Environ*., **25**, 151-162 (2000)

[15] U. A. Sedran, *Catal. Rev. Sci. Eng*., **36**, 405-431 (1994)

[16] M. Stocker, *Micropor. Mesopor. Mater*., **29**, 3-48 (1999)

[17] U. Olsbye, S. Svelle, M. Bjørgen, P. Beato, T. V. W. Janssens, F. Joensen, S. Bordiga, K. P. Lillerud, *Angew. Chem. Int. Ed*., **51**, 5810-5831 (2012)

[18] J. Kim, M. Choi, R. Ryoo, *J. Catal*., **269**, 219-228 (2010)

[19] F. J. Keil, *Micropor. Mesopor. Mater*., **29**, 49-66 (1999)

[20] J. Li, H. Chang, L. Ma, J. Hao, R. T. Yang, *Catal. Today*, **175**, 147-156 (2011)

[21] A. Fritz, V. Pitchon, *Appl. Catal. B: Environ*., **13**, 1-25 (1997)

[22] A. Grossale, I. Nova, E. Tronconi, D. Chatterjee, M. Weibel, J. Catal., 256, 312-322 (2008)

[23] U. Deka, A. Juhin, E. A. Eilertsen, H. Emerich, M. A. Green, S. T. Korhonen, B. M. Weckhuysen, A. M. Beale, *J. Phys. Chem. C*, **116**, 4809-4818 (2012)

[24] Y. Li, J. N. Armor, *Appl*. *Catal*. *B*: *Environ*., **2**, 239-256 (1993)

[25] Y. Li, J. N. Armor, *J. Catal*., **150**, 376-387 (1994)

[26] R. Burch, S. Scire, *Appl. Catal. B: Environ*., **3**, 295-318 (1994)

[27] M. C. Campa, S. D. Rossi, G. Ferraris, V. Indovina, *Appl. Catal. B: Environ*., **8**, 315-331 (1996)

[28] D. Kaucký, A. Vondrová, J. Dědeček, B. Wichterlová, *J. Catal*., **194**, 318-329 (2000)

[29] D. Kaucký, J. Dědeček, B. Wichterlová, *Micropor. Mesopor. Mater*., **31**, 75-87 (1999)

[30] A. Boix, E. E. Miró, E. A. Lombardo, M. A. Bañares, R. Mariscal, J. L. G. Fierro, *J. Catal.*, **217**, 186-194 (2003)

[31] S. Wang, W. Guo, L. Zhu, H. Wang, K. Qiu, K. Cen, *J. Phys. Chem. C*, **119**, 524-533 (2015)

[32] X. Zhang, Q. Shen, C. He, C. Ma, Z. Liu, Z. Hao, *Chem. Eng. J*., **226**, 95-104 (2013)

[33] H.V. Thang, K. Frolich, M. Sharzhy, P. Eliášová, M. Rubeš, J. Čejka, R. Bulánek, P. Nachtigall, *Phys. Chem. Chem. Phys.*, **18**, 18063-18073 (2016)

[34] E. K. Zajac, J. Datka, *Micropor. Mesopor. Mater*., **109**, 49-57 (2008)

[35] J. Dědeček, V. Balgová, V. Pashkova, P. Klein, B. Wichterlová, *Chem. Mater.*, **24**, 3231-3239 (2012)

[36] K. Aruga, *J. Unconv. Oil Gas Resour*., **14**, 1-5 (2016)

[37] https://www.businessinsider.com/eia-shale-gas-2035-2012-1 (EIA, Annual Energy Outlook 2012 Early Release)

[38] A. H. Kakaee, A. Paykani, M. Ghajar, *Renewable Sustainable Energy Rev*., **38**, 64-78 (2014)

[39] B. Cheng, J. Xu, Q. Deng, Z. Liao, Y. Wang, O. L. Faboya, S. Li, J. Liu, P. Peng, *Mar*. *Pet*. *Geol*., **121**, 104591 (2020)

[40] J. R. H. Ross, M. C. F. Steel. A. Zeini-Isfahani, *J. Catal*, **52**, 280-290 (1978)

[41] J. Xu, G. F. Froment, *AIChE J*., **35**, 88-96 (1989)

[42] F. Besenbacher, I. Chorkendorff, B. S. Clausen, B. Hammer, A. M. Molenbroek, J. K. Nørskov, I. Stensgaard, *Science*, **279**, 1913-1915 (1998)

[43] J. Barcicki, A. Denis, W. Grzegorczyk, D. Nazimek, T. Borowiecki, *React*. *Kinet*. *Catal*. *Lett*., **5**, 471-478 (1976)

[44] J. P. Van Hook, *Catal*. *Rev*., **21**, 1-51 (1980)

[45] J. D. Holladay, J. Hu, D. L. King, Y. Wang, *Catal. Today*, **139**, 244-260 (2009)

[46] S. J. Blanksby, G.B. Ellison, *Acc*. *Chem*. *Res*., **36**, 255-263 (2003)

[47] B. Wang, S. Albarracín-Suazo, Y. Pagán-Torres, E. Nikolla, *Catal. Today*, **285**, 147-158 (2017)

[48] H. S. Bengaard, J. K. Norskov, J. Sehested, B. S. Clausen, L. P. Nielsen, A. M. Molenbroek, J. R. Rostrup-Nielsen, *J. Catal*., **209**, 365-384 (2002)

[49] E. Achenbach, E. Riensche, *J. Power Sources*, **52**, 283-288 (1994)

[50] F. Abild-Pedersen, O. Lytken, J. Engbaek, G. Nielsen, I. Chorkendorff, J. K. Norskov, Surf. Sci., **590**, 127-137 (2005)

[51] J. M. Wei, E. Iglesia, *J. Catal*., **224**, 370-383 (2004)

[52] R. M. Watwe, H. S. Bengaard, J. R. Rostrup-Nielsen, J. A. Dumesic, J. K. Norskov, *J. Catal*., **189**, 16-30 (2000)

[53] J. R. Rostrup-Nielsen, T. S. Christensen, I. Dybkjaer, *Stud. Surf. Sci. Catal*., **113**, 81-95 (1998)

[54] N. C. Triantafyllopoulos, S. G. Neophytides, *J. Catal*., **217**, 324-333 (2003)

[55] T. Takeguchi, Y. Kani, T. Yano, R. Kikuchi, K. Eguchi, K. Tsujimoto, Y. Uchida, A. Ueno, K. Omoshiki, M. Aizawa, *J. Power Sources*, **112**, 588-595 (2002)

[56] J. Rostrup-Nielsen, J. K. Norskov, *Top. Catal*., **40**, 45-48 (2006)

[57] D. Chen, K. O. Christensen, E. Ochoa-Fernandez, Z. X. Yu, B. Totdal, N. Latorre, A. Monzon, A. Holmen, *J. Catal*., **229**, 82-96 (2005)

[58] S. Helveg, C. Lopez-Cartes, J. Sehested, P. L. Hansen, B. S. Clausen, J. R. Rostrup-Nielsen, F. Abild-Pedersen, J. K. Norskov, *Nature*, **427**, 426-429 (2004)

[59] D. L. Trimm, *Catal. Today*, **37**, 233-238 (1997)

[60] E. Nikolla, J. Schwank, S. Linic, *J. Catal*., **250**, 85-93 (2007)

[61] E. Nikolla, J. W. Schwank, S. Linic, *Catal. Today*, **136**, 243-248 (2008)

[62] E. Nikolla, J. Schwank, S. Linic, *J. Catal*., **263**, 220-227 (2009)

[63] J. Guo, H. Lou, H. Zhao, D. Chai, X. Zheng, *Appl. Catal. A: Gen*., **273**, 75-82 (2004)

[64] S. Teuner, *Hydrocarbon Process*., **64**, 106-107 (1985)

[65] B. Delmon, *Appl. Catal. B*, **1**, 139-147 (1992)

[66] J.-H. Kim, D. J. Suh, T.-J. Park, K.-L. Kim, *Appl. Catal. A: Gen*., **197**, 191-200 (2000)

[67] A. M. Gadalla, B. Bower, *Chem. Eng. Sci*., **43**, 3049-3062 (1988)

[68] J. R. Rostrup-Nielsen, J.-H. B. Hasen, *J. Catal*., **144**, 38-49 (1993)

[69] J. T. Richardson, S. A. Paripatyadar, *Appl. Catal*., **61**, 293-309 (1990)

[70] A. T. Ashcroft, A. K. Cheetham, M. L. H. Green, P. D. F. Vernon, *Nature*, **352**, 225-226 (1991)

[71] O. Yamazaki, T. Nozaki, K. Omata, K. Fujimoto, *Chem. Lett*., **21**, 1953-1954 (1992)

[72] M. Shah, T. Das, P. Mondal, *Fuel*, **313**, 122683 (2022)

[73] N. A. K. Aramouni, J. G. Touma, B. A. Tarboush, J. Zeaiter, M. N. Ahmad, *Renew. Sust. Energ. Rev*., **82**, 2570-2585 (2018)

[74] A. Erdöhelyi, J. Cserenyi, F. Solymosi, *J. Catal*. **141**, 287-299 (1993)

[75] C. A. Ortiz-Bravo, C. A. Chagas, F. S. Toniolo, *J. Nat. Gas Sci. Eng*., **96**, 104254 (2021)

[76] D. Fan, D. J. Dai, H. S. Wu, *Materials*, **6**, 101-115 (2013)

[77] P. Schwach, X. Pan, X. Bao, *Chem. Rev*., **117**, 8497-8520 (2017)

[78] Y. Gao, L. Neal, D. Ding, W. Wu, C. Baroi, A. M. Gaffney, F. Li, *ACS Catal*., **9**, 8592-8621 (2019)

[79] Y. H. Hou, W. C. Han, W. S. Xia, H. L. Wan, *ACS Catal*., **5**, 1663-1674 (2015)

[80] M. Zhao, S. Ke, H. Wu, W. Xia, H. Wan, *Ind. Eng. Chem. Res*., **58**, 22847-22856 (2019)

[81] D. Noon, A. Seubsai, S. Senkan, *ChemCatChem*, **5**, 146-149 (2013)

[82] T. W. Elkins, S. J. Roberts, H. E. Hagelin-Weaver, *Appl. Catal. A: Gen*., **528**, 175-190 (2016)

[83] A. S. Jones, D. Aziz, J. Ilsemann, M. Bäumer, H. Hagelin-Weaver, *Catal. Today*, **365**, 46-57 (2021)

[84] A. P. Ortiz-Espinoza, M. M. B. Noureldin, M. M. El-Halwagi, A. Jiménez-Gutiérreza, *Comput. Chem. Eng*., **107**, 237-246 (2017)

[85] V. Spallina, I. C. Velarde, J. A. M. Jimenez, H. R. Godini, F. Gallucci, M. V. Annaland, *Energy Convers. Manag.*, **154**, 244-261 (2017)

[86] B. L. Farrell, V. O. Igenegbai, S. Linic, *ACS Catal*., **6**, 4340-4346 (2016)

[87] R. Horn, R. Schlögl, *Catal. Lett*., **145**, 23-39 (2015)

[88] A. C. Rosenzweig, C. A. Frederick, S. J. Lippard, P. Nordlund, *Nature*, **366**, 537-543 (1993)

[89] R. L. Lieberman, A. C. Rosenzweig, *Nature*, **434**, 177-182 (2005)

[90] A. S. Hakemian, A. C. Rosenzweig, *Annu. Rev. Biochem*., **76**, 223-241 (2007)

[91] A. I. Olivos-Suarez, À. Szécsényi, E. J. M. Hensen, J. Ruiz-Martinez, E. A. Pidko, J. Gascon, *ACS Catal*., **6**, 2965-2981 (2016)

[92] Z. Guo, B. Liu, Q. Zhang, W. Deng, Y. Wang, Y. Yang, *Chem. Soc. Rev*., **43**, 3480-3524 (2014)

[93] R. Balasubramanian, S. M. Smith, S. Rawat, L. A. Yatsunyk, T. L. Stemmler, A. C. Rosenzweig, *Nature*, **465**, 115-119 (2010)

[94] R. A. Himes, K. Barnese, K. D. Karlin, *Angew. Chem. Int. Ed*., **49**, 6714-6716 (2010)

[95] A. R. Kulkarni, Z.-J. Zhao, S. Siahrostami, J. K. Nørskov, F. Studt, *Catal. Sci. Technol*., **8**, 114-123 (2018)

[96] D. K. Pappas, E. Borfecchia, M. Dyballa, K. A. Lomachenko, A. Martini, G. Berlier, B. Arstad, C. Lamberti, S. Bordiga, U. Olsbye, S. Svelle, P. Beato, *ChemCatChem*, **11**, 621-627 (2019)

[97] E. V. Kondratenko, T. Peppel, D. Seeburg, V. A. Kondratenko, N. Kalevaru, A. Martin, S. Wohlrab, *Catal. Sci. Technol*., **7**, 366-381 (2017)

[98] S. E. Bozbag, P. Šot, M. Nachtegaal, M. Ranocchiari, J. Bokhoven, C. Mesters, *ACS Catal*., **8**, 5721-5731 (2018)

[99] P. Vanelderen, B. E. R. Snyder, M.-L. Tsai, R. Hadt, J. Vancauwenbergh, O. Coussens, R. Schoonheydt, B. Sels, E. I. Solomon, *J. Am. Chem. Soc*., **137**, 6383-6392 (2015)

[100] H. V. Le, S. Parishan, A. Sagaltchik, C. Göbel, C. Schlesiger, W. Malzer, A. Trunschke, R. Schomäcker, A. Thomas, *ACS Catal*., **7**, 1403-1412 (2017)

[101] M. Ravi, M. Ranocchiari, J. A. van Bokhoven, *Angew. Chem. Int. Ed*., **56**, 16464-16483 (2017)

[102] M. Álvarez, P. Marín, S. Ordóñez, *Mol. Catal*., **487**, 110886 (2020)

[103] W. Taifan, J. Baltrusaitis, *Appl. Catal. B: Environ*., **198**, 525-547 (2016)

[104] L. Wang, L. Tao, M. Xie, G. Xu, J. Huang, Y. Xu, *Catal. Lett*., **21**, 35-41 (1993)

[105] Y. Xu, L. Lin, *Appl. Catal. A: Gen*., **188**, 53-67 (1999)

[106] F. Solymosi, A. Szöke, J. Cserényi, *Catal. Lett*. **39**, 157-161 (1996)

[107] F. Solymosi, J. Cserényi, A. Szöke, T. Bánsági, A. Oszkó, *J. Catal*., **165**, 150-161 (1997)

[108] D. Wang, J. H. Lunsford, M. P. Rosynek, (1996) *Top. Catal*., **3**, 289-297 (1996)

[109] C. L. Zhang, S. Li, Y. Yuan, W. X. Zhang, T. H. Wu, L. W. Lin, *Catal. Lett*., **56**, 207-213 (1998)

[110] D. Wang, J. H. Lunsford, M. P. Rosynek, *J. Catal*., **169**, 347-358 (1997)

[111] B. M. Weckhuysen, M. P. Rosynek, J. H. Lunsford, *Catal. Lett*., **52**, 31-36 (1998)

[112] H. Liu, T. Li, B. Tian, Y. Xu, *Appl. Catal. A: Gen*., **213**, 103-112 (2001)

[113] D. Ma, D. Wang, L. Su, Y. Shu, Y. Xu, X. Bao, *J. Catal*., **208**, 260-269 (2002)

[114] M. Rahman, A. Infantes-Molina, A. S. Hoffman, S. R. Bare, K. L. Emerson, S. J. Khatib, *Fuel*, **278**, 118290 (2020)

[115] J. F. Haw, W. Song, D. M. Marcus, J. B. Nicholas, *Acc. Chem. Res*., **36**, 317-326 (2003)

[116] M. Bjørgen, S. Svelle, F. Joensen, J. Nerlov, S. Kolboe, F. Bonino, L. Palumbo, S. Bordiga, U. Olsbye, *J. Catal*., **249**, 195-207 (2007)

[117] N. Tajima, T. Tsuneda, F. Toyama, K. Hirao, *J. Am. Chem. Soc*., 120, 8222-8229 (1998)

[118] S. R. Blaszkowski, R. A. Santen, *J. Am. Chem. Soc*., **119**, 5020-5027 (1997)

[119] J.S. Beck, D.H. Olson, S.B. McCullen, U.S. Patent 5 367 099 (1994)

[120] D. Mitsuyoshi, K. Kuroiwa, Y. Kataoka, T. Nakagawa, M. Kosaka, K. Nakamura, S. Suganuma, Y. Araki, N. Katada, *Micropor. Mesopor. Mater*., **242**, 118-126 (2017)

[121] S. J. X. He, M. A. Long, M. A. Wilson, M. L. Gorbaty, P. S. Maa, *Energy Fuels*, **9**, 616-619 (1995)

[122] T. Baba, H. Sawada, *Phys. Chem. Chem. Phys*., **4**, 3919-3923 (2002)

[123] D. B. Lukyanov, T. Vazhnova, *J. Mol. Catal. A Chem*., **305**, 95-99 (2009)

[124] S. S. Arzumanov, I. B. Moroz, D. Freude, J. Haase, A. G. Stepanov, *J. Phys. Chem. C*, **118**, 14427-14432 (2014)

[125] M. O. Adebajo, M. A. Long, R. L. Frost, *Catal. Commun*., **5**, 125-130 (2004)

[126] K. Nakamura, A. Okuda, K. Ohta, H. Matsubara, K. Okumura, K. Yamamoto, R. Itagaki, S. Suganuma, E. Tsuji, N. Katada, *ChemCatChem*, **10**, 3806-3812 (2018)

[127] K. Nakamura, K. Okumura, E. Tsuji, S. Suganuma, N. Katada, *ChemCatChem*, 12, 2333-2340 (2020)

Chapter 2 Selective Formation of Active Cobalt Species for Direct Methylation of Benzene with Methane on MFI Zeolite by Co-presence of Secondary Elements

2-1 Introduction

Supply of natural gas, including such a non-conventional resource as shale gas, is increasing, and its main component, methane, has attracted much attention as a chemical resource alternative to petroleum. Many researchers have studied about chemical processes using methane such as partial oxidation into methanol [1-7] and dehydroaromatization [8-13]. However, selectivity of partial oxidation of methane has still been low, leading to formation of CO_2 and energy loss [14]. Selectivity of dehydroaromatization of methane has not been high, leading to production of carbonaceous polymers and deactivation of catalysts [15-17].

Meanwhile, methylation of benzene ring with methane can be an option for effective conversion of methane into valued compounds. For example, combining the methylation of benzene into toluene shown by Eq. (1) and the shape selective disproportionation of toluene into a pair of benzene and para-xylene [18,19] should convert toluene and

methane into para-xylene, whose demand as a raw material of polyethylene terephthalate is large.

$CH_4 + C_6H_6 \rightarrow CH_3\text{-}C_6H_6 + H_2$ (1)

In previous reports, zeolite-supported transition metal species such as H-*BEA, Cu/*BEA, Cu/MFI [20], Ag/MFI [21], Pt/MFI [22], In/MFI [23] and Zn/MFI [24] showed catalytic activities for the reaction (1). We recently found that the catalytic activity of Co/MFI for the reaction (1) was remarkable among the zeolite-supported transition metals. The activity was found in the limited cobalt loading region. On a support MFI ([Al] = 1.3 mol kg^{-1}, SiO_2/Al_2O_3 molar ratio = 22), the toluene yield was mainly increased with increasing Co in the region of Co/Al = 0.3-0.4 and showed the maximum at Co/Al = 0.6. Further loading reduced the activity. The XAS (X-ray absorption spectroscopy) revealed that the oxidation state was approximately +II over the above cobalt loading range. The cobalt species was mono-atomically held by the ion-exchange site at Co/Al < 0.6, as supported by the maximum Lewis acidity at Co/Al = 0.6, whereas Co/Al > 0.6 resulted in the aggregation of CoO particles. It is therefore considered that the mono-atomic dispersion is required to generate the activity, whereas the aggregates have no activity. The latter is in agreement with a fact that cobalt species showed activity only on the MFI zeolite for the methylation of benzene with methane (1) but not on other examined supports [25].

In addition, one can find unique dependence of activity on the cobalt loading in the presented relationship between the cobalt loading and activity [25]. The activity was negligible in the region of Co/Al < 0.2, and it was generated mainly in the region of Co/Al = 0.2 to 0.6; the activity was significantly increased at Co/Al = 0.3-0.4. Although the main conclusion of our previous paper did not focus on this finding [25], the present study started from it. As shown above, the cobalt species was mono-atomically dispersed, and the oxidation state was +II over a range of Co/Al < 0.6. Therefore, the presence of at least two types of cobalt species with difference in the activity is speculated, even though the dispersion and oxidation state are similar; the active one probably formed at Co/Al > 0.3 and the inactive one formed at Co/Al < 0.2.

The zeolite-supported cobalt shows catalytic activity also for selective catalytic reduction (SCR) of NO_x with methane or ethane [26-30], and the activity has been known to be sensitive to the support zeolite and the location of ion-exchange site. Kaucký reported that the cobalt ions bound to framework oxygens at the main channel were most active among the cobalt ions in MOR and FER, whereas, in MFI, that coordinated to distorted 6-ring at the intersection of straight and sinusoidal channels possessed the highest activity [30]. It has been known that the locations of cobalt ions in the ion-exchange process are influenced by the co-presence of other metal ions [31-33]. Boix

investigated the effect of platinum additive on the catalytic activity for the SCR of NO_x with methane on Co/MFI [33]. They concluded that the mono-atomic cobalt species were preferentially dispersed on the main channel walls of MFI, while they moved to lattice sites with higher coordination number with addition of platinum ions. Based on this knowledge, it is predicted that the activity of Co/MFI for the reaction (1) is modified by the secondary added elements.

In this study, we investigate the ion-exchange behavior of cobalt in the co-presence of additional elements to relate the types of cobalt species with the nature of ion-exchange site. The influences of various elements on the catalytic activity of Co/MFI for the methylation of benzene with methane (1) are studied to find a method of improving the catalytic activity.

2-2 Experimental

2-2-1 Catalyst preparation

Samples of Co+M (M: secondary elements) were prepared by a co-ion-exchange method. Powder of NH_4-MFI zeolite ([Al] = 1.3 mol kg^{-1}, SiO_2/Al_2O_3 molar ratio = 22, purchased from Tosoh Corp.) was put into a mixed aqueous solution of cobalt nitrate and secondary metal nitrate (in the cases of M = Mg, Ca, Sc, Fe, Ni, Cu, Zn, Sr, Ag, In, La,

Ce and Pb) or chloride (in the case of M = Nb) with the amounts of Co and M corresponding to the molar ratios of Co/Al (Al in the zeolite) = M/Al = 2.0. The solution was stirred at 343 K for 4 h, filtered and dried at 383 K overnight. As references, Co/MFI and M/MFI (M = Mg, Ni, Zn and Pb) catalysts were also prepared by the ion-exchange using a pure cobalt nitrate aqueous solution with Co/Al = 0.2, 0.3, 0.4, 0.45, 0.6 or 2.0, or solutions of secondary metal nitrates with M/Al ratio = 2.0 (M = Mg, Zn and Pb) and Ni/Al ratio = 0.2. The solution was also stirred at 343 K for 4 h, filtered and dried at 383 K overnight. In addition, cobalt and magnesium were loaded on MFI by "two steps ion-exchange method". First, Co/MFI or Mg/MFI were prepared by the ion-exchange method (Co/Al = Mg/Al = 2.0) as above, and then, the other metal (Mg or Co) was loaded by the same method. The obtained catalysts are denoted as Co_Mg (first: Co, second: Mg) and Mg_Co (first: Mg, second: Co).

The amounts of cobalt and second metals in the final solids were measured by inductively coupled plasma - atomic emission spectroscopy (ICP-AES, Rigaku ICP CIROS). Hereafter, Co/MFI and M/MFI catalysts are denoted as Co*X* and M*Y* (*X* and *Y* shows the Co/Al and M/Al molar ratio), respectively.

2-2-2 Physicochemical Characterization

Valence and microstructure of cobalt species were analyzed by XAS at BL01B1 in Japan Synchrotron Radiation Research Institute (JASRI, SPring-8, Proposal number 2018A1075). The sample was compressed at 10 MPa to form a thin wafer with 1 cm of diameter. A Co-foil and Co oxides (CoO and Co_3O_4) were also measured as references. The Co K-edge absorption spectra for all samples and references were collected in the quick mode using a Si (111) monochromator at room temperature in atmosphere. The beam size at the sample position was 5 mm (horizontal) × 1 mm (vertical). The normalizing method of XANES spectra was as below. First, the pre-edge region was fitted and used it as a background. Next, the post-edge region was fitted, and the intensity of XAFS spectra was normalized by the difference of the intensity at pre-edge from that at post-edge.

2-2-3 Catalytic Tests

Catalytic reaction of direct methylation of benzene with methane was carried out using a fixed-bed flow reactor. The catalyst (0.300 g) was placed in a Pyrex tube, and pretreated in a flow of nitrogen (1.23 mmol min^{-1}) in the atmospheric pressure at 823 K for 1 h. Then, a mixture of methane (99.9 % from Iwatani Co.) and benzene (vaporized from a liquid sample 99.5% from FUJIFILM Wako Pure Chemical Co.) was fed to the

catalyst bed (98.6 and 2.7 kPa, 1.2 and 0.033 mmol min^{-1}, respectively, corresponding to $W_{cat}/F_{benzene}$ = 147 g_{cat} h $mol_{benzene}^{-1}$) at 773 K. The outlet materials were trapped by hexane at 273 K with a known amount of 1,4-diisopropylbenzene as an internal standard compound and analyzed with a flame ionization detector-gas chromatograph (FID-GC, Shimadzu GC-2014).

2-3 Results

Table 2-1 shows Co/Al, M/Al and Co+M/Al molar ratios of Co*X* and Co+M measured by ICP analysis. Amount of cobalt loaded on Co*X* increased with increasing the concentration of cobalt nitrate in the aqueous solution employed for the ion exchange, and the maximum Co/Al molar ratio was 0.42, given by the Co/Al = 2.0 solution. The Co/Al ratio on the solid was thus close to 0.5 where excess of cobalt nitrate was employed for the ion-exchange, indicating that the cobalt played as a divalent cation during the ion-exchange process. Dědeček and co-researchers indicated that divalent cobalt ion was easily ion-exchanged on a pair of Al atoms within a certain short distance on a zeolite in mild ion-exchange conditions [34] as employed in the present study. As stated above,

Table 2-1. Chemical compositions of Co/MFI, M/MFI and Co+M/MFI catalysts

Catalyst	Period of M	Valence of M	Amount in prepared solution		Amount in final solids					
			Co/Al	M/Al	[Al] / mol kg^{-1}	[Co] / mol kg^{-1}	[M] / mol kg^{-1}	Co/Al	M/Al	(Co+M)/Al
Co0.18			0.2		1.5	0.26		0.18		
Co0.23			0.3		1.3	0.29		0.23		
Co0.29			0.4		1.4	0.41		0.29		
Co0.32			0.45		1.4	0.46		0.32		
Co0.33			0.60		1.5	0.49		0.33		
Co0.42			2.00		1.4	0.60		0.42		
Mg0.43	3rd	+2		2.00	1.1		0.47		0.43	
Ni0.15	4th	+2		0.20	1.0		0.16		0.15	
Zn0.52	4th	+2		2.00	1.1		0.54		0.52	
Pb0.48	6th	+2		2.00	1.2		0.56		0.48	
Co+Mg	3rd	+2	2.00	2.00	1.2	0.29	0.27	0.24	0.22	0.46
Co+Ca	4th	+2	2.00	2.00	0.9	0.15	0.35	0.17	0.38	0.55
Co+Sc	4th	+3	2.00	2.00	0.8	0.42	0.05	0.53	0.07	0.60
Co+Fe	4th	+2	2.00	2.00	1.1	0.33	1.43	0.29	1.26	1.55
Co+Ni	4th	+2	2.00	2.00	1.2	0.36	0.16	0.30	0.13	0.43
Co+Cu	4th	+2	2.00	2.00	1.3	0.36	0.18	0.28	0.14	0.42
Co+Zn	4th	+2	2.00	2.00	1.3	0.31	0.25	0.23	0.19	0.42
Co+Sr	5th	+2	2.00	2.00	1.2	0.37	0.25	0.31	0.21	0.52
Co+Nb	5th	+5	2.00	2.00	1.1	0.38		0.36	2.08※	2.44※
Co+Ag	5th	+1	2.00	2.00	1.2	0.47	0.13	0.38	0.11	0.49
Co+In	5th	+3	2.00	2.00	1.4	0.50	0.48	0.37	0.36	0.73
Co+La	6th	+3	2.00	2.00	1.0	0.45	0.02	0.47	0.02	0.49
Co+Ce	6th	+3	2.00	2.00	1.1	0.50	0.02	0.45	0.02	0.47
Co+Pb	6th	+2	2.00	2.00	1.3	0.20	0.36	0.15	0.28	0.43

most of the ion-exchange sites in MFI were occupied by the cobalt divalent ions, suggesting that most Al atoms in the present MFI sample were located within a short distance.

Table 2-2. Chemical compositions of samples prepared by two step ion-exchange

Catalyst	First exchange	Second exchange	Amount in prepared solution		Amount in final solids					
			Co/Al	Mg/Al	[Al] / mol kg^{-1}	[Co] / mol kg^{-1}	[Mg] / mol kg^{-1}	Co/Al	Mg/Al	(Co+Mg)/Al
Mg_Co	Mg	Co	2.00	2.00	1.1	0.18	0.40	0.17	0.37	0.54
Co_Mg	Co	Mg	2.00	2.00	1.0	0.36	0.18	0.37	0.18	0.55

Most of the Co+M samples with divalent M cations (Mg, Ca, Ni, Cu, Zn, Sr and Pb) had ca. 0.5 (0.42-0.55) of the (Co+M)/Al molar ratios, indicating that the ion-exchange sites were generally occupied by Co and M divalent ions. The Co/Al molar ratio on Co+M tended to increase with increasing the atomic number of the secondary element. On the other hand, the Co+M containing cations with other valences showed a largely different trend; Fe, Nb and In showed obviously higher (Co+M)/Al ratios, probably because they were aggregated on the external surfaces of zeolites [35]. On the contrary, the M/Al ratio on Co+M (M = trivalent cation, Sc, La or Ce) was merely lower than those of the other Co+M.

Table 2-2 shows the chemical compositions of Co+Mg/MFI prepared by the two steps ion-exchange method. The amounts of elements loaded in the first step was higher than those in the second step.

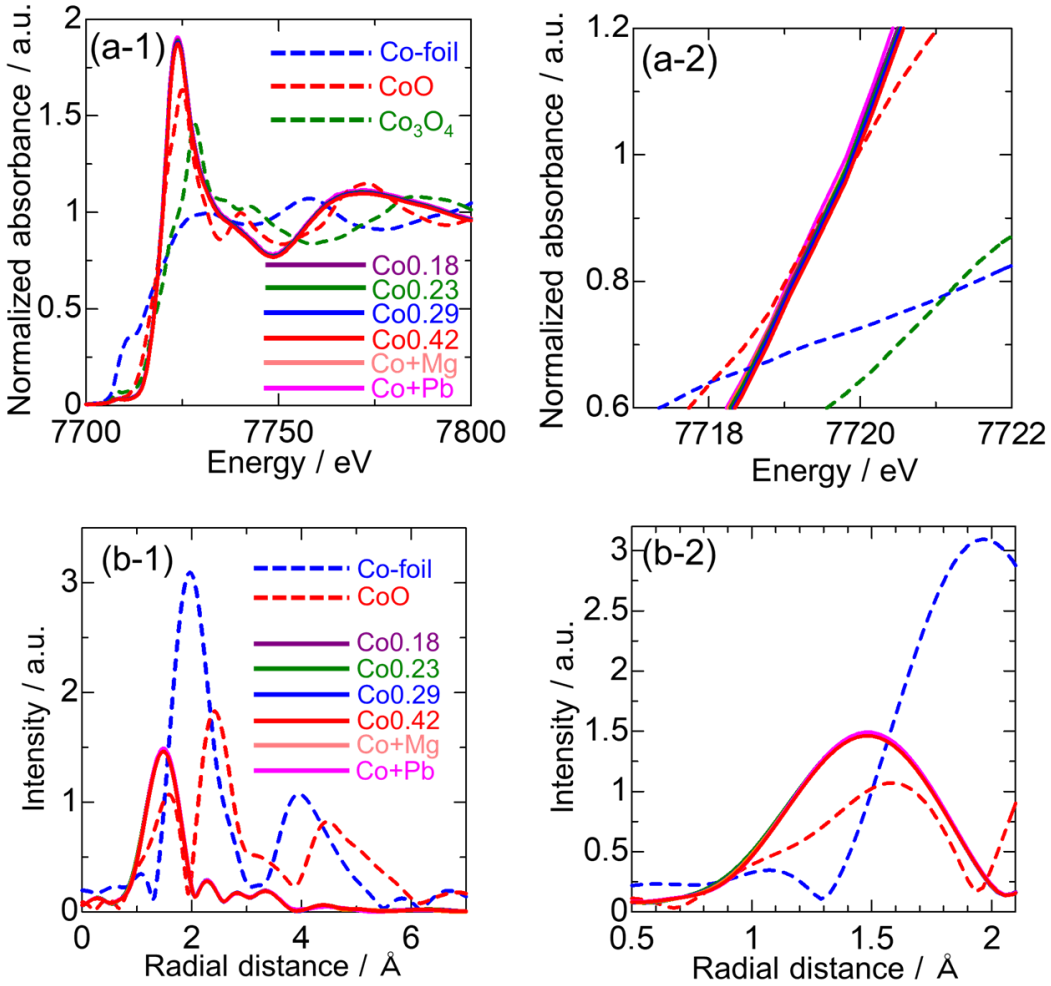

Figure 2-1. (a-1, a-2) XANES spectra and (b-1, b-2) radial distribution functions of Co K-edge EXAFS of Co/MFI (Co/Al ratio = 0.2-0.42), Co+M/MFI (M = Mg, Pb) and reference samples. (a-1) and (b-1) are the whole figures. (a-2) is the enlarged portion of 7717-7722 eV of XANES, while (b-2) is the enlarged portion of 0.5-2.1 Å of EXAFS.

Figure 2-1 (a) shows the Co-K edge XANES (X-ray absorption near edge structure)

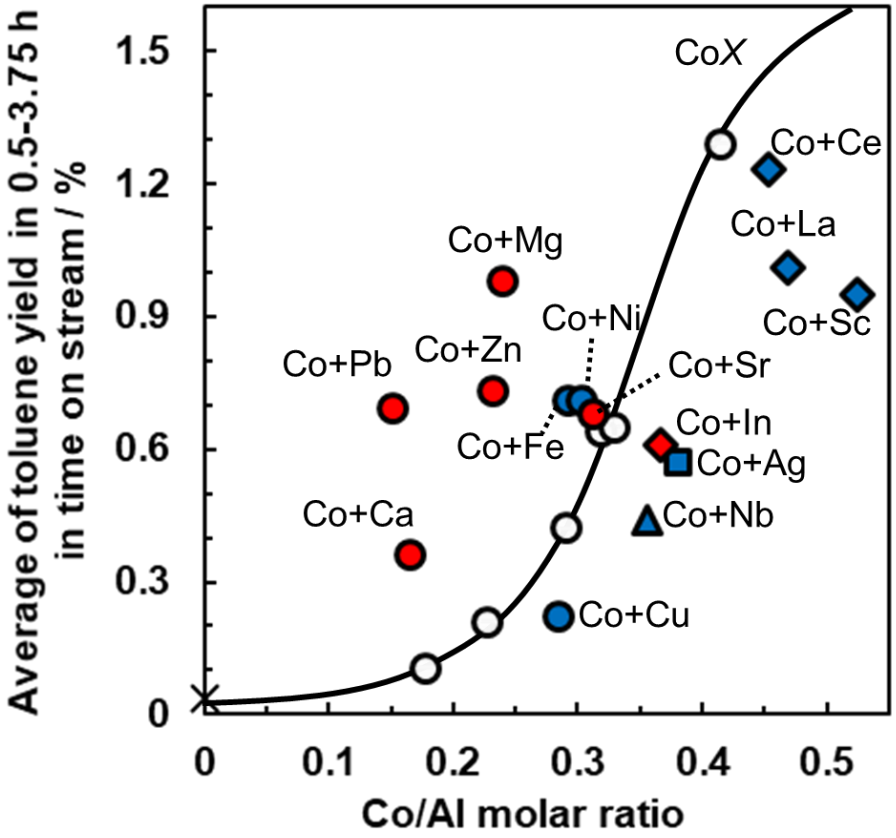

Figure 2-2. Relationship between catalytic activity for methylation of benzene with methane (773 K, P_{CH4} = 98.6 kPa, P_{C6H6} = 2.7 kPa, $W_{cat}/F_{benzene}$ = 147 g_{cat} h $mol_{benzene}^{-1}$) and amount of cobalt on (○) Co/MFI (Co/Al ratio = 0.2-0.42), Co+M/MFI; M = (■) monovalent, (●) divalent, (◆) trivalent and (▲) pentavalent ions, together with H-form of MFI (×). In addition, the typical and transition metals are given in red and blue colors, respectively.

spectra of Co*X*, Co+Mg and Co+Pb, together with the reference materials. The spectra of all the Co/MFI samples had similar absorption edge to that of bulk CoO, indicating that

the oxidation state of cobalt on MFI was +II, as already reported on Co ion exchanged or impregnated on MFI [25]. The Co+Mg and Co+Pb samples also had the same absorption edges as Co*X* even though the magnesium or lead was loaded on MFI with cobalt. Figure 2-1 (b) shows the radial distribution function of Co K-edge EXAFS (extended X-ray absorption fine structure). As our previous report on Co ion exchanged or impregnated on MFI [25], the spectra of all the Co*X* and Co+M (M = Mg or Pb) samples showed only a distribution peak at 0.15 nm, attributed to Co-O, indicating that cobalt species were mono-atomically dispersed on MFI. This tells us that such a species as Z-Co^{2+}-O-Mg^{2+}-Z (Z: Zeolite) was not predominantly formed on Co+M. These XAS measurements were carried out in atmosphere at ambient temperature. Therefore, these results show the microstructures of Co before the reaction but not the working state.

Figure 2-2 shows the catalytic activities of Co*X* and Co+M for the methylation of benzene with methane (1) as a function of the Co/Al molar ratio, where the activity is shown by the average toluene yield in 0.5-3.75 h of the time on stream based on the time course (Figure 2-3 and 2-4). On Co*X*, the catalytic activity was sensitively dependent on the Co/Al ratio. The activity was very small at Co/Al < 0.2 and then drastically increased with increasing the cobalt loading in the range of Co/Al = 0.3-0.4. The experimental fact has been reported in our previous paper, and origin of the decrease of activity found at

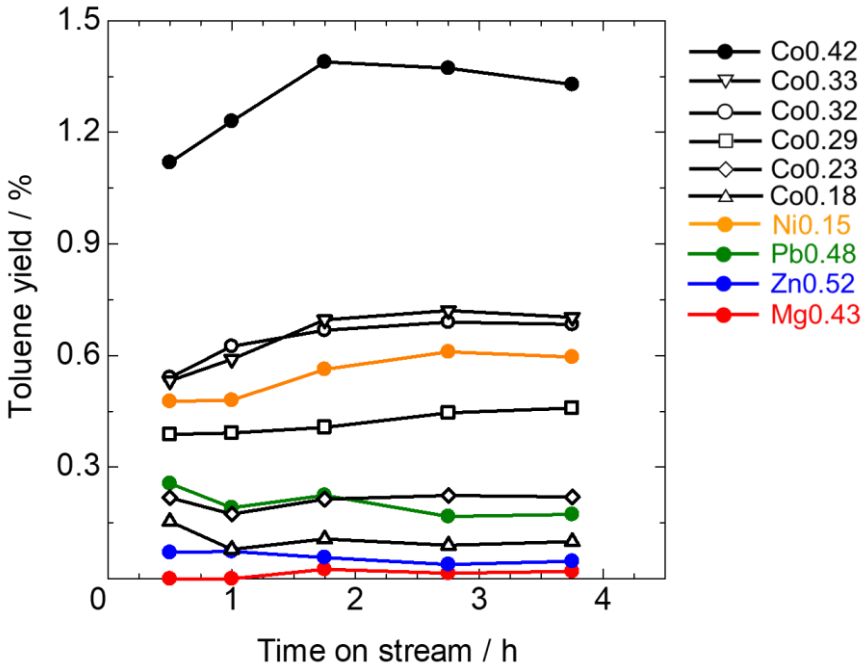

Figure 2-3. Time course of toluene yield at 773 K, P_{CH4} = 98.6 kPa, P_{C6H6} = 2.7 kPa and $W_{cat}/F_{benzene}$ = 147 g_{cat} h $mol_{benzene}^{-1}$ over Co/MFI (Co/Al = 0.18-0.42) and M/MFI (M = Ni, Pb, Zn and Mg). The toluene yields of all catalysts were relatively stable for 4 h.

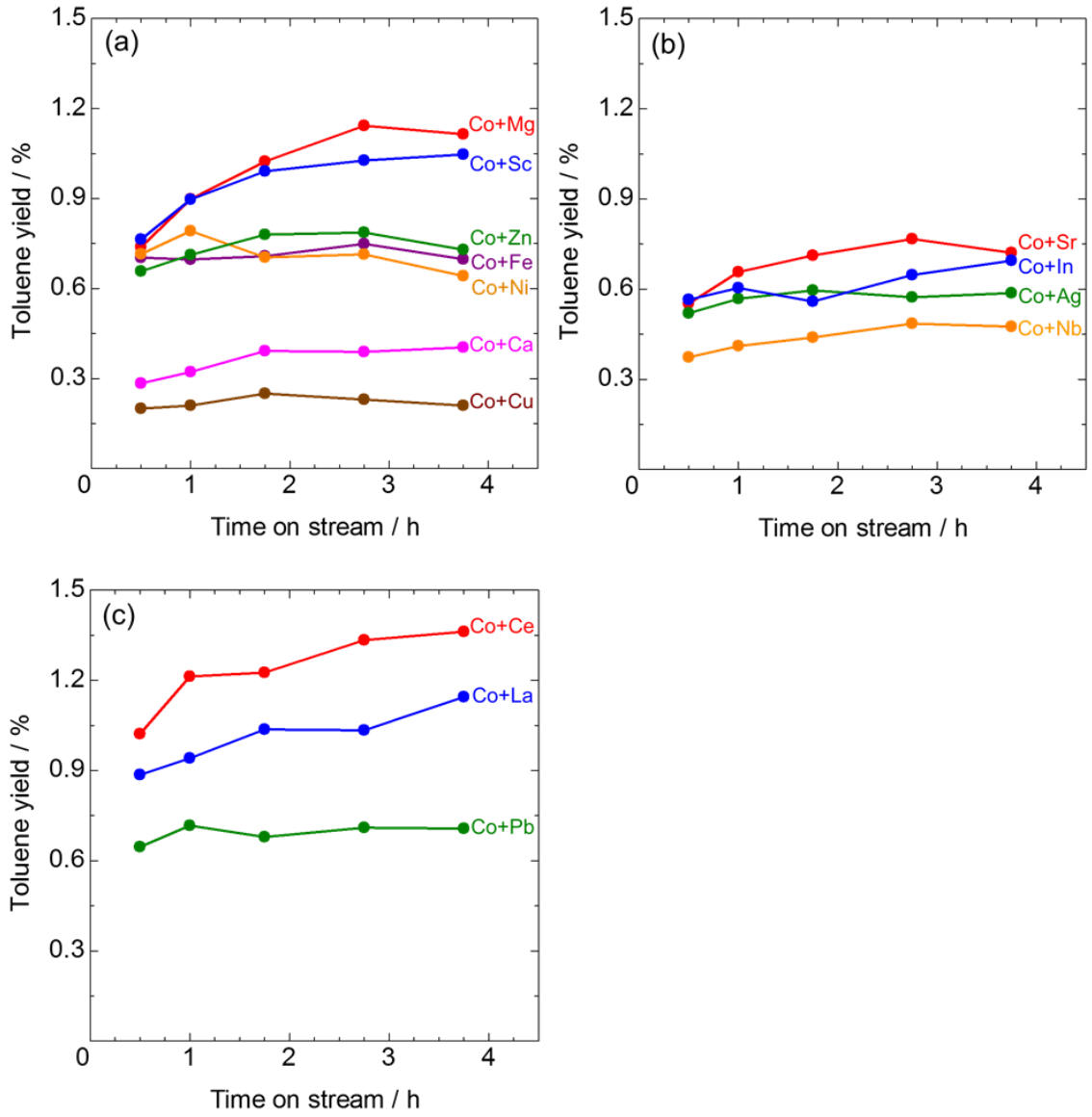

Figure 2-4. Time course of toluene yield at 773 K, P_{CH4} = 98.6 kPa, P_{C6H6} = 2.7 kPa and $W_{cat}/F_{benzene}$ = 147 g_{cat} h $mol_{benzene}^{-1}$ over Co+M/MFI; M = (a) 3rd, 4th, (b) 5th and (c) 6th period element ions. The toluene yields of all catalysts were relatively stable for 4 h.

Co/Al > 0.6 after the activity showed the maximum at Co/Al = 0.6 has been investigated; the XAFS and TEM analyses evidenced that the aggregation of Co species into CoO crystals diminished the activity at Co/Al > 0.6 [25].

Apart from it, here we focus on the activity changes in the range of Co/Al = 0-0.25 by the addition of second elements, where the simple Co loading generated little activity. Some of secondary elements significantly modified the activity; Mg, Pb, Zn and Ca

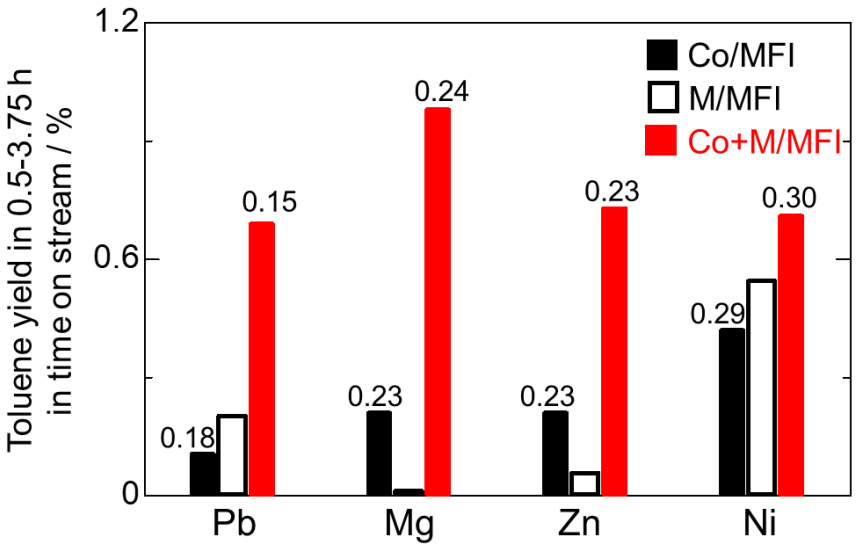

Figure 2-5. Comparison of catalytic activities for methylation of benzene with methane (773 K, P_{CH4} = 98.6 kPa, P_{C6H6} = 2.7 kPa, $W_{cat}/F_{benzene}$ = 147 g_{cat} h $mol_{benzene}^{-1}$) over Co+M/MFI (M = Pb, Mg, Zn, Ni), M/MFI and Co/MFI with equivalent cobalt contents. The digits indicate the Co/Al molar ratios.

enhanced the activity of Co/MFI with the equivalent cobalt loading, while Cu, Nb, Ag, In, Ce, La and Sc obviously suppressed the activity. Here one can summarize that the typical elements (red symbols) generally enhanced the activity, whereas the transition elements (blue) generally suppressed the activity.

Figure 2-5 shows the catalytic activities of Co+M (M = Pb, Mg, Zn and Ni) together with those of Co*X* with the equivalent cobalt contents and M*X*. On Co+Pb, Co+Mg and Co+Zn, the catalytic activity was drastically enhanced by adding of the second elements, even though M*X* (M = Pb, Mg and Zn) showed low catalytic activity. In contrast, Ni/MFI showed the relatively high toluene yield in the present conditions, i.e., in a flow of methane and benzene vapor. It has been known that silicate-supported Ni showed high activity to methane dehydrogenation (methane decomposition) into carbon and dihydrogen [36-38]. It is believed that Ni/MFI had also high activity for methane decomposition in the present conditions, where methane was the main component of reactant gas. The formed dihydrogen should cause the hydrogenolysis of benzene [39] in which the major product was toluene. The reason for the high apparent toluene yield on Ni/MFI is thus speculated to the activity for the dehydrogenation of methane and hydrogenolysis of benzene. The combined catalyst Co+Ni/MFI showed the activity not much higher than Co/MFI, telling us that the enhancement of activity of Co/MFI by the

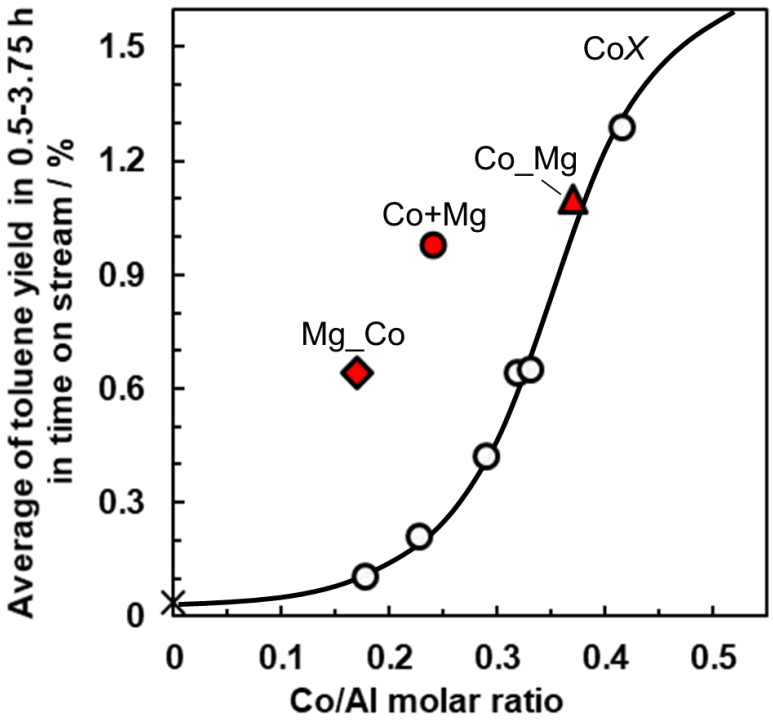

Figure 2-6. Relationship between catalytic activity for methylation of benzene with methane (at 773 K, P_{CH4} = 98.6 kPa, P_{C6H6} = 2.7 kPa, $W_{cat}/F_{benzene}$ = 147 g_{cat} h $mol_{benzene}^{-1}$) and amount of cobalt on (○) Co/MFI (Co/Al ratio = 0.2-0.42), (●) Co+Mg/MFI and the catalysts prepared by two steps ion-exchange method; (▲) Co_Mg (first: Co, second: Mg), (◆) Mg_Co (first: Mg, second: Co).

additional elements does not require the activity of added elements themselves for the methylation of benzene with methane. The addition of Mg, Pb and Zn generated the high activity, and the behavior was obviously different from that of Ni.

Figure 2-6 shows the relationship between the catalytic activity and cobalt content

on Co+M/MFI with different preparation methods. The Mg_Co sample on which Mg was loaded on the first step of the ion-exchanging showed the catalytic activity much higher than that of Co*X* with the equivalent cobalt content. The activity increase behavior of Mg_Co was similar to that found on Co+Mg, where Co and Mg were simultaneously introduced. On the contrary, the Co_Mg sample on which Mg was loaded by the second step of the ion-exchanging showed the catalytic activity similar to that of Co*X*.

2-4 Discussion

The Co/Al ratio on the Co*X* samples (prepared by simple cobalt ion-exchange) was ca. 0.5 where excess of cobalt nitrate was employed. Furthermore, we have observed that the number of Brønsted acid sites was approximately equal to the number of Al atoms before the ion-exchange, and two Brønsted acid sites were diminished by introduction of one Co^{2+} cation [25]. These observations indicate that the cobalt played as a divalent cation during the ion-exchange process. Similarly, the Co+M samples (M = Mg, Ca, Ni, Cu, Zn, Sr and Pb; prepared by the simultaneous exchange with Co and M) had ca. 0.5 (0.42-0.55) of the (Co+M)/Al molar ratios, indicating that both of Co and M played as divalent cations.

The low cobalt loading (Co/Al < 0.2) on Co/MFI generated negligible activity, while

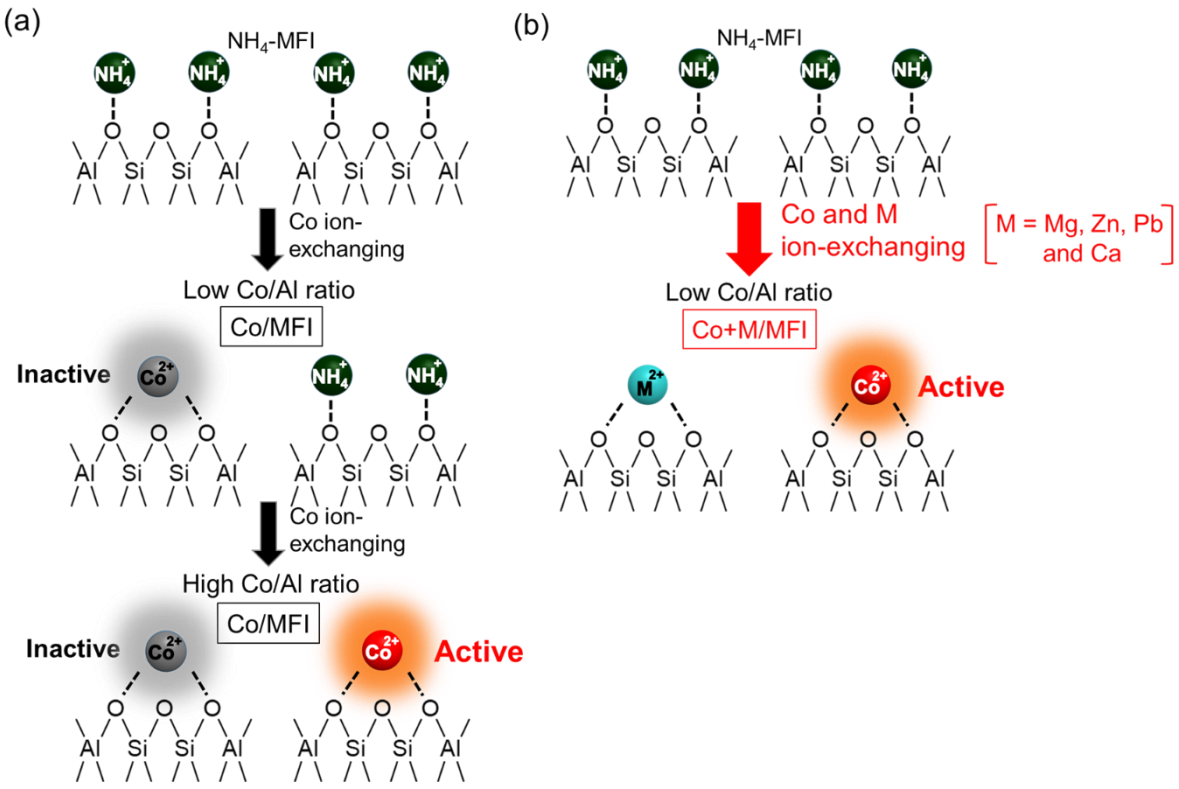

Figure 2-7. Schematic drawing of ion-exchange on (a) Co/MFI and (b) Co+M/MFI.

the high cobalt loading (Co/Al = 0.3-0.4), but within the region not forming the CoO aggregates, created the high activity for the methylation of benzene with methane (1). It tells us that the cobalt species on the ion-exchange site of MFI is classified into at least two types: the active and inactive ones. The XANES exhibited that the valence of both of them was commonly +II, and the EXAFS showed the principally mono-atomic dispersion of both types. The catalytic activity had been found only on a specific support, MFI zeolite, among various zeolites and silica [25], and here it was clarified that the activity was generated only limited cases, even the valence and microstructure of cobalt species were

kept as above. Based on these facts, we speculate that the activity was generated by the environment of mono-atomically dispersed cobalt species with oxidation state +II given by some specific interactions from the ion-exchange site. Therefore, the presence of at least two types of ion-exchange site with different interactions with Co^{2+} is supposed; the site giving high activity to cobalt species (hereafter active position) and the site not giving the activity (hereafter inactive position).

It is explained that the inactive cobalt species is formed at lower cobalt content, and active cobalt species is formed at relatively higher cobalt content (Figure 2-7 (a)). It is suggested that the divalent cobalt ion on the inactive position was thermodynamically stable. Even at the low cobalt content, the divalent typical element ions, i.e., Mg, Zn, Pb and Ca, improved the activity. In the ion-exchange procedure, the cobalt and these additives played as the independent divalent cations, and directly link such as Co-O-M was not observed by EXAFS. These facts deny the possibility of direct chemical modification of cobalt species by these typical elements, and therefore it is reasonable to explain that the added elements suppressed formation of the inactive cobalt species. It is thus speculated that the divalent typical element ions were more easily introduced onto the inactive positions than cobalt ions, blocking in the formation of inactive cobalt species (Figure 2-7 (b)). This hypothesis is consistent with that Mg_Co showed the high activity,

but Co_Mg did not.

Thus, preferential ion exchange of some specific sites is supposed to result in the enhancement of activity of Co species on MFI. The effect was found on Mg, Ca, Zn and Pb, i.e., typical elements with +II of the valence in the ion exchange solutions. The ion radius, acid-base property and extent of localization of charge may affect on the interaction between the cation and zeolite framework, and therefore they will influence the preferential exchange, but further study is necessary to clarify the key factors.

On the other hand, modification of the chemical nature of ion exchange site, e.g., Brønsted acid strength in H-form, by the additional elements has been reported [40-42]. Here the probability of such a modification effect on the acidic property by the added element is discussed. As stated in previous section, we found that the Brønsted acidity of original zeolite was lost with covering the ion exchange site with Co species. It means that, at least in the state of catalyst before the reaction, a Brønsted acid site was unnecessary for the generation of activity. However, the Brønsted acidic nature of ion exchange site may be regenerated by the (partial or total) reduction of Co^{2+} during the reaction. It is thus still possible that such Brønsted acidic nature played a role for the catalysis, especially in the alkylation step, and it was modified by the added elements. In our prediction, the probability of this reason is small, because the sum of amounts of ion

exchanged Co and added element was generally ca. 0.5 of the amount of Al, suggesting that the Co and added element separately occupied the ion exchange sites. On the other hand, Co species on MFI showed Lewis acidity. It seems important for the methylation of benzene ring, as found in the transmethylation of toluene on Ni/MFI [43]. We are currently analyzing details in Lewis acidity of Co species on MFI and will report as a paper in the future.

Dědeček et al. reported that the ion-exchange sites of cobalt ions on MFI could be classified into α, β and γ sites by difference of cobalt surrounding location and coordination numbers, which showed different absorption bands in visible light region [30, 31, 34]. It is speculated that difference in the activity of Co species among the ion-exchange sites is due to the electronic property of Co which is reflected by UV-vis spectrum, and therefore the identification of α, β and γ sites should be important. It needs the measurements in dehydrated environment, and the interpretation requires discussion which should be the subject of our next study.

Fundamental reason for the high activity of Co for the methylation of benzene with methane has not been clear, because the activity was found only on a very specific combination of element (Co) and support (MFI zeolite). The present paper focuses on the experimental observation of the activity of Co/MFI catalysts modified with the second

elements, but further analysis of the modified catalysts is believed to clarify the reason for activity of Co/MFI for the methylation of benzene with methane.

2-5 Conclusions

The catalytic activity for methylation of benzene with methane was generated only in the region Co/Al = 0.2 to 0.6 by the simple ion-exchange of cobalt onto MFI zeolite. The physicochemical characterizations indicated the presence of active and inactive cobalt species due to the difference in the nature of ion-exchange site. Addition of such divalent typical elements as Mg, Zn, Pb and Ca before or during the ion-exchange step of Co enhanced the activity, probably because the typical element ions blocked the inactive positions and concentrate Co on the active positions.

Acknowledgements

This study was partly supported by JST CREST Grant Number JPMJCR17P1, Japan.

References

[1] V. I. Sobolev, K. A. Dubkov, O. V. Panna, G. I. Panov, *Catal. Today*, **24**, 251-252 (1995)

[2] M. H. Groothaert, P. J. Smeets, B. F. Sels, P. A. Jacobs, R. A. Schoonheydt, *J. Am. Chem. Soc*., **127**, 1394-1395 (2005)

[3] E. M. Alayon, M. Nachtegaal, M. Ranocchiari, J. A. Bokhoven, *Chem. Commun.*, **48**, 404-406 (2012)

[4] V. L. Sushkevich, D. Palagin, M. Ranocchiari, J. A. Bokhoven, *Science*, **356**, 523-527 (2017)

[5] S. Grundner, M. A. C. Markovits, G. Li, M. Tromp, E. A. Pidko, E. J. M. Hensen, A. Jentys, M. Sanchez-Sanchez, J. A. Lercher, *Nat. Commun*., **6**, 7546 (2015)

[6] K. Narsimhan, K. Iyoki, K. Dinh, Y. R. Leshkov, *ACS Cent. Sci*., **2**, 424-429 (2016)

[7] N. V. Beznis, A. N. C. Laak, B. M. Weckhuysen, J. H. Bitter, *Micropor. Mesopor. Mater*., **138**, 176-183 (2011)

[8] L. Wang, L. Tao, M. Xie, G. Xu, J. Huang, Y. Xu, *Catal. Lett*., **21**, 35-41 (1993)

[9] Y. Xu, L. Lin, *Appl. Catal. A: Gen*., **188**, 53-67 (1999)

[10] F. Solymosi, A. Szöke, J. Cserényi, *Catal. Lett*. **39**, 157-161 (1996)

[11] F. Solymosi, J. Cserényi, A. Szöke, T. Bánsági, A. Oszkó, *J. Catal*., **165**, 150-161

(1997)

[12] D. Wang, J. H. Lunsford, M. P. Rosynek, (1996) *Top. Catal*., **3**, 289-297 (1996)

[13] C. L. Zhang, S. Li, Y. Yuan, W. X. Zhang, T. H. Wu, L. W. Lin, *Catal. Lett*., **56**, 207-213 (1998)

[14] R. A. Periana, *Science*, **358**, eaan5970 (2017)

[15] B. M. Weckhuysen, M. P. Rosynek, J. H. Lunsford, *Catal. Lett.*, **52**, 31-36 (1998)

[16] H. Liu, T. Li, B. Tian, Y. Xu, *Appl. Catal. A: Gen*., **213**, 103-112 (2001)

[17] D. Ma, D. Wang, L. Su, Y. Shu, Y. Xu, X. Bao, *J. Catal*., **208**, 260-269 (2002)

[18] J.S. Beck, D.H. Olson, S.B. McCullen, U.S. Patent 5 367 099 (1994)

[19] D. Mitsuyoshi, K. Kuroiwa, Y. Kataoka, T. Nakagawa, M. Kosaka, K. Nakamura, S. Suganuma, Y. Araki, N. Katada, *Micropor. Mesopor. Mater*., **242**, 118-126 (2017)

[20] S. J. X. He, M. A. Long, M. A. Wilson, M. L. Gorbaty, P. S. Maa, *Energy Fuels*, **9**, 616-619 (1995)

[21] T. Baba, H. Sawada, *Phys. Chem. Chem. Phys*., **4**, 3919-3923 (2002)

[22] D. B. Lukyanov, T. Vazhnova, *J. Mol. Catal. A Chem*., **305**, 95-99 (2009)

[23] A. A. Gabrienko, S. S. Arzumanov, I. B. Moroz, I. P. Prosvirin, A. V. Toktarev, W. Wang, A. G. Stepanov, *J. Phys. Chem. C*, **118**, 8034-8043 (2014)

[24] X. Wang, J. Xu, G. Qi, B. Li, C. Wang, F. Deng, *J. Phys. Chem. C*, **117**, 4018-4023

(2013)

[25] K. Nakamura, A. Okuda, K. Ohta, H. Matsubara, K. Okumura, K. Yamamoto, R. Itagaki, S. Suganuma, E. Tsuji, N. Katada, *ChemCatChem* **10**, 3806-3812 (2018)

[26] Y. Li, J. N. Armor, *Appl*. *Catal*. *B*: *Environ*., **2**, 239-256 (1993)

[27] Y. Li, J. N. Armor, *J. Catal*., **150**, 376-387 (1994)**.**

[28] R. Burch, S. Scire, *Appl. Catal. B: Environ*., **3**, 295-318 (1994)

[29] M. C. Campa, S. D. Rossi, G. Ferraris, V. Indovina, *Appl. Catal. B: Environ*., **8**, 315-331 (1996)

[30] D. Kaucký, A. Vondrová, J. Dědeček, B. Wichterlová, *J. Catal*., **194**, 318-329 (2000)

[31] J. Dědeček, D. Kaucký, B. Wichterlová, *Micropor. Mesopor. Mater*., **35**, 483-494 (2000)

[32] X. Zhang, Q. Shen, C. He, C. Ma, Z. Liu, Z. Hao, *Chem. Eng. J*., **226**, 95-104 (2013)

[33] A. Boix, E. E. Miró, E. A. Lombardo, M. A. Bañares, R. Mariscal, J. L. G. Fierro, *J. Catal.*, **217**, 186-194 (2003)

[34] J. Dědeček, Z. Sobalik, B. Wichterlová, *Catal. Rev*., **54**, 135-223 (2012)

[35] M. Rutkowska, L. Chmielarz, M. Jabłońska, C. J. Oers, P. Cool, *J. Porous. Mater.*, **21**, 91-98 (2014)

[36] J. Ashok, S. N. Kumar, A. Venugopal, V. D. Kumari, M. Subrahmanyam, *J. Power*

Sources, **164**, 809-814 (2007)

[37] M. N. Uddin, W. M. A. W. Daud, H. F. Abbas, *Energy Convers. Manag*., **90**, 218-229 (2015)

[38] M. Inaba, K. Murata, M. Saito, I. Takahara, N. Mimura, *React. Kinet. Catal. Lett*., **77**, 109-115 (2002)

[39] T. Sano, K. Okabe, H. Hagiwara, H. Takaya, H. Shoji, K. Matsuzaki, *J. Mol. Catal*., **40**, 113-117 (1987)

[40] G. Qi, Q. Wang, J. Xu, J. Trébosc, O. Lafon, C. Wang, J. P. Amoureux, F. Deng, *Angew. Chem. Int. Ed*., **55**, 15826-15830 (2016)

[41] P. Gao, Q. Wang, J. Xu, G. Qi, C. Wang, X. Zhou, X. Zhao, N. Feng, X. Liu, F. Deng, *ACS Catal*., **8**, 69-74 (2018)

[42] M. Niwa, T. Noda, K. Suzuki, N. Morishita, N. Katada, *Micropor. Mesopor. Mater*., **146**, 208-215 (2011)

[43] S. Suganuma, K. Nakamura, A. Okuda, N. Katada, *Mol. Catal*., **435**, 110-117 (2017)

Chapter 3 Investigation of Reaction Mechanism on Co/MFI Catalyst for Methylation of Benzene with Methane by using in situ IR spectroscopy

3-1 Introduction

Natural gas, whose main component is methane, has been expected to be an alternative resource for energy and chemicals [1]. Since the energy for cleavage of C-H bond in methane is the largest among hydrocarbons [2], it has been believed that the conversion of methane into valued compounds is difficult. The activation of methane by catalysts is therefore demanded. Methylation of benzene with methane (1) has also been proposed for the use of methane as a part of valued chemical, because the produced toluene has multiple demands, e.g., para-xylene production via disproportionation.

$$CH_4 + C_6H_6 \rightarrow CH_3\text{-}C_6H_5 + H_2 \qquad (1)$$

We recently found that Co/MFI possessed marked activity for methylation of benzene with methane at 773 K compared with various combinations of metal elements and zeolites [3, 4].

We have reported that the atomic dispersion of Co^{2+} species on the ion exchange site of MFI zeolite ([Al] = 1.35 mol kg^{-1}) at Co / Al = 0.25 - 0.6 had high activity for the reaction (1) [3, 4]. We have also previously founded that even Co species on MFIs with different Al concentrations ([Al] = 0.4 – 1.0 mol kg^{-1}) exhibited catalytic activity [3]. However, the reaction mechanism of the methylation of benzene by methane on Co/MFI was not clear in our previous findings.

On the other hand, in situ FT-IR studies have recently been used as a means to elucidate the reaction mechanism for various reactions [5-10]. Saepurahman et al. clarified the reaction mechanism for methylation of benzene with methanol on H-MFI and H-BEA catalysts by examining the acid sites and products on catalysts during the reaction using in situ FT-IR [5]. Zheng et al. have used in situ FT-IR technique to elucidate the reaction mechanism for isomerization of xylene with surface-modified H-MFI, and investigated the relationship between the Brønsted acid sites and catalytic activity [6]. In addition, in situ IR has been used to investigate the reaction mechanisms of benzene

alkylation with propylene on MWW zeolite catalyst [7] and NH_3-SCR reaction catalyzed by Cu-CHA zeolites [8]. Kukulska-Zajac et al. reported that when C_6H_6 was adsorbed on Ag^+ and Cu^+ on zeolite, the d-electrons of the metal ion were π-back-donated to the π^* antibonding orbitals of C_6H_6, and thus the IR spectrum of adsorbed C_6H_6 shifted to lower wavenumber side than that of free C_6H_6 in the liquid phase [11, 12]. Archipov et al. also reported similar results on Cu/FAU and CuMFI [13, 14]. Therefore, C_6H_6 adsorbed on the metal on zeolite and free C_6H_6 (in gas or liquid phase) can be distinguished by in situ IR spectra.

With the above background, in this study, the reaction mechanism of the methylation of benzene with methane over Co/MFI catalyst was clarified by using in situ IR technique.

3-2 Experimental

3-2-1 Catalyst preparation

Na-MFI zeolite ([Al] = 0.6 mol kg^{-1}, SiO_2 / Al_2O_3 molar ratio = 52, provided by Mizusawa Industrial Chemicals, Ltd.) were converted to NH_4 form by the three times repetition of ion exchange with ammonium nitrate aqueous solution (NH_4 / Al = 1000%) at 343 K for 4 h.

Co/MFI were prepared by impregnation and ion exchange method. In the impregnation method, powder of 1 g of NH_4-MFI (SiO_2 / Al_2O_3 molar ratio = 52) was put into 100 mL of aqueous solution containing the cobalt nitrate (Co / Al molar ratio = 0.6), and the mixture was stirred at 343 K up to most of the solvent (water) was removed by vaporization. The yielded solid was further dried again at 383 K for 3 h in atmosphere. In this way, Co/MFI (52) was obtained. In the ion exchange method, powder of 1 g of NH_4-MFI zeolite ([Al] = 1.3 mol kg^{-1}, SiO_2 / Al_2O_3 molar ratio = 22, purchased from Tosoh Corp.) was put into 100 mL of aqueous solution containing the cobalt nitrate (Co / Al molar ratio = 2), and the mixture was stirred at 343 K for 4 h. The filtered solid was washed with ion exchanged water and filtered for three times, and dried at 383 K for 12 h in atmosphere. In this way, Co/MFI (22) was obtained. The Al and Co contents in the final solids of Co/MFI(22) were measured with an aid of ICP-OES, and the Co/Al ratio was 0.4.

3-2-2 in situ IR measurement

In the experiments with C_6H_6 and Ar flowing, followed by CH_4 or N_2 flow on Co/MFI samples, the sample wafer (15 mg, 1 cm diameter) was first attached in the IR cell which was installed in a MicrotracBEL IRMS-TPD analyzer, and flowed O_2 (1.23

mmol min^{-1}) in the atmospheric pressure at room temperature for 30 min. Then, the temperature of sample was raised to 823 K at 10 K min^{-1} and the sample was pretreated for 1 h. After the pre-treatment, the temperature was lowered to 773 K under O_2, and evacuated under vacuum for 10 min. Then, C_6H_6 was introduced into the system by bubbling liquid C_6H_6 at 273 K with Ar (1.23 mmol min^{-1}). Ar and vaporized C_6H_6 were flowed in the atmospheric pressure at 773 K for 30 min. Thereafter Ar and C_6H_6 were stopped, and at the same time CH_4 (1.23 mmol min^{-1}) or N_2 (1.23 mmol min^{-1}) was flowed alone in the atmospheric pressure at 773 K. The IR spectra were recorded under vacuum, C_6H_6 + Ar flow, CH_4 or N_2 flow. In each spectrum, the spectrum under vacuum was subtracted as background to cancel the spectrum derived from the MFI framework or daily errors (CO_2 and water vapor, etc.). The IR spectra were recorded with a FT/IR-4700 spectrometer (JASCO Corp.) quipped in an MCT detector. The IR spectrum was integrated 70 times. Spectral resolution was 4 cm^{-1}.

The blank experiment was measured without any sample in the cell, and the IR spectra of the free species in the gas phase were obtained. The spectrum of $C_6H_5CH_3$ was obtained in the same way as that of C_6H_6, by bubbling liquid $C_6H_5CH_3$ at 273 K with N_2 to introduce the vapor of $C_6H_5CH_3$.

3-3 Results and Discussion

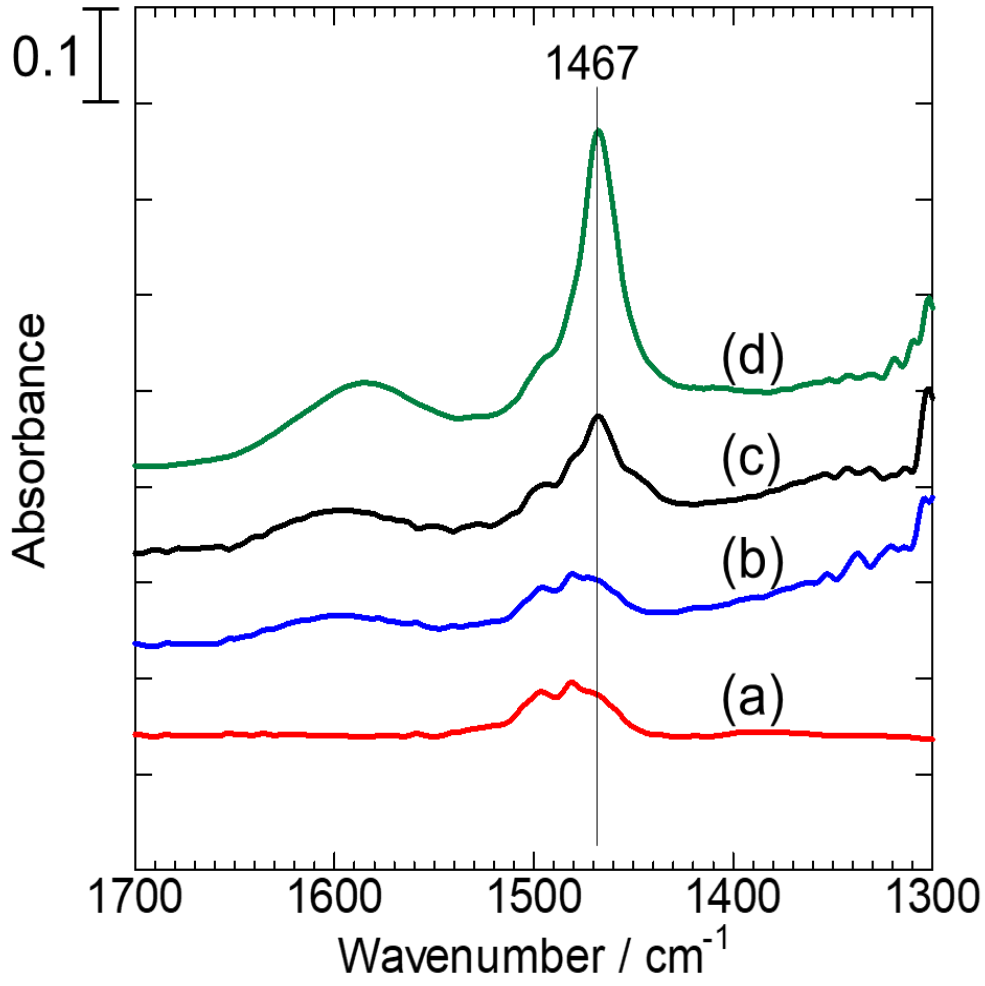

Figure 3-1. FT-IR spectra under C_6H_6 and Ar flowing (absorbance under C_6H_6 and Ar flow – absorbance under vacuum) (a) in the blank experiment at 753 K, (b) on H-MFI(52) at 753 K, (c) on Co/MFI(52) at 773 K and (d) on Co/MFI(22) at 773 K.

Figure 3-1 (a) shows the IR spectrum under gaseous C_6H_6 and Ar flowing (absorbance under C_6H_6 and Ar flow – absorbance under vacuum) in the blank experiment at 753 K. The broad peak around 1480 cm^{-1} was observed. This peak derived from the stretching vibration of the C-C ring of gaseous (free) C_6H_6, as reported in the past [11-14]. Figure 3-1 (b) shows the IR spectrum under gaseous C_6H_6 and Ar flowing (absorbance under C_6H_6 and Ar flow – absorbance under vacuum) on H-MFI(52) zeolite at 753 K. In the C-C stretching region (around 1480 cm^{-1}), there were no peaks other than free C_6H_6. Figure 3-1 (c) shows the IR spectrum under gaseous C_6H_6 and Ar flowing (absorbance under C_6H_6 and Ar flow – absorbance under vacuum) on Co/MFI(52) at 773 K. On Co/MFI(52), in addition to the broad peak at c.a. 1480 cm^{-1}, the relatively sharp peak at 1467 cm^{-1} was observed. Kukulska-Zajac et al. have previously reported that the IR spectra of C_6H_6 (C-C stretching vibration) adsorbed on Ag/MFI and Cu/MFI at 430 K were found at 1472 cm^{-1} and 1467 cm^{-1}, respectively [11, 12]. Archipov et al. have reported that the C-C stretch band of C_6H_6 adsorbed on Cu/HY at 298 K was observed at 1471 cm^{-1} [13]. The peak of C_6H_6 adsorbed on M/zeolite shifted to lower wavenumber side than that of gaseous (free) C_6H_6 (1480 cm^{-1}), which is thought to be due to π-back donation of d-electrons of the metal to the π^* antibonding orbitals of C_6H_6 [11, 12]. Based on the literatures, the peak at 1467 cm^{-1} in Figure 3-1 (c) was attributed to the C-C

stretching vibration of C_6H_6 adsorbed on Co/MFI(52). The 1467 cm^{-1}-peak was attributed to C_6H_6 adsorbed on the Co species (not the Brønsted acid site) on the MFI, since there was no peak at 1467 cm^{-1} on H-MFI(52) as shown in Figure 3-1 (b). Figure 3-1 (d) shows the IR spectrum under gaseous C_6H_6 and Ar flowing (absorbance under C_6H_6 and Ar flow – absorbance under vacuum) on Co/MFI(22) at 773 K. The sharp peak at 1467 cm^{-1} was observed on Co/MFI(22) as well as on Co/MFI(52) (Figure 3-1 (c)), indicating that C_6H_6 was also adsorbed on the Co species on MFI(22). Comparing Figure 3-1 (c) and (d), the absorbance of 1467 cm^{-1}-peak on Co/MFI(22) was higher than that on Co/MFI(52). This may be due to the higher amount of Al (i.e. ion exchange sites) on MFI(22) than on MFI(52), which results in a higher amount of Co species adsorbed on C_6H_6.

Figure 3-2 A (a) and B (a) show the IR spectrum under gaseous CH_4 flowing (absorbance under CH_4 flow – absorbance under vacuum) in the blank experiment at 753 K. The peaks at 1300 - 1400 cm^{-1} and 1540 cm^{-1} were found, which were attributed to C-H deformation bands of free CH_4 in the gas phase [15, 16]. Figure 3-2 A (b) and B (b) show the IR spectrum under gaseous $C_6H_5CH_3$ and N_2 flowing (absorbance under $C_6H_5CH_3$ and N_2 flow – absorbance under vacuum) on Co/MFI(52) at 753 K. The shoulder peak around 1500 cm^{-1} and the bands at 1480 cm^{-1} and 1440 cm^{-1} were observed. According to the previous paper, the shoulder peak around 1500 cm^{-1} was attributed to

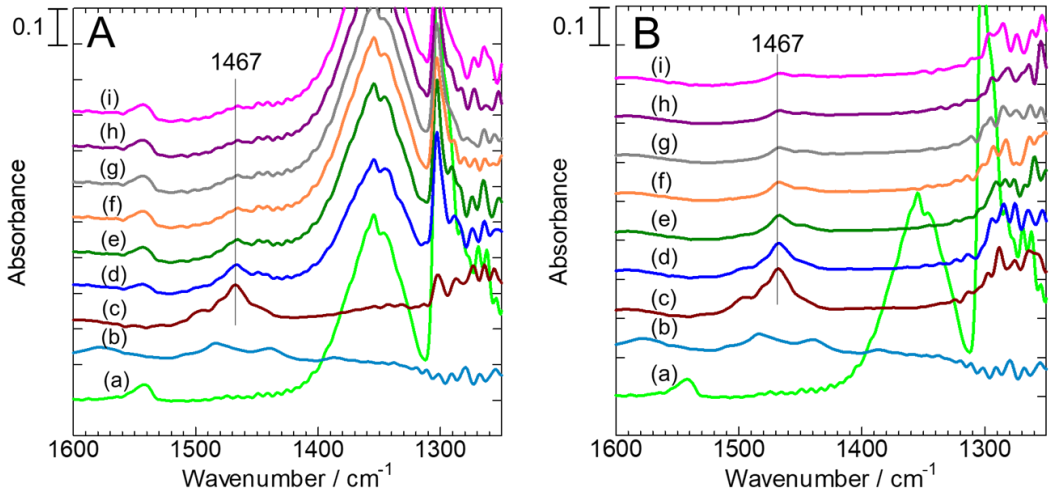

Figure 3-2 A. IR spectra under (a) CH_4 flowing (absorbance under CH_4 flow – absorbance under vacuum) in the blank experiment at 753 K, (b) $C_6H_5CH_3$ and N_2 flowing (absorbance under $C_6H_5CH_3$ and N_2 flow – absorbance under vacuum) on Co/MFI(52) at 753 K, (c) C_6H_6 and Ar flowing (absorbance under C_6H_6 and Ar flow – absorbance under vacuum) (d-i) after CH_4 (d) 1 min, (e) 2 min, (f) 3 min, (g) 4 min, (h) 5 min and (i) 6 min flowing (absorbance under CH_4 flow – absorbance under vacuum) on Co/MFI(52) at 773 K.

B. IR spectra under (a) CH_4 flowing (absorbance under CH_4 flow – absorbance under vacuum) in the blank experiment at 753 K, (b) $C_6H_5CH_3$ and N_2 flowing (absorbance under $C_6H_5CH_3$ and N_2 flow – absorbance under vacuum) on Co/MFI(52) at 753 K, (c) C_6H_6 and Ar flowing (absorbance under C_6H_6 and Ar flow – absorbance under vacuum) (d-i) after N_2 (d) 1 min, (e) 2 min, (f) 3 min, (g) 4 min, (h) 5 min and (i) 6 min flowing (absorbance under N_2 flow – absorbance under vacuum) on Co/MFI(52) at 773 K.

the C-C stretching vibration of $C_6H_5CH_3$ in the gas phase [17], and the peak at 1480 cm^{-1} was derived from $C_6H_5CH_3$ (C-C stretching) adsorbed on Co/MFI [17-19]. The band at 1440 cm^{-1} was attributed to $C_6H_5CH_3$ (C-C stretching vibration) in the gas phase or adsorbed on Co/MFI [17, 20].

Figure 3-2 A (c-i) show the IR spectra of C_6H_6 and Ar flowing, followed by C_6H_6 and Ar stopping, and simultaneously flowing CH_4 on Co/MFI(52) at 773 K. (c) is the IR spectrum under C_6H_6 + Ar flow (absorbance under C_6H_6 and Ar flow – absorbance under vacuum), and (d-i) are the IR spectra under CH_4 1 - 6 min flow (absorbance under CH_4 flow – absorbance under vacuum). After the flow of CH_4, the peaks originating from C_6H_6 in the gas phase (1480 cm^{-1}) and C_6H_6 adsorbed on Co species on MFI (1467 cm^{-1}) decreased, and the peaks attributed to CH_4 in the gas phase (1300 - 1400 and 1540 cm^{-1}) increased. There were no peaks derived from $C_6H_5CH_3$ (1440, 1480 and 1500 cm^{-1}) formed by the reaction of C_6H_6 and CH_4. The IR spectra of the experiments performed by replacing CH_4 with N_2 are shown in Figure 3-2 B (c-i). Even when N_2 was flowed instead of CH_4, the peak at 1467 cm^{-1} decreased. Therefore, it was found that C_6H_6 adsorbed on Co/MFI was desorbed even when only N_2 was flowed. Figure 3-3 A shows the IR spectra of C_6H_6 desorbed (absorbance under CH_4 1-6 min flow - absorbance under C_6H_6 and Ar flow) from Co/MFI(52) by CH_4 1 – 6 min flow at 773 K, and Figure 3-3 B shows the IR spectra of C_6H_6 desorbed (absorbance under N_2 1-6 min flow - absorbance under C_6H_6 and Ar flow) from Co/MFI(52) by N_2 1 – 6 min flow at 773 K. Comparing Figure 3-3 A and B, it can be seen that the decrease rate of the peak at 1467 cm^{-1} was faster in the CH_4 flow (A), which means that the desorption of C_6H_6 adsorbed on Co/MFI was faster. In

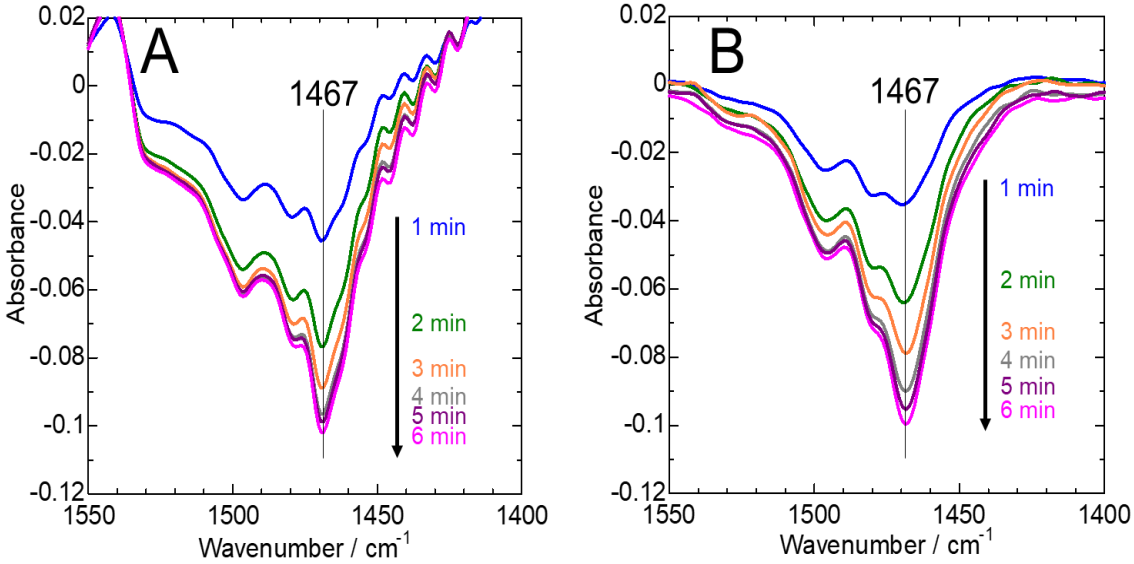

Figure 3-3 A. IR spectra of C_6H_6 desorbed (absorbance under CH_4 1-6 min flow - absorbance under C_6H_6 and Ar flow) from Co/MFI(52) by CH_4 1 – 6 min flow at 773 K. B. IR spectra of C_6H_6 desorbed (absorbance under N_2 1-6 min flow - absorbance under C_6H_6 and Ar flow) from Co/MFI(52) by N_2 1 - 6 min flow at 773 K,

addition, the desorption of C_6H_6 in the CH_4 flowing ended after about 4 min, whereas in the N_2 stream, the desorption was clearly observed even 5 - 6 min. This is thought to be due to the reaction of C_6H_6 adsorbed on Co/MFI with CH_4, resulting in faster desorption of C_6H_6 than under N_2 flow. Figure 3-4 (c-h) show IR difference spectra of Figure 3-2 A (d-i) and B (d-i) ((absorbance under CH_4 flow – absorbance under vacuum) – (absorbance under N_2 flow – absorbance under vacuum)). From Figure 3-4 (c)-(e), negative peaks around 1467 cm^{-1} were observed. This indicates that the desorption of C_6H_6 species

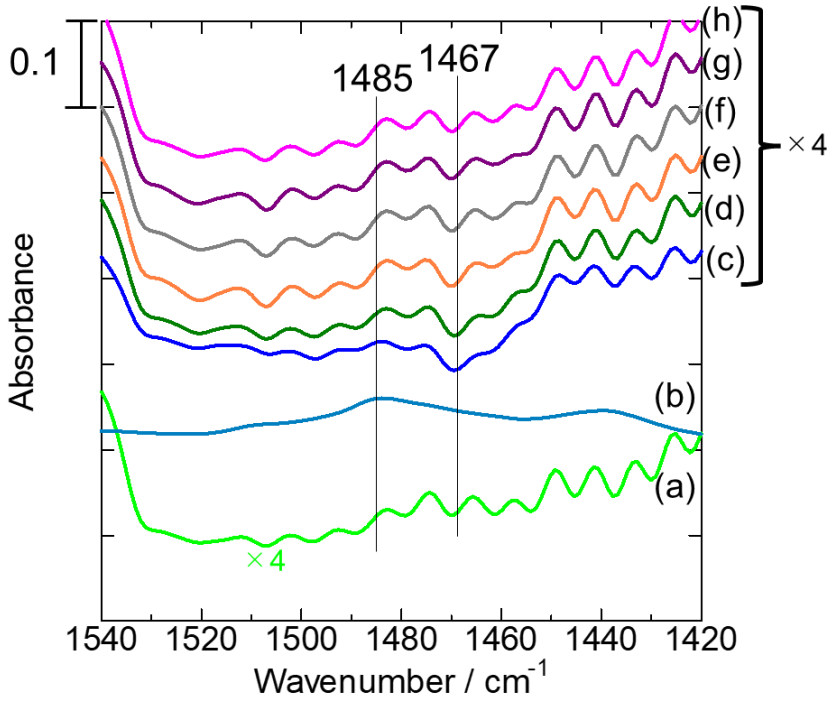

Figure 3-4. IR spectra under (a) CH_4 flowing (absorbance under CH_4 flow – absorbance under vacuum) in the blank experiment at 753 K, (b) $C_6H_5CH_3$ and N_2 flowing (absorbance under $C_6H_5CH_3$ and N_2 flow – absorbance under vacuum) on Co/MFI(52) at 753 K, (c-h) IR difference spectra of Figure 3-2 A (d-i) and Figure 3-2 B (d-i) ((absorbance under CH_4 flow – absorbance under vacuum) – (absorbance under N_2 flow – absorbance under vacuum)).

adsorbed on Co/MFI was faster in CH_4 1 - 3 min flow than in N_2 1 - 3 min flow as shown in Figure 3-3. Although there was no clear toluene-derived peak, there seemed to be a positive peak at 1485 cm^{-1} in Figure 3-4 (c) with a trace amount of toluene, indicating that toluene may have been formed after 1 min of CH_4 flowing.

The same experiment was conducted by replacing the catalyst with Co/MFI (22) as shown in Figure 3-5 A and B. Figure 3-5 A (c) is the IR spectrum under C_6H_6 + Ar flow

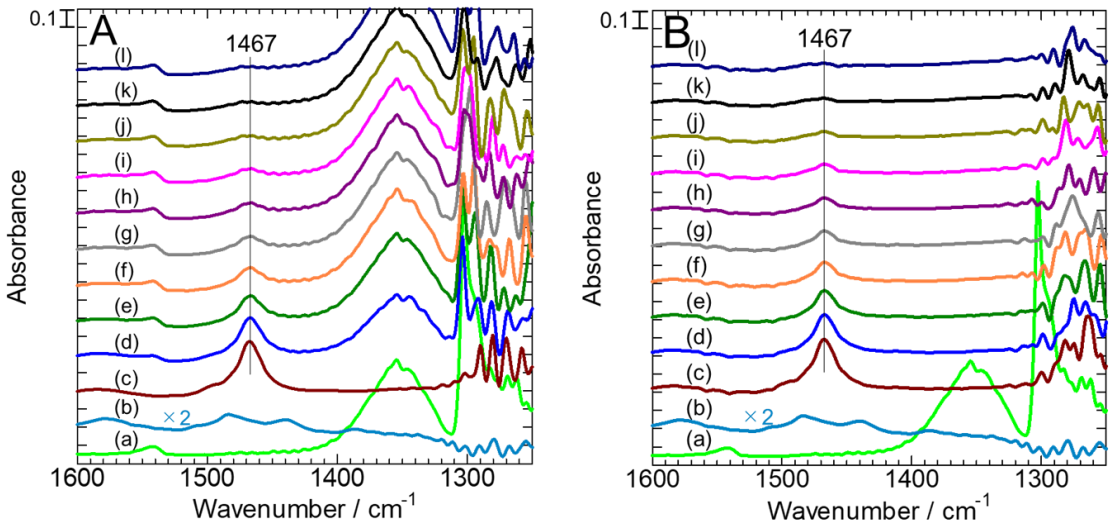

Figure 3-5 A. IR spectra under (a) CH_4 flowing (absorbance under CH_4 flow – absorbance under vacuum) in the blank experiment at 753 K, (b) $C_6H_5CH_3$ and N_2 flowing (absorbance under $C_6H_5CH_3$ and N_2 flow – absorbance under vacuum) on Co/MFI(52) at 753 K, (c) C_6H_6 and Ar flowing (absorbance under C_6H_6 and Ar flow – absorbance under vacuum) (d-l) after CH_4 (d) 1 min, (e) 2 min, (f) 3 min, (g) 4 min, (h) 5 min, (i) 6 min, (j) 10 min, (k) 20 min and (l) 30 min flowing (absorbance under CH_4 flow – absorbance under vacuum) on Co/MFI(22) at 773 K.

B. IR spectra under (a) CH_4 flowing in the blank experiment at 753 K, (b) $C_6H_5CH_3$ and N_2 flowing (absorbance under $C_6H_5CH_3$ and N_2 flow – absorbance under vacuum) on Co/MFI(52) at 753 K, (c) C_6H_6 and Ar flowing (absorbance under C_6H_6 and Ar flow – absorbance under vacuum) (d-i) after N_2 (d) 1 min, (e) 2 min, (f) 3 min, (g) 4 min, (h) 5 min and (i) 6 min , (j) 10 min, (k) 20 min and (l) 30 min flowing (absorbance under N_2 flow – absorbance under vacuum) on Co/MFI(22) at 773 K.

(absorbance under C_6H_6 and Ar flow – absorbance under vacuum), and (d-l) are the IR spectra under CH_4 1 - 30 min flow (absorbance under CH_4 flow – absorbance under vacuum) on Co/MFI(22) at 773 K. After the flow of CH_4, the peaks originating from C_6H_6 in the gas phase (1480 cm^{-1}) and C_6H_6 adsorbed on Co species on MFI (1467 cm^{-1})

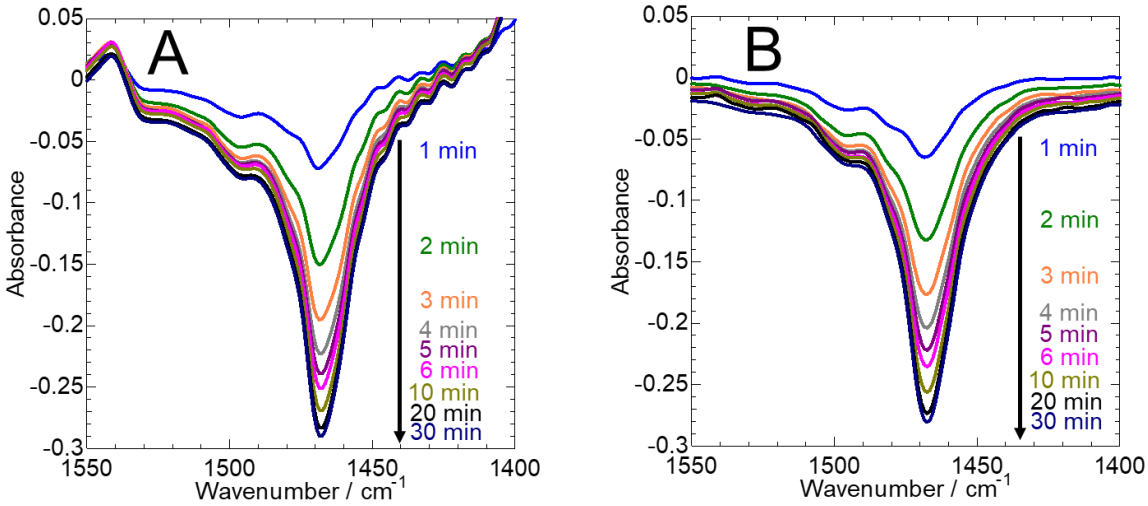

Figure 3-6 A. IR spectra of C_6H_6 desorbed (absorbance under CH_4 1-30 min flow - absorbance under C_6H_6 and Ar flow) from Co/MFI(22) by CH_4 1 – 30 min flow at 773 K. B. IR spectra of C_6H_6 desorbed (absorbance under N_2 1-30 min flow - absorbance under C_6H_6 and Ar flow) from Co/MFI(22) by N_2 1 - 30 min flow at 773 K,

decreased, and the peaks attributed to CH_4 in the gas phase (1300 - 1400 and 1540 cm^{-1}) increased as in the case of Co/MFI(52) (Figure 3-2 A (c-i)). There were no peaks derived from $C_6H_5CH_3$ (1440, 1480 and 1500 cm^{-1}) formed by the methylation of C_6H_6 with methane (Figure 3-5 A (d-l)). The IR spectra of the experiments performed by replacing CH_4 with N_2 on Co/MFI(22) are shown in Figure 3-5 B (c-l). After the flow of N_2, the peaks of free C_6H_6 in the gas phase (1480 cm^{-1}) and C_6H_6 adsorbed on Co species on MFI (1467 cm^{-1}) decreased. Figure 3-6 A shows the IR spectra of C_6H_6 desorbed (absorbance under CH_4 1-30 min flow - absorbance under C_6H_6 and Ar flow) from Co/MFI(22) by CH_4 1 – 30 min flow at 773 K, and Figure 3-6 B shows the IR spectra of C_6H_6 desorbed

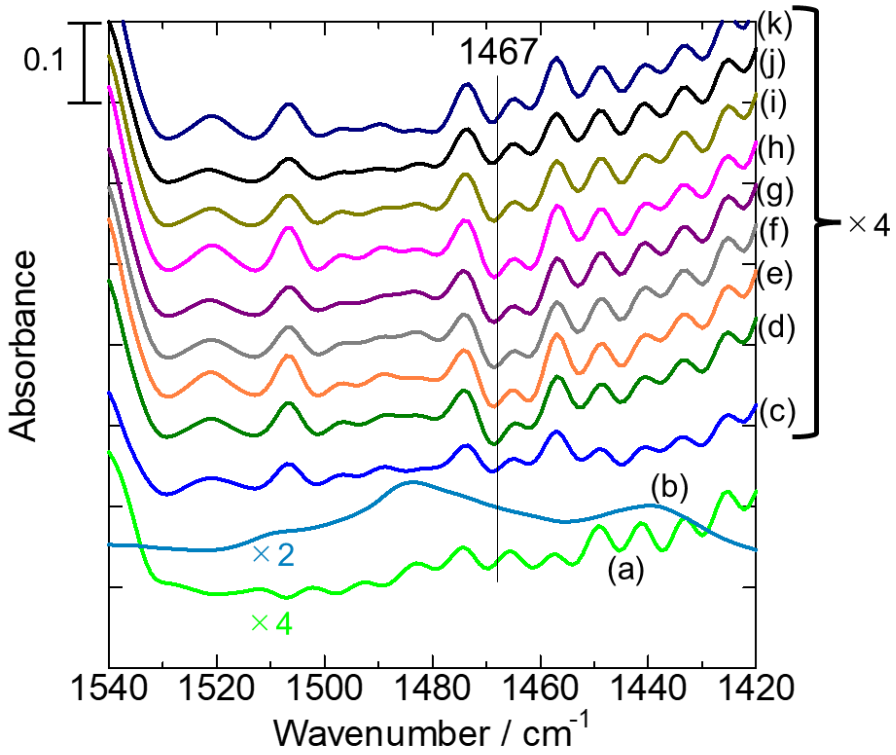

Figure 3-7. IR spectra under (a) CH_4 flowing (absorbance under CH_4 flow – absorbance under vacuum) in the blank experiment at 753 K, (b) $C_6H_5CH_3$ and N_2 flowing (absorbance under $C_6H_5CH_3$ and N_2 flow – absorbance under vacuum) on Co/MFI(52) at 753 K, (c-k) IR difference spectra of Figure 3-5 A (d-l) and Figure 3-5 B (d-l) ((absorbance under CH_4 flow – absorbance under vacuum) – (absorbance under N_2 flow – absorbance under vacuum)).

(absorbance under N_2 1-30 min flow - absorbance under C_6H_6 and Ar flow) from Co/MFI(22) by N_2 1 – 30 min flow at 773 K. Comparing Figure 3-6 A and B, although not as different as in Co/MFI(52) (Figure 3-3 A and B), the desorption of C_6H_6 was found to be faster in the CH_4 flow than in the N_2 flowing. Figure 3-7 (c-k) show IR difference spectra of Figure 3-5 A (d-l) and 3-5 B (d-l) ((absorbance under CH_4 flow – absorbance under vacuum) – (absorbance under N_2 flow – absorbance under vacuum)). From Figure

3-7 (d-i), negative peaks around 1467 cm^{-1} were observed in about 2 - 10 min of gas (CH_4 or N_2) flow. On Co/MFI (22), the reaction between benzene and methane proceeded under CH_4 circulation, and the desorption rate of adsorbed species of C_6H_6 was faster than that under N_2 flow similar to Co/MFI(52). However, no positive peak derived from $C_6H_5CH_3$ (1440, 1480 and 1500 cm^{-1}) was observed.

From the above experimental results, it was found that C_6H_6 species adsorbed on Co species on MFI when C_6H_6 was introduced on Co/MFI. The electronic state of C_6H_6 adsorbed on Co species changed compared with that of (free) C_6H_6 in the gas phase. In the experiments in which C_6H_6 was flowed, followed by flowing of CH_4 or N_2, the desorption rate of C_6H_6 adsorbed on Co species on MFI was faster with CH_4 than with N_2. This indicates that the C_6H_6 previously adsorbed on the Co species on the MFI reacted with CH_4, and the methylation of C_6H_6 proceeded.

3-4 Conclusions

From the in situ IR spectra, it was found that C_6H_6 was adsorbed on the Co species on MFI by the introduction of C_6H_6 into Co/MFI. The electronic state of C_6H_6 adsorbed on Co species differed compared with that of free C_6H_6 in the gas phase. It was suggested that the C_6H_6 adsorbed on the Co species on MFI reacted with CH_4 and the methylation

of C_6H_6 proceeded.

Acknowledgements

This study was partly supported by JST CREST Grant Number JPMJCR17P1, Japan.

References

[1] M. Ravi, M. Ranocchiari, J. A. Bokhoven, *Angew. Chem. Int. Ed*., **56**, 16464-16483 (2017)

[2] A. E. Shilov, G. B. Shul'pin, *Chem. Rev*., **97**, 2879-2932 (1997)

[3] K. Nakamura, A. Okuda, K. Ohta, H. Matsubara, K. Okumura, K. Yamamoto, R. Itagaki, S. Suganuma, E. Tsuji, N. Katada, *ChemCatChem*, **10**, 3806-3812 (2018)

[4] H. Matsubara, E. Tsuji, Y. Moriwaki, K. Okumura, K. Yamamoto, K. Nakamura, S. Suganuma, N. Katada, *Catal. Lett*., **149**, 2627-2635 (2019)

[5] Saepurahman, M. Visur, U. Olsbye, M. Bjørgen, S. Svelle, *Top. Catal*., **54**, 1293-1301 (2011)

[6] S. Zheng, A. Jentys, J. A. Lercher, *J. Catal*., **241**, 304-311 (2006)

[7] J. Fu, C. Ding, *Catal. Commun*., **6**, 770-776 (2005)

[8] H. Kubota, C. Liu, T. Amada, K. Kon, T. Toyao, Z. Maeno, K. Ueda, A. Satsuma, N.

Tsunoji, T. Sano, K. Shimizu, *Catal. Today*, **376**, 73-80 (2021)

[9] A. Westermann, B. Azambre, M. C. Bacariza, I. Graca, M. F. Ribeiro, J. M. Lopes, C. Hanriques, *Appl. Catal. B: Environ*., **174**, 120-125 (2015)

[10] A. Satsuma, K. Shimizu, *Prog. Energy Combust. Sci*., **29**, 71-84 (2003)

[11] E. Kukulska-Zajac, P. Kozyra, J. Datka, *Appl. Catal. A: Gen*., **307**, 46-50 (2006)

[12] E. Kukulska-Zajac, J. Datka, *Micropor. Mesopor. Mater*., **109**, 49-57 (2008)

[13] T. Archipov, S. Santra, A. B. Ene, H. Stoll, G. Rauhut, E. Roduner, *J. Phys. Chem. C*, **113**, 4107-4116 (2009)

[14] A. B. Ene, T. Archipov, E. Roduner, *J. Phys. Chem. C*, **114**, 14571-14578 (2010)

[15] J. Wu, S. Li, G. Li, C. Li, Q. Xin, *Appl. Surf. Sci*., **81**, 37-41 (1994)

[16] C. Li, W. Yan, Q. Xin, *Catal. Lett*., **24**, 249-256 (1994)

[17] R. M. Serra, E. E. Miró, A. V. Boix, *Micropor. Mesopor. Mater*., **127**, 182-189 (2010)

[18] Y. Shi, X. Yang, F. Tian, C. Jia, Y. Chen, *J. Nat. Gas Chem*., **21**, 421-425 (2012)

[19] Z. Zhang, X. Yuan, S. Miao, H. Li, W. Shan, M. Jia, C. Zhang, *Catalysts*, **9**, 829 (2019)

[20] M. A. Larrubia, G. Busca, *Appl. Catal. B: Environ*., **39**, 343-352 (2002)

Chapter 4 Position and Lewis Acidic Property of Active Cobalt Species on MFI Zeolite for Catalytic Methylation of Benzene with Methane

4-1 Introduction

Natural gas, whose main component is methane, has been expected to be an alternative resource for energy and chemicals [1]. Since the energy for cleavage of C-H bond in methane is the largest among hydrocarbons [2], it has been believed that the conversion of methane into valued compounds is difficult. The activation of methane by catalysts is therefore demanded. As a typical expected use of methane, much attention has been drawn to the reactions of methane into methanol [3, 4] and aromatic hydrocarbons [5]. However, the former reaction has low selectivity, or low energy efficiency, and the latter reaction has disadvantage due to a side reaction into carbonaceous resulting in the quick deactivation of catalyst. Up to now, these problems have obstructed the effective use of methane.

On the other hand, methylation of benzene with methane (1) has also been proposed for the use of methane as a part of valued chemical, because the produced toluene has multiple demands, e.g., para-xylene production via disproportionation.

$$CH_4 + C_6H_6 \rightarrow CH_3\text{-}C_6H_5 + H_2 \quad (1)$$

The preceding studies showed the activities for this reaction of some zeolite-based catalysts as H-*BEA, Cu/*BEA [6], Ag/MFI [7], Pt/MFI [8] and In/MFI [9]. We recently found that Co/MFI possessed marked activity for this reaction at 773 K compared with various combinations of metal elements and zeolites [10, 11].

We have reported that the atomic dispersion of Co^{2+} species on the ion exchange site of MFI zeolite ([Al] = 1.35 mol kg^{-1}) at Co_{zeo}/Al_{zeo} = 0.25-0.6 had high activity for the reaction (1) [10]. The low activity at Co_{zeo}/Al_{zeo} > 0.6 was ascribed to the cobalt oxide aggregate formation. In addition, even in the region of Co_{zeo}/Al_{zeo} < 0.6 where most cobalt species were mono-atomically dispersed, at least two types of cobalt species; active and inactive ones were found at Co_{zeo}/Al_{zeo} > 0.25 and Co_{zeo}/Al_{zeo} < 0.25, respectively [11]. Furthermore, even in the low Co_{zeo}/Al_{zeo} region, co-presence of typical divalent elements such as Mg, Zn, Pb and Ca during the Co loading process was found to enhance the catalytic activity. Dependence of the activity on the Co loading was complicated, suggesting the presence of Co species with different activities. Identification of these species will

contribute to the design of catalyst with high performance. Analysis of local structure and chemical nature of Co species in these regions with and without second element should tell us important information for the nature of active Co species.

The difference in the local structure of active and inactive Co species is analyzed by the ultraviolet-visible (UV-vis) spectroscopy in this study as follows. According to Dědeček et al. [12, 13], ion exchange sites for divalent cations on a zeolite are classified into three types (α, β and γ sites) based on the coordination environment as shown in Figure 4-1. On MFI, it is proposed that the α site is located on the wall of 10-ring straight channel, the β site is located in 6-ring close to the intersection of straight and sinusoidal 10-ring channels, and the γ site is located on the pocket-like wall of sinusoidal channel

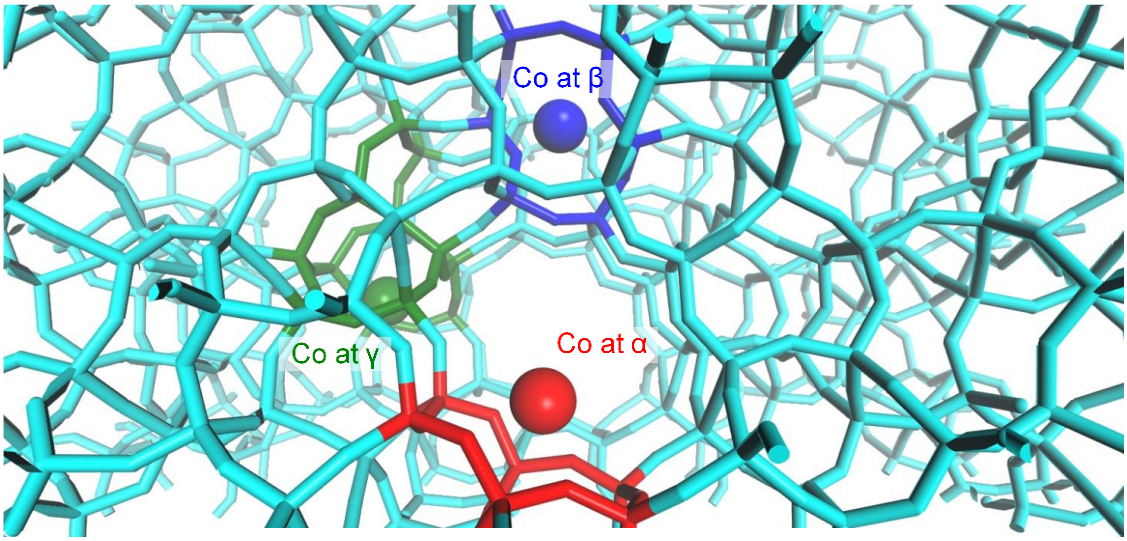

Figure 4-1. Positions of Co species in MFI structure.

[12], based on distribution of the Al atoms at crystallographically non-equivalent positions [14]. These principles are applied to the present Co/MFI and Co+second metal(M)/MFI zeolites to relate the structure and state of Co species with the catalytic activity for the methylation of benzene with methane.

We have developed an ammonia infrared-mass spectroscopy temperature-programmed desorption (IRMS-TPD) method to quantitative analysis of number and strength (molar standard enthalpy of desorption of ammonia, hereafter ΔH) of Brønsted and Lewis acid sites on a solid [15]. In our previous study, we have reported Lewis acidic nature of Co loaded on MFI [10]. Other researchers have also reported Co species on MFI showed Lewis acidity [16, 17]. Then, in this study, we investigate the Lewis acidic nature of Co/MFI and Co+M/MFI catalysts to unveil the relationship among the position, electron-withdrawing nature and catalytic activity of Co^{2+} on MFI zeolite. We will propose structural and chemical features of the MFI zeolite-supported Co species which possesses the catalytic activity for methylation of benzene with methane in this paper.

4-2 Experimental

4-2-1 Catalyst preparation

Table 4-1. Chemical compositions of samples

Sample	Composition of zeolite / nitrate solution mixture for ion exchange				Composition of final solid				
	$[Co]_{sol}$	$[M]_{sol}$	Co_{sol}/Al_{zeo}	M_{sol}/Al_{zeo}	$[Al]_{zeo}$	$[Co]_{zeo}$	$[M]_{zeo}$	Co_{zeo}/Al_{zeo}	M_{zeo}/Al_{zeo}
	/ mol L_{sol}^{-1}		molar ratio		/ mol $kg_{dry\ cat}^{-1}$			molar ratio	
Co-0.085	1.2×10^{-3}	0	0.1	0	1.50	0.13		0.085	
Co-0.16	2.3×10^{-3}	0	0.2	0	1.44	0.23		0.16	
Co-0.26	3.5×10^{-3}	0	0.3	0	1.25	0.33		0.26	
Co-0.28	4.7×10^{-3}	0	0.4	0	1.45	0.41		0.28	
Co-0.39	1.2×10^{-2}	0	1	0	1.43	0.56		0.39	
Co-0.42	2.3×10^{-2}	0	2	0	1.43	0.60		0.42	
Co-0.48	0.23	0	20*	0	1.40	0.67		0.48	
Mg-0.19	0	2.3×10^{-3}	0	0.2	1.47		0.29		0.19
Cu-0.34	0	2.3×10^{-2}	0	2	1.30		0.44		0.34
Pb-0.48	0	2.3×10^{-2}	0	2	1.18		0.56		0.48
Co-0.24+Mg-0.22	2.3×10^{-2}	2.3×10^{-2}	2	2	1.20	0.29	0.27	0.24	0.22
Co-0.28+Cu-0.14	2.3×10^{-2}	2.3×10^{-2}	2	2	1.29	0.36	0.18	0.28	0.14
Co-0.15+Pb-0.28	2.3×10^{-2}	2.3×10^{-2}	2	2	1.30	0.20	0.36	0.15	0.28

*: Three times repetition of ion exchange using solutions with Co 20 times more than Al in the used zeolite.

Samples of Co/MFI were prepared by an ion exchange method. Powder of 1 g of NH_4-MFI zeolite with [Al] = 1.35 mol kg^{-1} (SiO_2/Al_2O_3 = 22.1, Tosoh Corporation) was put into 100 mL of aqueous solution containing the desired amount of cobalt nitrate (Co_{sol}/Al_{zeo} molar ratio = 0.1, 0.2, 0.3, 0.4, 1, 2 and 20) as shown in Table 4-1, and the mixture was stirred at 343 K for 4 h. The filtered solid was washed with ion exchanged water and filtered for three times, and dried at 383 K for 12 h in atmosphere. Some samples were prepared by reverse ion exchange with ammonium nitrate from Co/MFI

with Co_{zeo}/Al_{zeo} = 0.48 in the final solid which had been prepared by the three times repetition of the ion exchange using excess of Co. On the other hand, the Co+M/MFI (M = Mg, Cu or Pb) samples were prepared by an ion exchange method using mixed aqueous solutions of Co+Mg, Co+Cu or Co+Pb nitrates at fixed molar ratios of Co_{sol}/Al_{zeo} = M_{sol}/Al_{zeo} = 2.0. As references, M/MFI samples were also prepared by ion exchange on NH_4-MFI with a solution of second metal nitrate (Mg_{sol}/Al_{zeo} = 0.2, Cu_{sol}/Al_{zeo} = 2.0, Pb_{sol}/Al_{zeo} = 2.0).

The Al, Co, Mg, Cu and Pb contents in the final solids of all the above samples were measured with an aid of inductively coupled plasma optical emission spectroscopy (ICP-OES, Rigaku Spectro Ciros CCD and Agilent 5110 ICP-OES) as shown in Table 4-1. Hereafter, Co/MFI, M/MFI and Co+M/MFI catalysts are denoted as Co-*X*, M-*Y* and Co-*X*+M-*Y* (*X* and *Y* show the Co_{zeo}/Al_{zeo} and M_{zeo}/Al_{zeo} molar ratios, in the final solid), respectively.

4-2-2 XRD analysis

XRD patterns was measured using an Ultima IV diffractometer (Rigaku) with a Cu Kα X-ray source operated at 40 kV of the voltage and 40 mA of the current.

4-2-3 UV-vis spectroscopy

The position of Co species was investigated with a UV-vis spectrometer (JASCO V550) using an in-situ diffuse reflectance cell at 773 K in N_2 flow with barium sulfate as a reference compound.

Here it is noteworthy that the pretreatment of catalytic reaction was carried out at 823 K as shown later, but that for UV-vis analysis was performed at 773 K. The Co/MFI was prepared from a Co salt in which the oxidation state of Co was +II, and we have reported that the oxidation state of Co species on the ion exchange site of MFI was principally kept to be +II even in a flow of methane/benzene in the reaction conditions. In addition, most of Co was evidenced to have mono-atomic dispersion [10]. Therefore, it is assumed that the oxidation state was kept at +II, and mono-atomic Co species (namely, Co^{2+}) was strongly held by the ion exchange site below 823 K. On the other hand, the purpose of pretreatment of UV-vis is to remove water which perturbates the spectrum. We selected 773 K as the pretreatment temperature for UV-vis measurements due to the limit of equipment. We believe it sufficient to remove water, and also the oxidation state and location of Co are believed to be kept as those in the catalytic reaction.

The absorption intensity was calculated from the Schuster-Kubelka-Munk equation

Table 4-2. UV-vis spectral components of the Co^{2+} ions in Co/MFI

Component	Wavenumber / cm^{-1}			
α	15128±46			
β	16002±26	17109±30	18695±10	21081±36
γ	20059±22	22011±42		

$F(R_\infty) = (1-R_\infty)^2/2R_\infty$, where R_∞ was a diffuse reflectance from a semi-infinite layer, and $F(R_\infty)$ was assumed to be proportional to the absorbance. The thus obtained K-M spectrum of Co^{2+} d-d transition region (13000 - 25000 cm^{-1}) was deconvoluted into seven components of the α, β and γ sites according to Dědeček et al [12]. The assumed UV-vis spectral components are shown in Table 4-2. Quantification of Co^{2+} at different sites was carried out as described in the following section from the comparison of UV-vis band intensities and ICP-AES analysis.

4-2-4 Ion exchange isotherm

In order to show the thermodynamic stability of cations at different sites, ion exchange isotherm was calculated [18-20]. Here the reaction formula of ion exchange from NH_4-form zeolite into Co-form is assumed as (2), where Co plays as a role of divalent cation.

$$NH_4 - Z + \frac{1}{2}Co^{2+}(aq) \rightarrow Co_{\frac{1}{2}} - Z + NH_4{}^{+}(aq) \qquad (2)$$

where –Z and (aq) show the states in zeolite and solution, respectively. The molar fractions of Co^{2+} among total cations in the solution (X_{sol}) and zeolite (Y_{zeo}) phases under the equilibrium state are calculated by (3) and (4), respectively, on the assumption that the number of ion exchange site was equal to the number of Al atoms.

$$X_{sol} = \frac{2[Co]_{aq}}{2[Co]_{aq} + [NH_4]_{aq}} \qquad (3)$$

$$Y_{zeo} = \frac{2[Co]_{zeo}}{[Al]_{zeo}} \qquad (4)$$

where the subscripts "aq" and "zeo" show the molar concentrations of discussed species in the solution (mol dm^{-3}) and zeolite (mol kg^{-1}), respectively, at the equilibrium. The values of $[Al]_{zeo}$ and $[Co]_{zeo}$ were experimentally determined by ICP-AES. The others are calculated as follows.

$$[\mathrm{Co}]_{\mathrm{aq}} = [\mathrm{Co}]_{\mathrm{aq},0} + \frac{W\left([\mathrm{Co}]_{\mathrm{zeo},0} - [\mathrm{Co}]_{\mathrm{zeo}}\right)}{V} \qquad (5)$$

$$[\mathrm{NH_4}]_{\mathrm{aq}} = [\mathrm{NH_4}]_{\mathrm{aq},0} + \frac{W\left([\mathrm{Al}]_{\mathrm{zeo},0} - 2[\mathrm{Co}]_{\mathrm{zeo},0} - [\mathrm{Al}]_{\mathrm{zeo}} + 2[\mathrm{Co}]_{\mathrm{zeo}}\right)}{V} \qquad (6)$$

where the subscripts "aq,0" and "zeo,0" show the molar concentrations of discussed species in the solution (mol dm^{-3}) and zeolite (mol kg^{-1}), respectively, before the ion exchange, while W and V show the weight of employed zeolite and the volume of solution, respectively. The concentrations $[Co]_{aq,0}$ and $[NH_4]_{aq,0}$ were calculated from the amounts of employed Co^{2+} and NH_4^+ nitrates, whereas $[Al]_{zeo,0}$ and $[Co]_{zeo,0}$ were measured by ICP-AES; $[Al]_{zeo,0}$ and $[Al]_{zeo}$ were similar, because the ion exchange procedure hardly affected the framework composition, but both experimentally observed values were here used for the calculations.

The above Y_{zeo} shows the quantity of total Co on the zeolite normalized with the ion exchange capacity. The amounts of Co^{2+} at each site Y_x (x = α, β or γ) were calculated from (7).

$$Y_x = \frac{\left[\mathrm{Co}^{2+}\right]_x}{\left[\mathrm{Co}^{2+}\right]_{x,\mathrm{Co\text{-}0.48}}} \qquad (7)$$

where $[Co^{2+}]_x$ show the concentration of Co^{2+} at x site (x = α, β or γ), and $[Co^{2+}]_{x,Co\text{-}0.48}$ show those on the Co-0.48 sample, i.e, Co/MFI prepared by the repetition of ion exchange with excess of cobalt nitrate. Procedure for quantification of Co^{2+} at α, β and γ sites was carries out based on the experimental observation of UV-vis and ICP-AES as described in the following section.

Equilibrium constant of the ion exchange (2) is described as (8), where x shows α, β or γ.

$$K_x = \left(\frac{Y_x}{X_{\mathrm{sol}}}\right)\left(\frac{1-X_{\mathrm{sol}}}{1-Y_x}\right)^{\frac{1}{2}} \qquad (8)$$

Here we assume independent equilibrium constants for α, β or γ sites. Dědeček et al. found that preferential distribution of Co at these sites on MFI [12], indicating such a difference in the equilibrium parameter. We here study the dependence of Co distribution on the total composition on this assumption. The equilibrium constants were calculated by curve fitting of the simulated relationship between Y_x and X_{sol}, and the experimentally observed ion exchange isotherm.

4-2-5 Ammonia IRMS-TPD measurements

The quantitative analysis of Lewis and Brønsted acid sites was performed by an ammonia infrared-mass spectroscopy temperature-programmed desorption (IRMS-TPD) method, which had been developed by our group [15]. After the pre-treatment in N_2 at 823 K in an automatic analyzer (Microtrac-BEL IRMS-TPD) reference IR spectra were recorded with heating a sample wafer (7 mg, 1 cm diameter), in a He flow (82 μmol s^{-1}, 6 kPa) at 0.0333 K s^{-1} up to 823 K; one spectrum per 1 K interval. Then, NH_3 was adsorbed at 343 K, and the temperature was again elevated in a flow of He with recording IR spectra and NH_3 concentration at the outlet with an aid of a mass spectrometer.

4-2-6 Reaction tests

Catalytic methylation of benzene with methane was performed using a fixed-bed flow reactor shown in our previous report [11]. The catalyst (0.300 g) was placed in a Pyrex tube, and pretreated in a flow of N_2 (1.23 mmol min^{-1}) in the atmospheric pressure at 823 K for 1 h. Then, a mixture of CH_4 (99.9% from Iwatani Industrial Gases Corporation) and C_6H_6 vaporized from a liquid C_6H_6 (special grade, FUJIFILM Wako Pure Chemical Corporation) was fed to the catalyst bed (98.6 and 2.7 kPa, 1.2 and 0.033

mmol min^{-1}, respectively, corresponding to $W_{cat}/F_{benzene}$ = 147 g_{cat} h $mol_{benzene}^{-1}$) at 773 K. The outlet materials were trapped by hexane at 273 K with a known amount of 1,4-diisopropylbenzene as an internal standard compound and analyzed with a flame ionization detector-gas chromatograph (FID-GC, Shimadzu GC-2014).

4-3 Results

4-3-1 XRD analysis

XRD patterns of NH_4-MFI support and Co/MFI catalysts are shown in Figure 4-2. MFI framework structure did not change or collapse after Co^{2+} loading. In addition, since the XRD patterns of Co species on MFI were not detected, it was found that Co species were well dispersed.

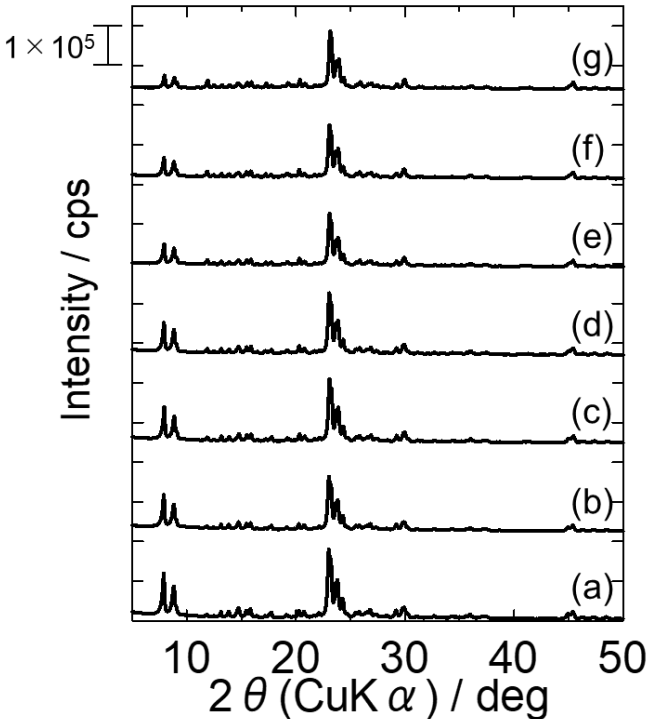

Figure 4-2. XRD patterns of (a) NH4-MFI and Co/MFI (Cozeo/Alzeo = (b) 0.047, (c) 0.12, (d) 0.16, (e) 0.27, (f) 0.32 and (g) 0.48).

4-3-2 Ion exchange isotherm of NH_4-MFI with Co^{2+}

Ion exchange isotherm is shown in Figure 4-3. In the region of low Co concentration of solution ($X_{sol} < 0.2$), the Co concentration on zeolite (Y_{zeo}) rapidly increased up to ca. 0.6 with increasing X_{sol}. Then Y_{zeo} gradually increased up to ca.

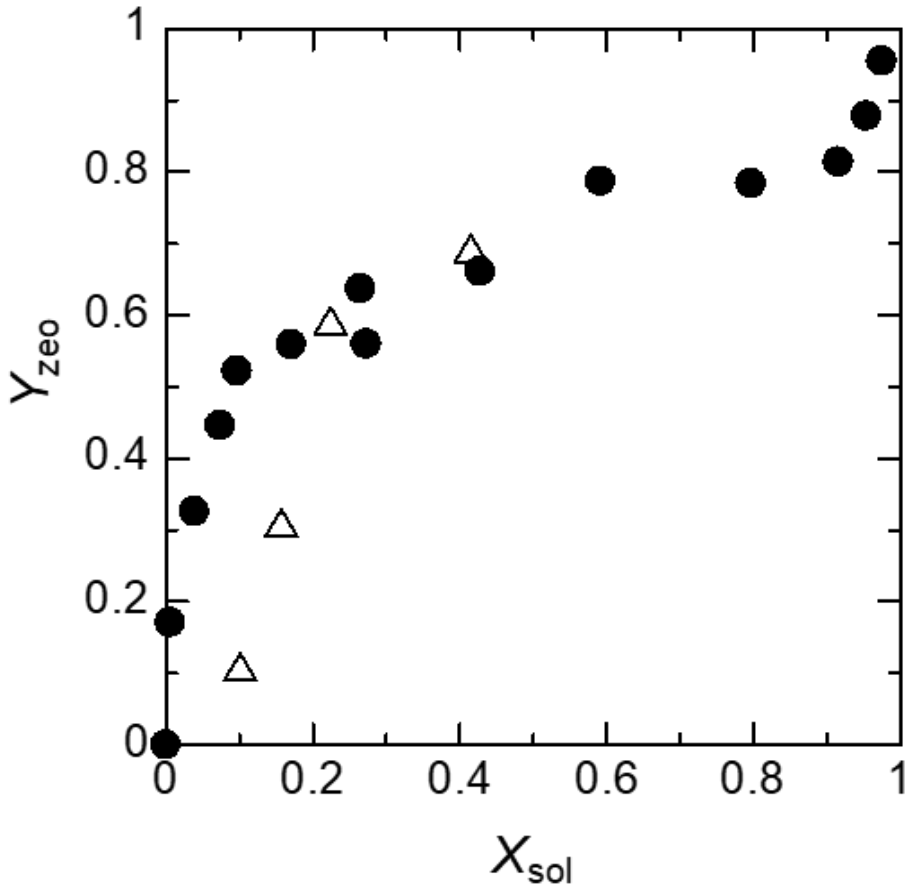

Figure 4-3. Ion exchange isotherm of NH_4^+ on MFI with Co^{2+} (filled circle) and Co^{2+} on MFI with NH_4^+ (triangle).

1, where Co ions occupied almost a half of ion exchange sites. Repetition of ion exchange using excess of cobalt nitrate (molar ratio of Co put into the employed solution/Al in the employed zeolite = 20) gave ca. 0.5 (exactly 0.48) of the Co/Al molar ratio in the final solid (Co_{zeo}/Al_{zeo}) as shown in Table 4-1, telling us that one Co^{2+} cation occupied two ion exchange sites. We have reported that the ammonia IRMS-TPD evidenced the loss of one Brønsted acid sites with ca. 0.5 of Co cation loading, and EXAFS exhibited the mono-atomic dispersion of Co^{2+} species in this Co concentration region [10], supporting that the ion exchange proceeded between NH_4^+ and Co^{2+} but not with such a mono valent species as $Co(OH)^+$. In addition, Figure 4-3 shows the relationship between Y_{zeo} and X_{sol} observed during the reverse ion exchange from the Co-form MFI with ammonium nitrate solution. From the start (X_{sol} = Y_{zeo} = 1) to the region where a considerable amount of Co was exchanged with NH_4 (X_{sol} = ca. 0.2, Y_{zeo} = 0.6), the relationship between Y_{zeo} and X_{sol} was similar to that observed during the ion exchange from the NH_4-form MFI with Co nitrate solution. This indicates that the ion exchange behavior was predominantly according to the equilibrium but less affected by kinetics (diffusion rate of ion in pores).

Equilibrium constant of the exchange from NH_4-form into Co-form was generally high than unity, indicating that one Co^{2+} cation possessed lower standard Gibbs energy (higher thermodynamic stability) than a pair of NH_4^+ at all kinds of the site. It is speculated that the volume of one Co^{2+} cation was smaller than that of a pair of NH_4^+ cations (or any other mono valent cations). Holding of a cation by an ion exchange site requires packing of the charged species into a small space, and this derives a principle that structural fitting of the cation and cavity involving the ion exchange site gives the thermodynamic stability.

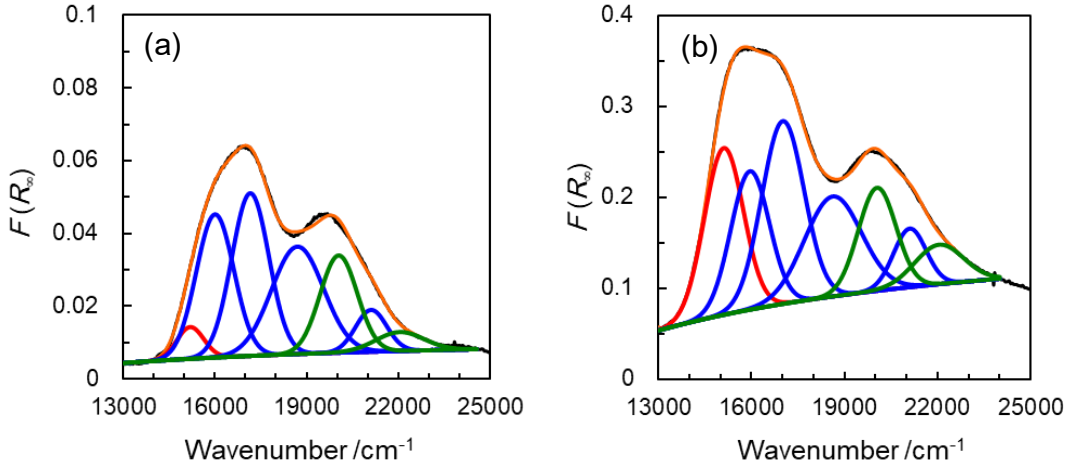

Figure 4-4. Examples of deconvolution of UV-vis spectra on (a) Co-0.085 and (b) Co-0.48 into components α, β and γ. Black line shows the observed spectra and yellow line shows the fitting curves comprising Gaussian curves of components α (one red line), β (four blue lines) and γ (two green lines).

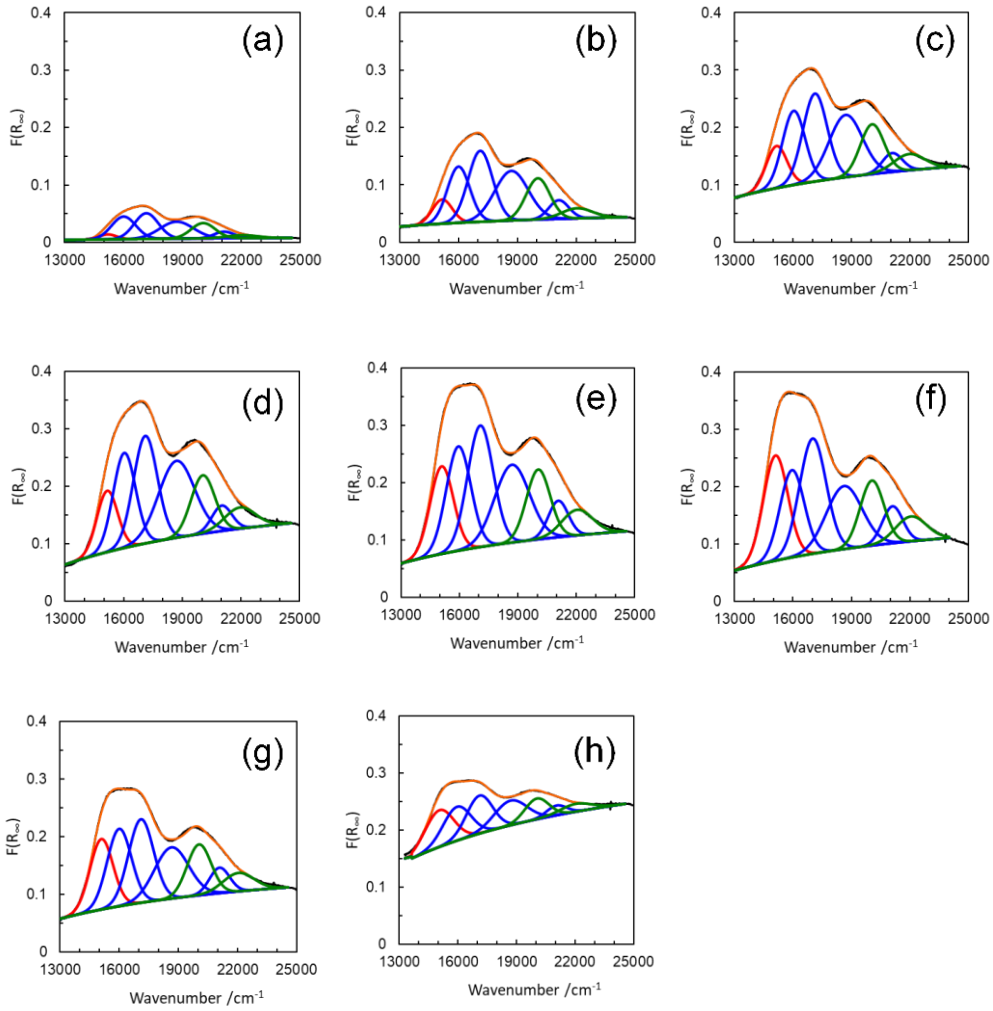

Figure 4-5. UV-vis spectra and their deconvolution of (a) Co-0.085, (b) Co-0.16, (c) Co-0.26, (d) Co-0.28, (e) Co-0.39, (f) Co-0.48, (g) Co-0.24+Mg-0.22 and (h) Co-0.15+Pb-0.28. Black line shows the observed spectra and yellow line shows the fitting curve comprsing Gaussian curves of compornet α (one red line), β (four blue lines) and γ (two green lines).

4-3-3 UV-vis spectroscopy

According to the principles found by Dědeček et al. [12], the components were

Table 4-3. Quantification of Co species at α, β and γ sites

Sample	$[Co]_{zeo}$	I_α	I_β	I_γ	$[Co]_\alpha$	$[Co]_\beta$	$[Co]_\gamma$
	/ mol kg^{-1}	/ cm^{-1}			/ mol kg^{-1}		
Co-0.085	0.13	10	207	51	0.0050	0.078	0.0064
Co-0.16	0.23	54	561	145	0.028	0.21	0.018
Co-0.26	0.33	98	699	188	0.051	0.26	0.024
Co-0.28	0.41	141	888	228	0.073	0.34	0.029
Co-0.39	0.56	244	1003	247	0.13	0.38	0.031
Co-0.48	0.67	289	917	258	0.15	0.35	0.033
Co-0.24+Mg-0.22	0.29	200	674	190	0.10	0.25	0.024
Co-0.15+Pb-0.28	0.20	117	328	83	0.061	0.12	0.010

extracted as shown in Figure 4-4 and 4-5 from the observed UV-vis spectra. Here, the wavenumbers of α, β and γ components in UV-vis spectrum were adjusted within the ranges shown in Table 4-2 to give best fitting with the experimentally observed spectrum according to Dědeček et al. [12]. The thus obtained band intensities (peak areas) of components (I_α, I_β and I_γ) were summarized in Table 4-3.

For the quantitative analysis, it was assumed that the molar extinction coefficients of Co^{2+} on these sites were unchanged throughout the experiments, and therefore the absorption coefficients as defined by Dědeček et al. [21], in inverse proportional to the molar extinction coefficients, were also constant. The relative intensities of absorption coefficients for Co^{2+} at α, β and γ sites were assumed to be 3.7 : 2.7 : 0.9, according to the measurements on Co/MFI [12]. Figure 4-6 indicates that the band intensity after

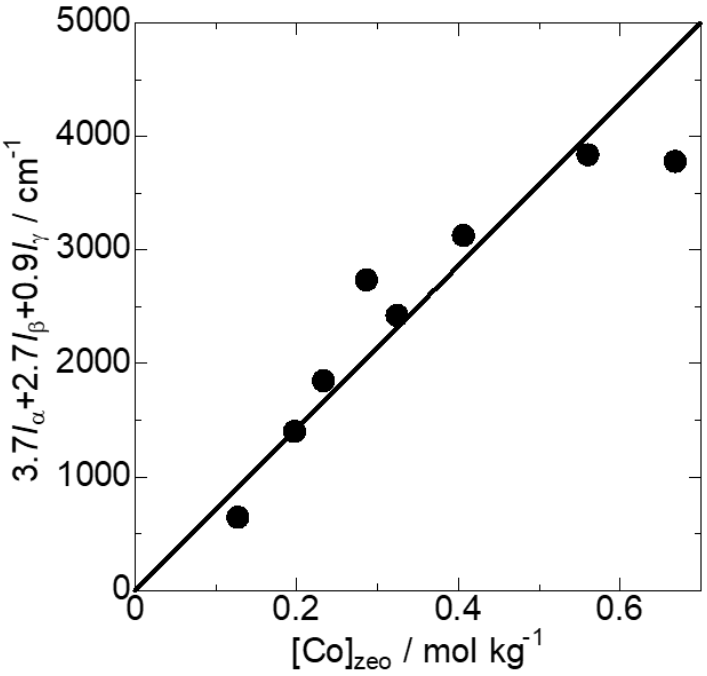

Figure 4-6. Plots of $3.7I_\alpha+2.7I_\beta+0.9I_\gamma$, where I_x shows the UV-vis band intensity of Co^{2+} at the site x, against Co content.

calibration with relative absorption coefficients, $3.7I_\alpha+2.7I_\beta+0.9I_\gamma$, was approximately proportional to the total Co^{2+} concentration in zeolites ($[Co]_{zeo}$). The absorption coefficients in these measurements were estimated to be 5.2×10^{-4}, 3.8×10^{-4} and 1.3×10^{-4} mol kg^{-1} $(cm^{-1})^{-1}$ for Co^{2+} at α, β and γ sites, respectively. The amounts of Co^{2+} at α, β and γ sites were finally calculated to be the products of these coefficients and peak intensities, as shown in Table 4-3.

The ion exchange behavior of NH_4-MFI zeolite with cobalt nitrate in the presently adopted conditions was predominantly according to the equilibrium but less affected by

kinetics (diffusion rate of ion in pores), as explained in Supporting Information. Co^{2+} possess higher thermodynamic stability than NH_4^+ at all kinds of the site on MFI, as a result of structural fitting of the cation and cavity [22].

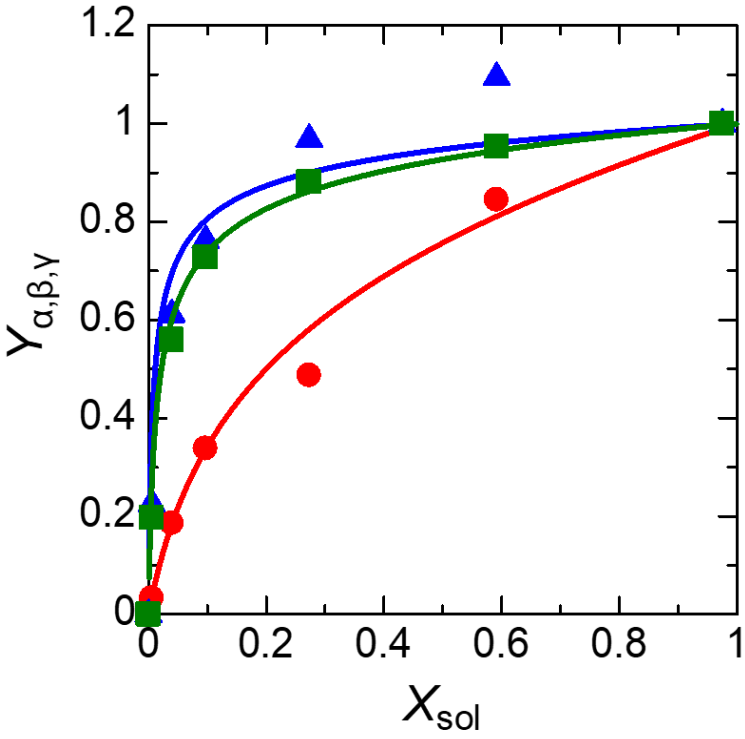

Figure 4-7. Ion exchange isotherms of NH_4^+ and Co^{2+} at α (●), β (▲), and γ (■) positions on MFI zeolite.

From to the amounts of Co^{2+} on α, β and γ sites, the ion exchange isotherms of these sites were yielded as shown in Figure 4-7. The experimental results (shown by dots) are approximately fitted with the curves calculated by (8) with the equilibrium constants of α, β and γ sites assumed to be 2.53, 13.2, and 9.36, respectively. The equilibrium constants

of ion exchange from NH_4^+ into Co^{2+} at α, β and γ sites are estimated to be these values. The constants higher than unity indicate that Co^{2+} was more preferentially held by the zeolite than NH_4^+ on all the sites, but it is noteworthy that the equilibrium constants of β and γ sites were obviously larger than that of α site. Therefore, the stability of Co^{2+} was especially high at the narrow sites which gave the low wavenumber of d-d transition due to the large number of coordinated oxygen atoms. A possible explanation is that Co^{2+} was strongly stabilized by electron donation from the oxygen atoms surrounding the β and γ sites, whereas Co^{2+} at the α site kept high chemical potential due to empty orbitals.

Figure 4-8 (a)-(c) shows the amounts of Co at α, β and γ sites as functions of the total Co loading shown by Co_{zeo}/Al_{zeo}. As a result of the above discussed equilibrium, the

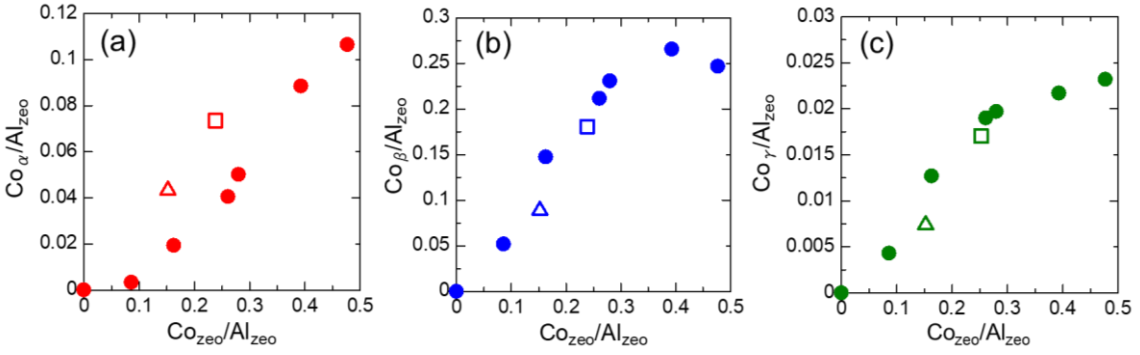

Figure 4-8. Co^{2+} concentrations at (a) α, (b) β and (c) γ sites plotted against total Co concentration on Co/MFI (filled circle), Co+Mg/MFI (square) and Co+Pb/MFI (triangle).

Co^{2+} ions were preferentially held by the β and γ sites in the region of initial loading (Co_{zeo}/Al_{zeo} = 0 - 0.25), and it looks that these sites were approximately saturated with Co^{2+} at ca. Co_{zeo}/Al_{zeo} = 0.25. In contrast, the loading of Co species at the α site was observed mainly in higher Co_{zeo}/Al_{zeo} and continued to increase up to Co_{zeo}/Al_{zeo} = 0.5. The preferential loading of Co^{2+} at the β and γ sites on the initial stage of ion exchange has been reported [12].

In Figure 4-8 (a)-(c), changes of the amounts of Co at α, β and γ sites by the addition of Mg and Pb are shown. The addition of these elements during the ion exchange resulted in obvious increase of Co at α and decrease of Co at β and γ compared to the simple loading of Co with the equivalent concentration. It has already been reported that the addition of Ca and Ba increased Co at α and decreased Co at β and γ [12]. The present observation is consistent, because one of the alkaline earth elements, namely Mg, provided the increase of Co at α and decrease of Co at β and γ.

4-3-4 Ammonia IRMS-TPD measurements

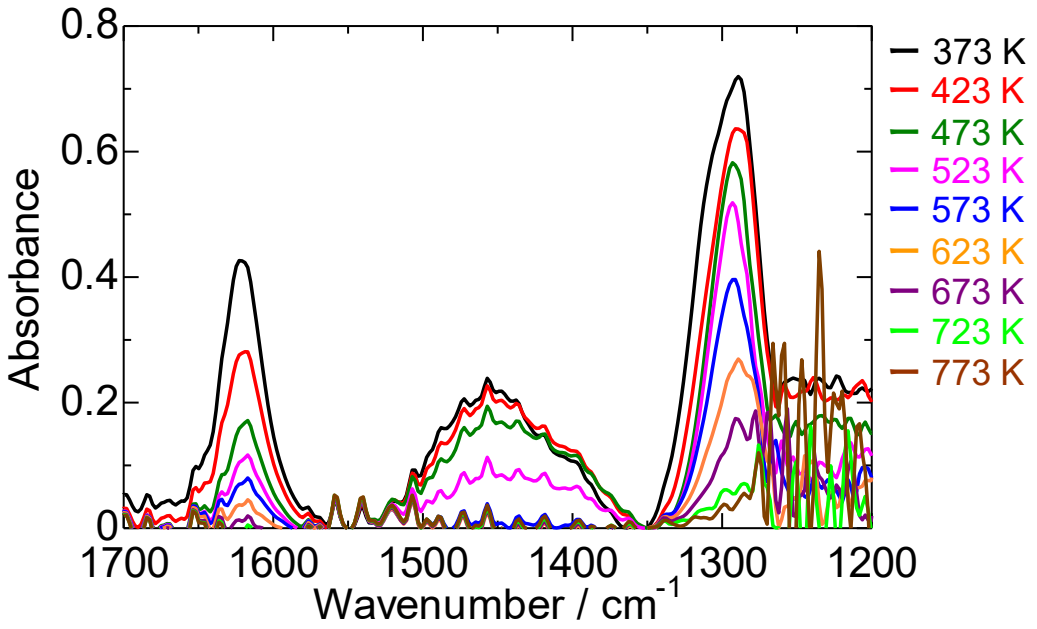

Figure 4-9. IR spectra of NH_3 adsorbed (absorbance after adsorption of NH_3 - absorbance before adsorption of NH_3) on Co/MFI (Co_{zeo}/Al_{zeo} = 0.42) at 373 - 773 K.

Figure 4-9 shows the IR spectra of NH_3 adsorbed on Co-0.42 at 373 - 773 K. In Figure 4-9, three bands are found at about 1620, 1450 and 1285 cm^{-1}. The 1450 cm^{-1}-band is ascribed to the symmetric deformation of NH_4^+ bounded to Brønsted acid site (ν_4 band of NH_4) on MFI zeolite [23]. The 1620 cm^{-1} and 1285 cm^{-1}-bands are assigned to the asymmetric and symmetric deformation of NH_3 coordinated to

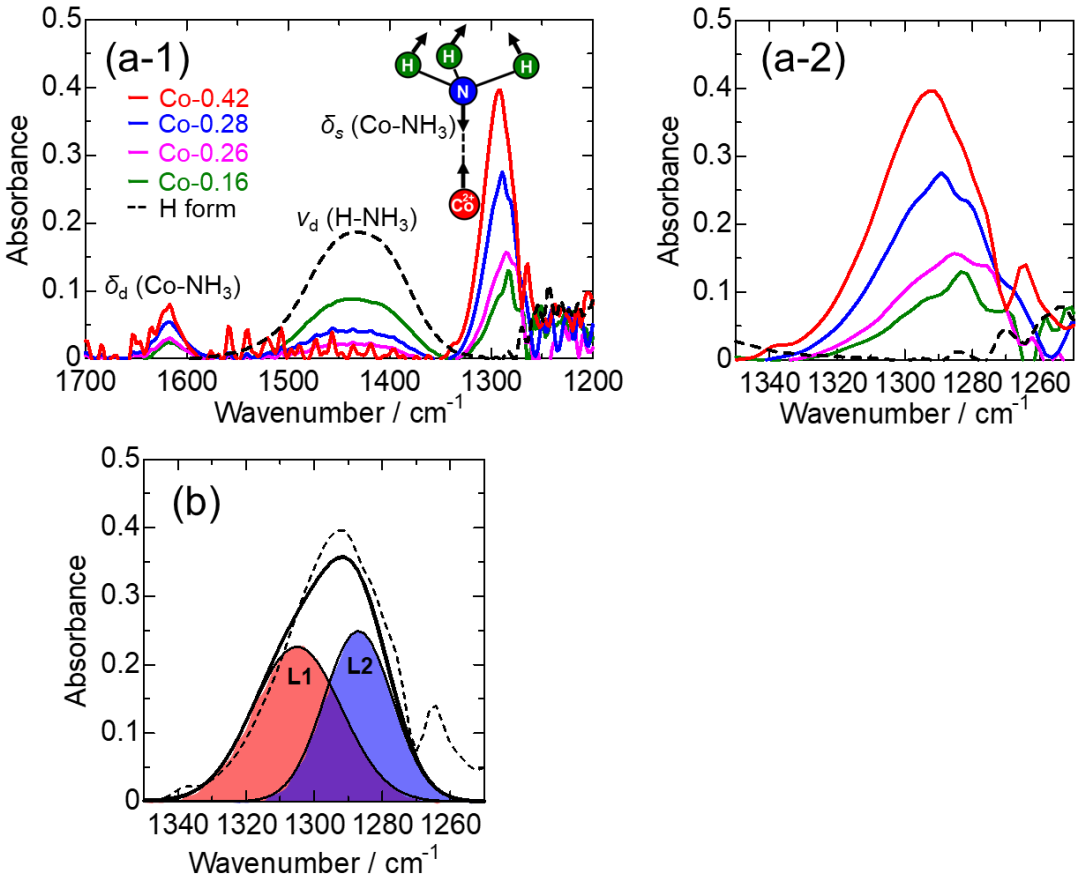

Figure 4-10. (a-1, a-2) IR spectra of NH_3 adsorbed on Co/MFI (Co_{zeo}/Al_{zeo} = 0.16 - 0.42, solid lines) and H-form MFI (black dashed line) at 573 K. (a-1) is the whole figure. The inset figure shows the symmetric deformation (δ_s) of NH_3 on Co species showing 1285 cm^{-1}-band. (a-2) is the enlarged portion of 1250 - 1350 cm^{-1}. (b) Deconvolution of the δ_s band into L1 (1305 cm^{-1}) and L2 (1287 cm^{-1}) components on Co-0.42 at 573 K. The dashed line shows the observed spectrum, and the solid lines show the calculated spectra.

Lewis acid site (L) on Al-containing zeolite (δ_d and δ_s bands of L-NH_3, the latter

one is drawn as inset part of Figure 4-10 (a-1)) [23, 24]. The absorbance of three bands decreased with increasing the temperature due to desorption of NH_3 from Brønsted and Lewis acid sites.

F igure 4-10 (a-1) shows the IR spectra of NH_3 adsorbed on Co/MFI and H-form MFI at 573 K. As shown in Figure 4-10 (a-1), only the ν_4 band of NH_4 at 1450 cm^{-1} was observed on the H-form MFI at 573 K (black dash line), indicating that only Brønsted acid sites existed on the H-form MFI. Intensities of the δ_d and δ_s bands of L-NH_3 at 1620 and 1285 cm^{-1} increased, and that of the ν_4 band of NH_4 at 1450 cm^{-1} decreased with increasing the Co loading. These results indicate that NH_4^+ cations on NH_4-MFI, which were the origin of protons in the heated H-form, were ion-exchanged with Co^{2+}, and the thus introduced Co species showed Lewis acidity as reported previously [10]. As shown in Figure 4-10 (a-2) (enlarged portion around 1300 cm^{-1}), the peak top of δ_s band of L-NH_3 shifted to the higher wavenumber side with increasing the Co content, implying that the δ_s band of L-NH_3 consisted of at least two fractions, and the quantities of them were varied by the Co content.

For quantitative analysis, as shown in Figure 4-10 (b), we assumed the higher wavenumber peak at 1305 cm^{-1}, hereafter denoted as L1 peak, and the lower one at 1285 cm^{-1}, denoted as L2 peak. All peaks of Co-0.16, Co-0.26, Co-0.28 and Co-0.42 at 373 K

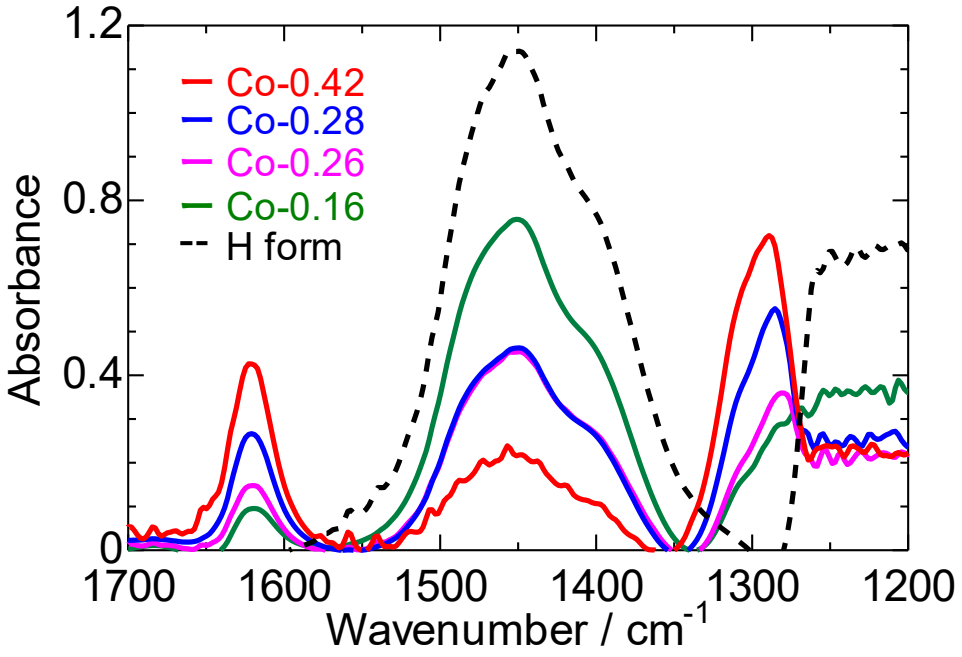

Figure 4-11. IR spectra of NH_3 adsorbed on Co/MFI (Co_{zeo}/Al_{zeo} = 0.16 - 0.42, solid lines) and H-form MFI (black dashed line) at 373 K.

clearly showed a shoulder peak at 1305 cm^{-1} (Figure 4-11). Therefore, the shoulder peak was assumed as the L1 peak. Then, the L2 peak position was determined by a curve fitting method of all the peaks of Co-0.16, Co-0.26, Co-0.28 and Co-0.42 between 340 K to 750 K. All the peaks of the Co/MFI were well deconvoluted into these assumed the two peaks.

Figure 4-12 (a) shows the δ_s bands of L-NH_3 on Co-0.24+Mg-0.22, Co-0.26 with equivalent Co content and Mg-0.19 at 573 K. As shown in Figure 4-12 (a), Mg-0.19 showed the peak at nearby 1280 cm^{-1} at 573 K, suggesting that Mg species on MFI

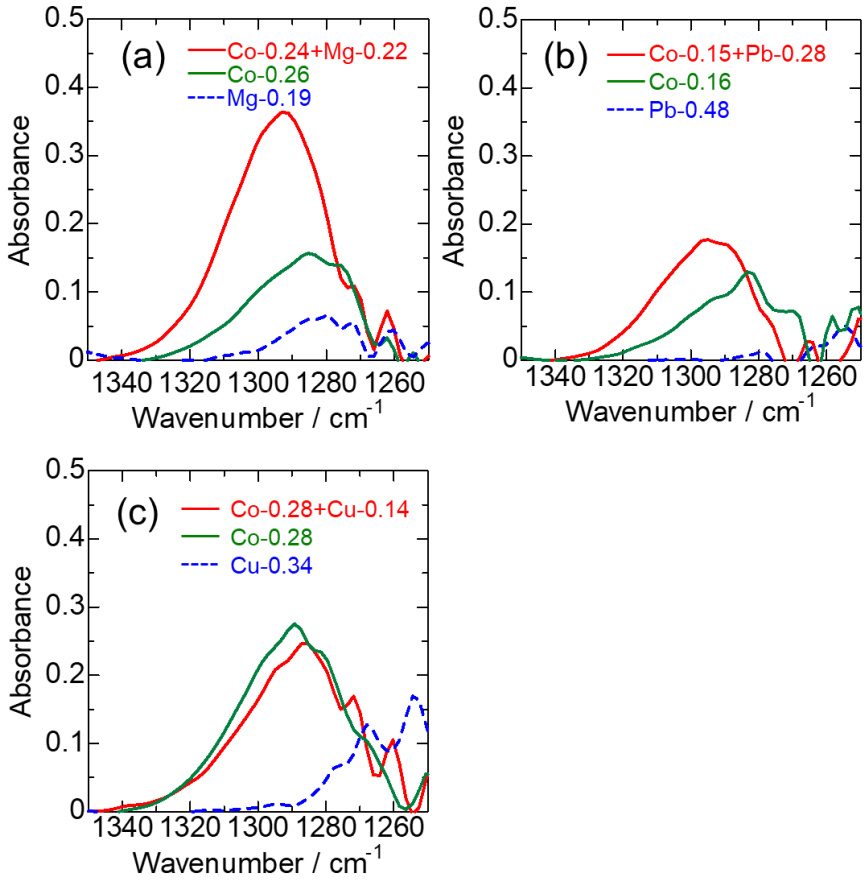

Figure 4-12. IR spectra of NH_3 adsorbed on Co+M/MFI [M = (a) Mg, (b) Pb and (c) Cu, red solid lines], Co/MFI (green solid lines) with equivalent Co content and M/MFI (blue dashed lines) at 573 K.

showed Lewis acidity. It should be emphasized that the δ_s band of L-NH_3 on Co-0.24+Mg-0.22 appeared at the higher wavenumber side compared to both Co-0.26 and Mg-0.19. It means that the high wavenumber shift of δ_s band of L-NH_3 on Co/MFI occurred at the low Co content by the co-presence of Mg, similarly to the shift observed at the high Co content on purely Co-promoted MFI. A similar behavior was observed on

Co-0.15+Pb-0.28 as displayed in Figure 4-12 (b). In contrast, the addition of Cu did not cause the high wavenumber shift. The peak position of Co-0.28+Cu-0.14 was slightly shifted to the lower wavenumber side (Figure 4-12 (c)).

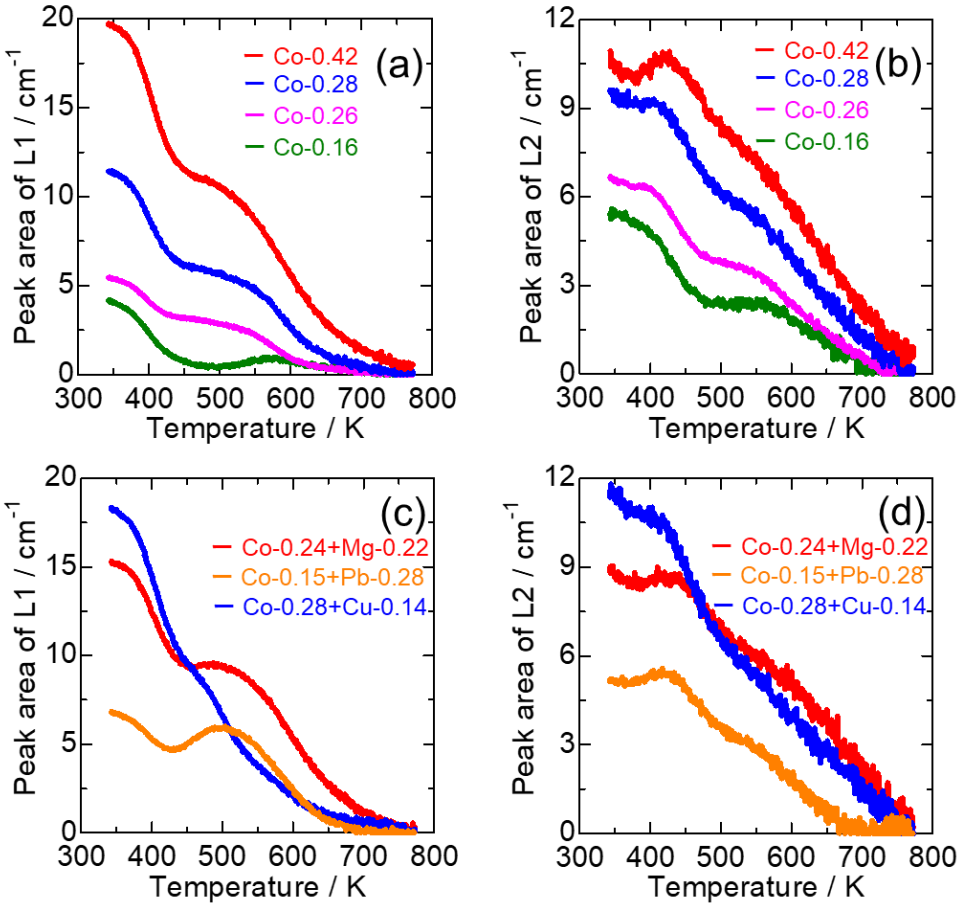

Figure 4-13. Peak areas of (a, c) L1 and (b, d) L2 bands plotted against temperature on (a, b) Co/MFI (Co_{zeo}/Al_{zeo} = 0.16 - 0.42) and (c, d) Co+M/MFI (M = Mg, Pb and Cu) catalysts

To investigate more details of the δ_s of the L-NH_3 band, the temperature dependences of amounts of species showing the L1 and L2 bands were analyzed. Figure 4-13 shows the plots of peak intensities (areas) of L1 and L2 bands on the Co/MFI and the Co+M/MFI catalysts against the temperature. In both plots, the decrease of intensity due to desorption of NH_3 was observed in two separated regions; 340 - 450 K and 500 - 750 K for L1, and 400 - 500 K and 550 - 800 K for L2. The quantities of these fractions seem to be different among the samples. For example, the L1 peak on Co-0.16 was almost completely diminished at about 450 K, whereas the peak areas of L1 on Co-0.26, Co-

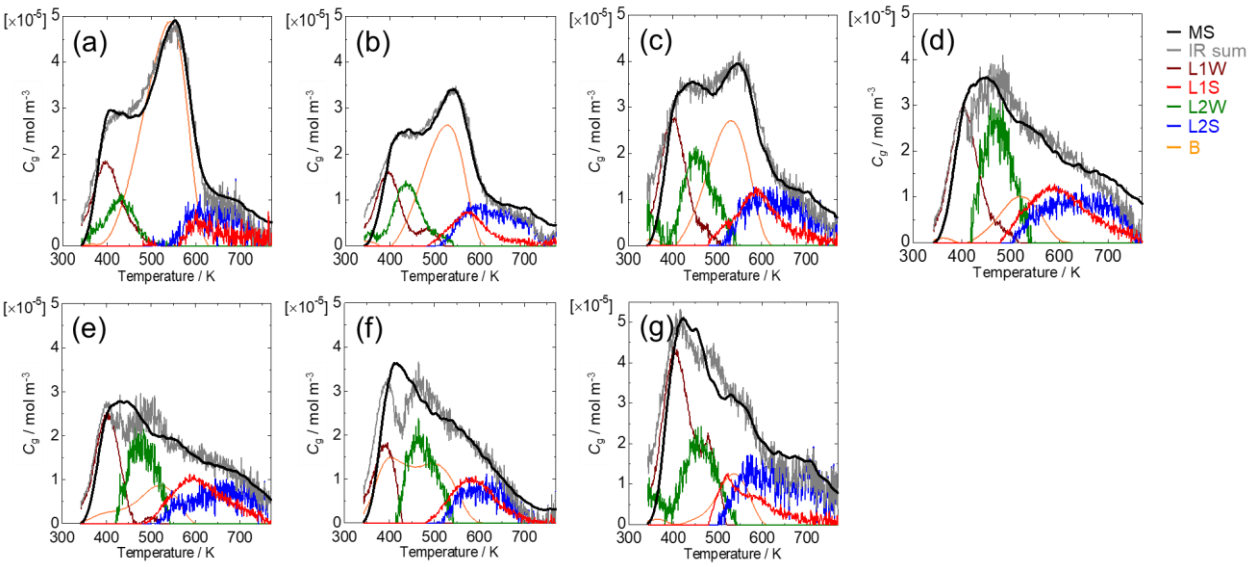

Figure 4-14. Fitting of IR- and MS-TPD calculating TPD spectrum of Lewis acid sites and Brønsted acid site on Co/MFI (Co_{zeo}/Al_{zeo} = (a) 0.16, (b) 0.26, (c) 0.28 and (d) 0.42) and Co+M/MFI (M = (e) Mg, (f) Pb and (g) Cu).

0.28 and Co-0.42 largely decrease at two temperature regions, i.e., 340 - 450 K and 500 - 750 K (Figure 4-13 (a)). These suggest the presence of total four types of Lewis acidic Co species showing different wavenumbers and ammonia desorption enthalpy (ΔH; so-called adsorption heat, reflected by the desorption temperature) [25]. Here they are denoted L1W, L1S, L2W and L2S; W and S show weak and strong, respectively. The L1W, L1S, L2W and L2S species also existed on Co+M/MFI catalysts (Figure 4-13 (c), (d)). The L1W and L1S species were clearly observed on Co-0.24+Mg-0.22 and Co-0.15+Pb-0.28, whereas only L1W species was observed on Co-0.28+Cu-0.14. The behaviors of L2 species of all Co-*X*+M-*Y* were similar to Co-0.28 and Co-0.42.

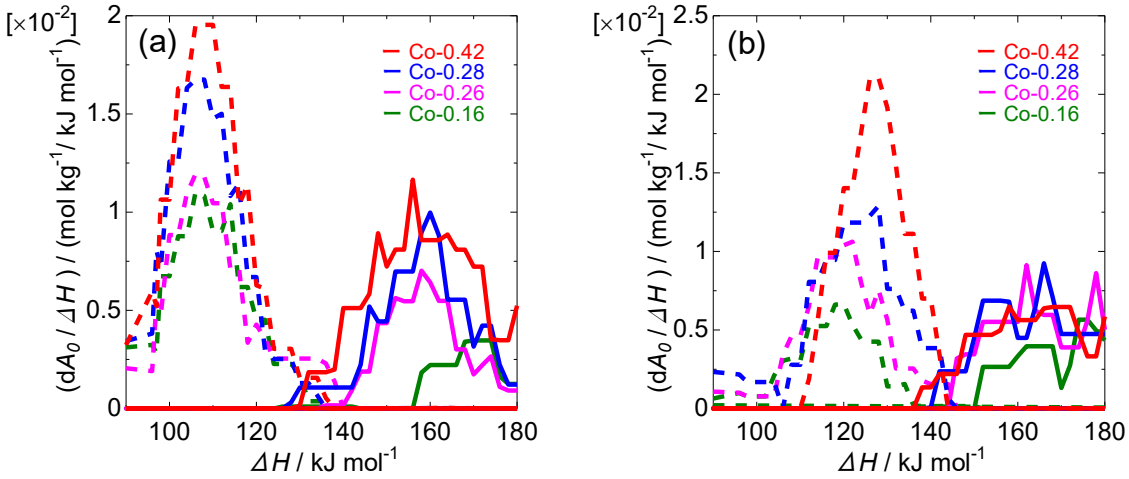

Figure 4-15. Ammonia desorption enthalpy of (a) L1W (dashed lines) and L1S (solid lines), (b) L2W (dashed lines) and L2S (solid lines) acid sites on Co/MFI (Co_{zeo}/Al_{zeo} = 0.16 - 0.42).

Principally according to our previously proposed method [26], the ammonia TPD profiles (temperature dependence of concentration of ammonia in gas phase) of Brønsted acid sites (B) and all the four types of Lewis acid sites (L1W, L1S, L2W and L2S) were

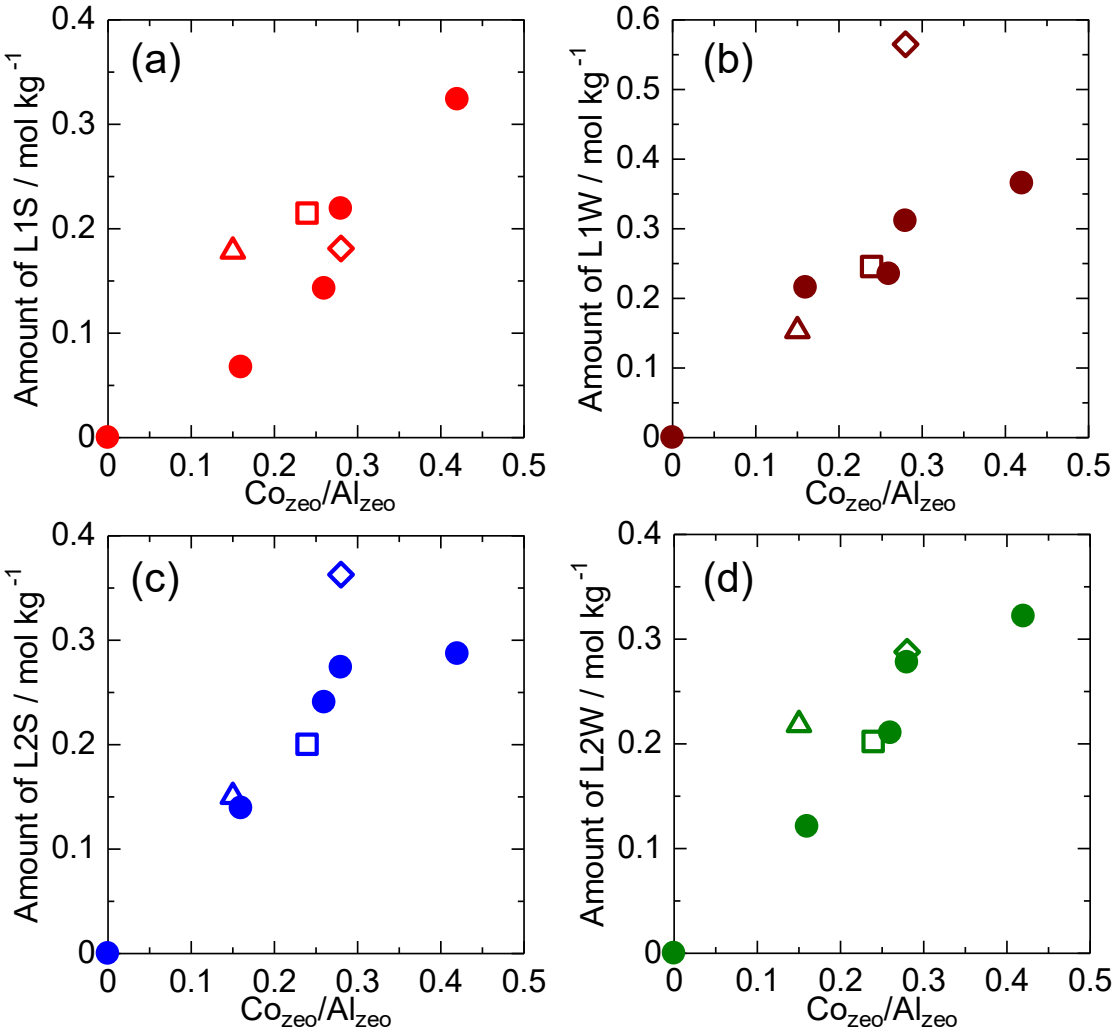

Figure 4-16. Amounts of (a) L1S, (b) L1W, (c) L2S and (d) L2W type acid sites plotted against Co_{zeo}/Al_{zeo} molar ratio on Co/MFI (filled circle) and Co+M/MFI [M = Mg (square), Cu (diamond) and Pb (triangle)].

determined to have absolute quantitative information, namely, to have the vertical axis with "mol" of the unit. It was assumed that the sum of concentrations of ammonia desorbed from Brønsted acid sites and four types of Lewis acid sites was equal to the concentration of ammonia (C_g, mol m^{-3}) detected by the mass spectrometer (MS). The ammonia TPD profiles of five types of acid sites were obtained as shown in Figure 4-14. The profile gives the amount ($A_{0,i}$, mol kg^{-1}) of the five types of acid sites. On the other hand, the distribution of ΔH was derived from the peak shape according to our previous paper [27] as shown in Figure 4-15.

Figure 4-16 shows the amounts of L1S, L1W, L2S and L2W type Lewis acid sites as a function of Co content on Co-*X* and Co-*X*+M-*Y*. The amount of L1S was small at lower Co_{zeo}/Al_{zeo} molar ratio and then rapidly increased with increasing the Co loading (Co_{zeo}/Al_{zeo} = 0.25 - 0.5), and also increased with adding Mg and Pb (Figure 4-16 (a)). On the other hand, the dependences on Co content of L1W, L2S and L2W were largely different from that of L1S; the amounts of these types mainly increased at Co_{zeo}/Al_{zeo} = 0 - 0.3 but not at 0.25 - 0.5 (Figure 4-16 (b)-(d)).

4-3-5 Catalytic activity

Figure 4-17 shows the change in catalytic activity for the methylation of benzene with methane by the loading of Co on MFI. As already reported [11], the activity of Co/MFIs was low in the low Co_{zeo}/Al_{zeo} region (Co_{zeo}/Al_{zeo} < 0.25), and significant increase of the activity was found at Co_{zeo}/Al_{zeo} = 0.25 - 0.5. The inactive Co species was first formed in Co_{zeo}/Al_{zeo} < 0.25. Then, the highly active Co species was generated in Co_{zeo}/Al_{zeo} = 0.25 - 0.5 [11]. Even in the low Co_{zeo}/Al_{zeo} region, the addition of Mg and

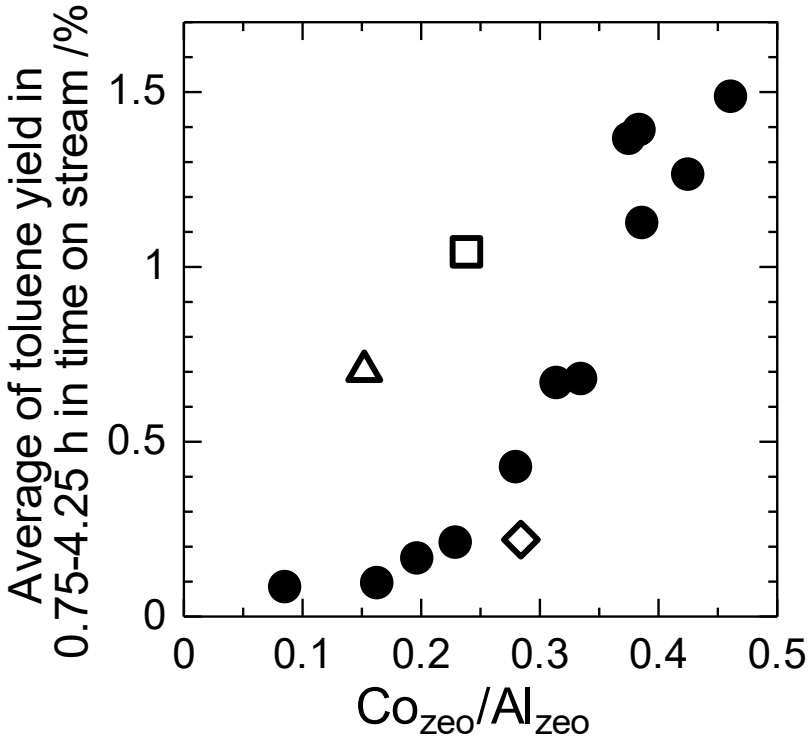

Figure 4-17. Catalytic activity for methylation of benzene with methane plotted against Co_{zeo}/Al_{zeo} molar ratio on Co/MFI (filled circle) and Co+M/MFI [M = Mg (square), Cu (diamond) and Pb (triangle)].

Pb enhanced the activity. In contrast, the addition of Cu suppressed the activity. It is suggested that the active Co species were selectively formed by addition of typically elements such as Mg and Pb. In contrast, the activity was suppressed by addition of transition metals such as Cu and Ag [11].

4-4 Discussion

The Co^{2+} cation at the α site increased mainly in the region of Co_{zeo}/Al_{zeo} = 0.2 - 0.5 by the simple ion exchange from NH_4-MFI into the Co-form (Figure 4-8 (a)). The catalytic activity for methylation of benzene with methane was mainly generated in the almost same Co_{zeo}/Al_{zeo} region (0.25 - 0.5). In contrast, at the initial stage of Co loading (Co_{zeo}/Al_{zeo} < 0.2), the Co^{2+} cations were mainly loaded at the β and γ sites (Figure 4-8 (b), (c)), and the activity was kept low. On this stage, we can draw two hypotheses; (I) Co^{2+} at the α site was active, while that at the β and γ sites were inactive; (II) such a Co species as dimer with Co-O-Co bond [28], which has been detected at relatively high Co loading on MFI [29], was the active species.

From EXAFS in our previous study [10, 11], most Co species at Co_{zeo}/Al_{zeo} < 0.6 were atomically dispersed, indicating that no or only small amount of Co dimers with Co-O-Co were formed during ion-exchange of Co^{2+}. The addition of Mg and Pb during the

ion exchange increased the Co^{2+} cation at the α site, and simultaneously the activity was enhanced. It tells us that, among the above two hypotheses, (I) was probable, because it is difficult to relate the addition of Mg and Pb with the formation of dimer, while the increase of Co^{2+} at the α site was observed in the two series of catalysts possessing the high activity. It is concluded that the Co species on the α site was active for the methylation of benzene with methane, while those at β and γ sites were inactive. One of

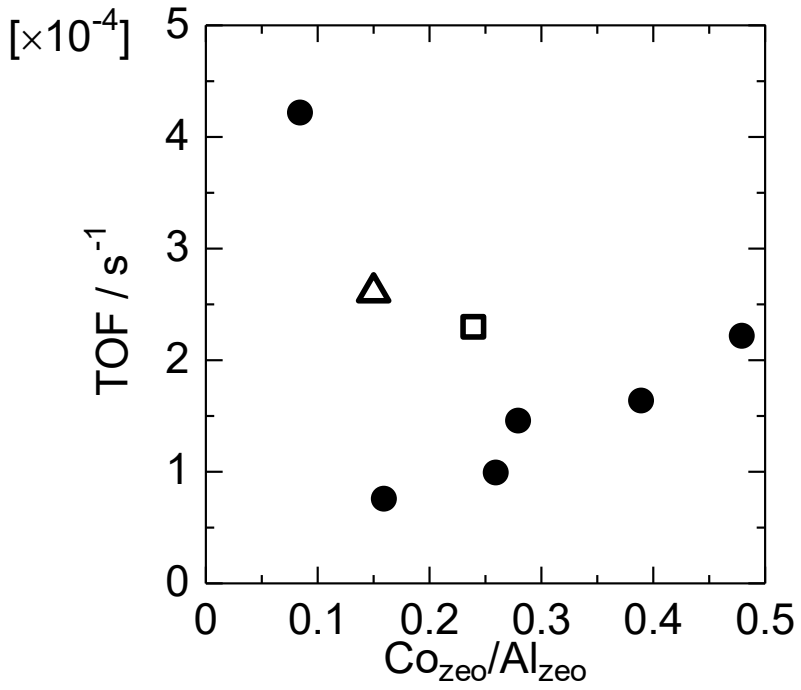

Figure 4-18. Turnover frequency (rate of toluene formation / amount of Co at α position) on Co/MFI (filled circle), Co+Mg/MFI (open square) and Co+Pb/MFI (open triangle).

the reasons of activity of the α site for direct methylation of benzene with methane is appropriate location of the α site; the α site is located on 10-ring with 0.56 nm of the diameter, which allow the diffusion of benzene (0.5 nm). Diffusion or interaction of benzene with Co^{2+} at the β and γ sites is possibly limited by steric hindrance, causing the low reaction rate of methylation of benzene with methane. Recently, our group reported that the ZSM-11 zeolite with MEL framework had larger probability of loading of Co^{2+} on the α site compared to ZSM-5 (MFI), and the Co/MEL showed high activity for this reaction [30].

The turnover frequency (TOF) was calculated on the assumption that the Co at α position was only the active site (Figure 4-18). The TOF was exceptionally high at $Co_{zeo}/Al_{zeo} = 0.09$, but it was presumably caused by large experimental errors due to small values of the reaction rate and amount of Co at α position. After ignoring this point, the TOF was generally low in the low Co_{zeo}/Al_{zeo} region, where the relatively large distribution of Co at β and γ positions. The TOF gradually increased with increasing Co and was relatively high in the co-presence of Mg and Pb even at the low Co_{zeo}/Al_{zeo}. High TOF at the high Co_{zeo}/Al_{zeo} or in the co-presence of Mg and Pb was caused by the high distribution of Co at α position as stated above. These findings suggest that Co at β and γ positions not only is inactive but also suppressed the activity of Co at α position through

some side reactions. The detail of the side reactions is the subject of future study.

Meanwhile, as a result of the ammonia IRMS-TPD measurements, the amount of L1S showed similar dependence on the Co content to that of catalytic activity; the L1S type Lewis acidity was mainly generated at Co_{zeo}/Al_{zeo} = 0.25 - 0.5, and also generated by adding Mg and Pb (Figure 4-16 (a)). On the contrary, the behaviors of L1W, L2S and L2W were largely different from that of catalytic activity (Figure 4-16 (b)-(d)). These suggest that the Co species having L1S type Lewis acidic nature was the active species for the methylation of benzene with methane. The amounts of the Co^{2+} at the α site and L1S site showed dependency on the Co content similar to the catalytic activity, indicating that the Co^{2+} at the α site with L1S nature was active for the desired reaction. As shown in Figure 4-19, the amounts of L1S of Co/MFI and Co+M/MFI were plotted against those of the Co^{2+} at the α site. The amount of L1S was approximately proportional to that of Co^{2+} at the α site.

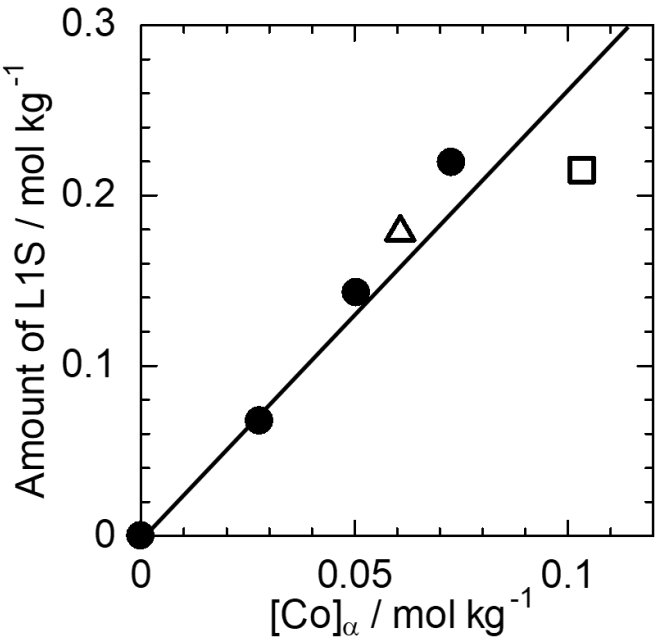

Figure 4-19. Amount of L1S type acid sites plotted against Co^{2+} concentrations at α site on Co/MFI (filled circle), Co+Mg/MFI (open square) and Co+Pb/MFI (open triangle).

The ion strength of ion exchange site and pore size are supposed to affect the Lewis acidic nature of supported cation. The latter has experimentally and theoretically been clarified [31]. Thus environment of Co species should affect its Lewis acidic nature. The α site is located on the wall of 10-ring straight channel. The β position is also facing to the 10-ring (sinusoidal channel), but the β site is at the center of 6-ring located at a small cavity of the curved sinusoidal channel, next to the intersection between the straight and sinusoidal channels. The γ site is also located on the sinusoidal channel wall (Figure 4-1)

[12]. The number of oxygen atoms coordinated to Co^{2+} was small at the α site, as directly evidenced by the low wavenumber of d-d transition (Figure 4-4). It implies that the electron withdrawing nature of Co^{2+} was kept strong at the α site, whereas the electron donation from oxygen was too strong at the β and γ sites to suppress the electron withdrawing ability, i.e., Lewis acidity. The L1 and L2 bands reflected symmetric deformation of NH_3 coordinated to Co species. The wavenumber of L1 was larger than that of L2 (Figure 4-10 (b)), i.e. energy of related bond was larger in the L1 type species than L2 species. For example, the N-Co bond was possibly stronger in the L1 type. It tells us that the Co species with L1 type nature has an ability of strong electron withdrawing from the coordinated base molecule. On the other hand, ΔH of L1S and L2S types were stronger than those of L1W and L2W species. It means that L1S and L2S types possess the nature of deeply stabilizing a base. Therefore, one can conclude that the L1S type Co species at the α site had the strong electron-withdrawing and base-stabilizing nature. It is proposed that the active Co species for methylation of benzene with methane had strong Lewis acidity from both viewpoints of electron-withdrawing and base-stabilizing nature.

Figure 4-20 shows possible reaction scheme on Co/MFI for the direct methylation of benzene with methane. Physical adsorption of benzene is presumed to be readily proceed. The reaction is one kind of the dehydrogenation, and therefore, the nature of Co

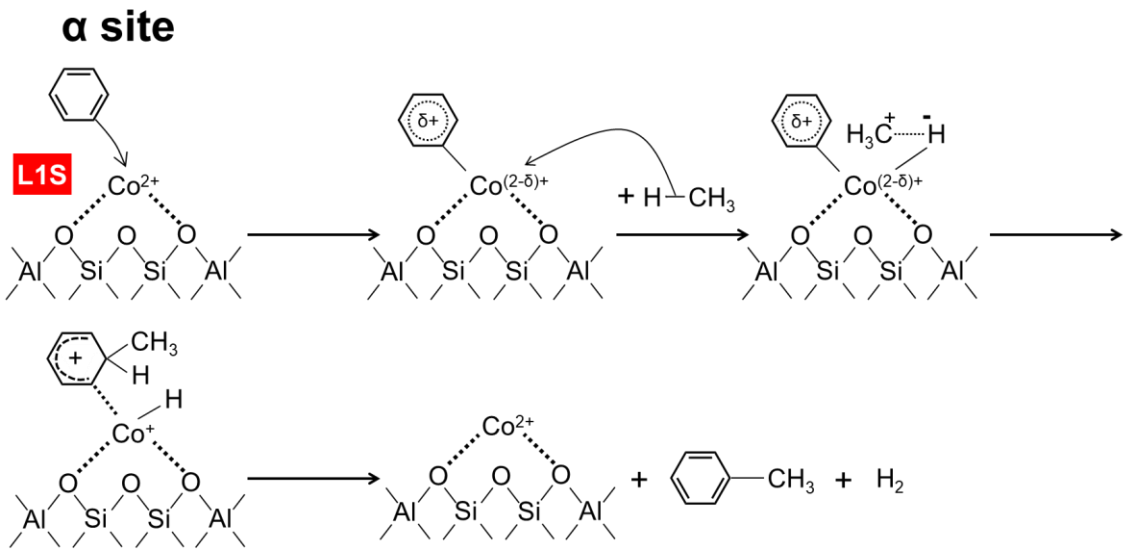

Figure 4-20. Amount of L1S type acid sites plotted against Co^{2+} concentrations at α site on Co/MFI (filled circle), Co+Mg/MFI (open square) and Co+Pb/MFI (open triangle).

as a transition metal fundamentally contributes to cleavage the C-H bond of CH_4. In addition, on the active Co/MFI (Co_{zeo}/Al_{zeo} = 0.25 - 0.5, or Mg- or Pb-promoted), the L1S Co species at the α site strongly withdraws electrons from methane, leading to withdrawing of hydride ion (H^-). Then, the formed CH_3^+ attacks to adsorbed benzene to readily form a toluene molecule via an aromatic alkenium cation.

4-5. Conclusions

The Co species on α site of MFI zeolite was mainly formed in relatively high

Co_{zeo}/Al_{zeo} loading region, and in addition, the co-existence of Mg and Pb increased the Co species on α site. The active species for direct methylation of benzene with methane was identified to be the Co species on α site with strong base-stabilizing and electron-withdrawing nature (L1S type). It is suggested that the L1S type Co species at α site withdrew H^- from CH_4, and the formed $^+CH_3$ should provide the methylation of benzene.

Acknowledgements

This study was partly supported by JST CREST Grant Number JPMJCR17P1, Japan, and JSPS KAKENHI Grant Number JP 19J15344.

References

[1] M. Ravi, M. Ranocchiari, J. A. Bokhoven, *Angew. Chem. Int. Ed*., **56**, 16464-16483 (2017)

[2] A. E. Shilov, G. B. Shul'pin, *Chem. Rev*., **97**, 2879-2932 (1997)

[3] M. Stöcker, *Micropor. Mesopor. Mater*., **29**, 3–48 (1999)

[4] J. F. Haw, W. Song, D. M. Marcus, J. B. Nicholas, *Acc. Chem. Res*., **36**, 317-326 (2003)

[5] L. Wang, L. Tao, M. Xie, G. Xu, J. Huang, Y. Xu, *Catal. Lett*., **21**, 35-41 (1993)

[6] S. J. X. He, M. A. Long, M. A. Wilson, M. L. Gorbaty, P. S. Maa, *Energy Fuels*, **9**, 616-619 (1995)

[7] T. Baba, H. Sawada, *Phys. Chem. Chem. Phys*., **4**, 3919-3923 (2002)

[8] D. B. Lukyanov, T. Vazhnova, *J. Mol. Catal. A Chem*., **305**, 95-99 (2009)

[9] S. S. Arzumanov, I. B. Moroz, D. Freude, J. Haase, A. G. Stepanov, *J. Phys. Chem. C*, **118**, 14427-14432 (2014)

[10] K. Nakamura, A. Okuda, K. Ohta, H. Matsubara, K. Okumura, K. Yamamoto, R. Itagaki, S. Suganuma, E. Tsuji, N. Katada, *ChemCatChem*, **10**, 3806-3812 (2018)

[11] H. Matsubara, E. Tsuji, Y. Moriwaki, K. Okumura, K. Yamamoto, K. Nakamura, S. Suganuma, N. Katada, *Catal. Lett*., **149**, 2627-2635 (2019)

[12] J. Dědeček, D. Kaucký, B. Wichterlová, *Micropor. Mesopor. Mater*., **35**, 483-494 (2000)

[13] D. Kaucký, J. Dědeček, B. Wichterlová, *Micropor. Mesopor. Mater*., **31**, 75-87 (1999)

[14] T. Yokoi, H. Mochizuki, S. Namba, J. N. Kondo, T. Tatsumi, *J. Phys. Chem. C*, **119**, 15303-15315 (2015)

[15] M. Niwa, N. Katada, *Chem. Rec.*, **13**, 432-455 (2013)

[16] M. Mhamdi, S. Khaddar-Zine, A. Ghorbel, *Appl. Catal. A: Gen*., **357**, 42-50 (2009)

[17] L. B. Pierella, C. Saux, S. C. Caglieri, H. R.Bertorello, P. G. Bercoff, *Appl. Catal. A: Gen*., **347**, 55-61 (2008)

[18] M. S. Berber-Mendoza, R. Leyva-Ramos, P. Alonso-Davila, L. Fuentes-Rubio, R. M. Guerrero-Coronado, *J. Colloid Interface Sci*., **301**, 40-45 (2006)

[19] M. Jeffroy, A. Boutin, A. H. Fuchs, *J. Phys. Chem. B*., **115**, 15059-15066 (2011)

[20] H. S. Sherry, *J. Phys. Chem.*, **70**, 1158-1168 (1966)

[21] J. Dědeček, B. Wichterlová, *J. Phys. Chem. B*, **103**, 1462-1476 (1999)

[22] D. W. Breck, Zeolite Molecular Sieves: Structure, Chemistry, and Use, *John Wiley and Sons*, New York, London, Sydney, Toronto (1974)

[23] S. Suganuma, Y. Murakami, J. Ohyama, T. Torikai, K. Okumura, N. Katada, *Catal. Lett*., **145**, 1904-1912 (2015)

[24] K. Nakamoto, Infrared and Raman Spectra of Inorganic and Coordination Compounds, sixth ed., *Wiley*, New York (2009)

[25] N. Katada, *Mol. Catal*., **458**, 116-126 (2018)

[26] M. Niwa, K. Suzuki, N. Katada, T. Kanougi, T. Atoguchi, *J. Phys. Chem. B*, **109**, 18749-18757 (2005)

[27] N. Katada, T. Tsubaki, M. Niwa, *Appl. Catal. A: Gen*., **340**, 76-86 (2008)

[28] G. Fierro, M. A. Eberhardt, M. Houalla, D. M. Hercules, W. K. Hall, *J. Phys. Chem*.

100, 8468-8477 (1996)

[29] M. Mhamdi, S. Khaddar-Zine, A. Ghorbel, *Appl. Catal. A: Gen*., **357**, 42-50 (2009)

[30] P. Hu, K. Nakamura, H. Matsubara, K. Iyoki, Y. Yanaba, K. Okumura, T. Okubo, N. Katada, T. Wakihara, *Appl. Catal. A: Gen*., **601**, 117661 (2020)

[31] H. V. Thang, K. Frolich, M. Sharzhy, P. Eliášová, M. Rubeš, J. Čejka, R. Bulánek, P. Nachtigall, *Phys. Chem. Chem. Phys*., **18**, 18063-18073 (2016)

Chapter 5 Effect of Al Concentrations in Co/MFI Catalysts for Selective Methylation of Benzene with Methane

5-1 Introduction

Supply of natural gas, including such a non-conventional resource as shale gas, is increasing, and its main component, methane, has attracted much attention as a chemical resource alternative to petroleum. Methylation of benzene ring with methane can be an option for effective conversion of methane into valued compounds. For example, combining the methylation of benzene into toluene shown by Eq. (1) and the shape selective disproportionation of toluene into a pair of benzene and para-xylene [1, 2] should convert toluene and methane into para-xylene, whose demand as a raw material of polyethylene terephthalate is large.

$$CH_4 + C_6H_6 \rightarrow CH_3\text{-}C_6H_6 + H_2 \qquad (1)$$

We recently found that the catalytic activity of Co/MFI for the reaction (1) was remarkable among the zeolite-supported transition metals [3]. As shown in Chapters 2 and 4, the activity of Co/MFI ([Al] = 1.35 mol kg^{-1}, SiO_2 / Al_2O_3 molar ratio = 22) was low in the low Co / Al region (Co /Al < 0.25), and significant increase of the activity was

found at Co / Al = 0.25 - 0.5. The inactive Co species was first formed in Co / Al < 0.25. Then, the highly active Co species was generated in Co / Al = 0.25 - 0.5. Even in the low Co / Al region, the addition of Mg and Pb enhanced the activity [4, 5]. According to Dědeček et al. [6, 7], ion exchange sites for divalent cations on a zeolite are classified into three types (α, β and γ sites) on a pair of Al atoms within a certain short distance on a zeolite in mild ion-exchange conditions. On MFI, it is proposed that the α site is located on the wall of 10-ring straight channel, the β site is located in 6-ring close to the intersection of straight and sinusoidal 10-ring channels, and the γ site is located on the pocket-like wall of sinusoidal channel [6], based on distribution of the Al atoms at crystallographically non-equivalent positions [8]. As shown in Chapter 4, the Co species on α site of MFI zeolite was mainly formed in relatively high Co / Al loading region, and in addition, the co-existence of Mg and Pb increased the Co species on α site. The active species for direct methylation of benzene with methane was identified to be the Co species on α site with strong base-stabilizing and electron-withdrawing nature (L1S type) [5].

For catalysts with Co impregnated on MFIs with different Al concentrations (Co/Al = 0.6), we have previously reported higher catalytic activity with higher Al concentrations at 773 K. The highest activity was obtained with the MFI with the highest Al concentration ([Al] = 1.35 mol kg^{-1}, SiO_2 / Al_2O_3 = 22) [3]. However, Co/MFI with [Al]

= 1.35 mol kg^{-1} prepared by impregnation or ion-exchange method proceeded the simple dehydrogenation of methane as a side reaction, as shown in equation (2) [3, 9].

$$CH_4 \rightarrow C + 2H_2 \qquad (2)$$

The coke produced in this reaction is undesirable because it deposits on the catalyst and causes catalyst degradation. Therefore, it is necessary to improve the catalyst to inhibit the side reaction and selectively proceed with the methylation of benzene ring.

On the other hand, in Co/zeolite, it has been reported that the supported Co species varies with the Al concentration in the zeolite. According to Dědeček et al., unpaired Al corresponds to the concentration of Al of two Al atoms in different rings unable to coordinate a bare divalent cation, but accommodating divalent $[Co(II)(H_2O)_6]^{2+}$ complex or Co-oxo species ($[Co(III)O]^{+}$) in dehydrated zeolites [10]. Our research group has previously reported that methylation of benzene by methane proceeded in Co/MFI and Co/MEL, and that low silica (Si / Al = 17-18) had a higher methylation selectivity than high silica (Si / Al = 36) in both MFI and MEL [11]. The Al in zeolites can be classified into two types: the $Al_{Framework}$, which is within the zeolite framework and serves as an ion exchange site (i.e. brings negative charge), and the $Al_{Extra\text{-}framework}$, which is outside the framework and does not serve as an ion exchange site. As has been reported in the past, the $[Al]_{Framework}$ in zeolites can be accurately quantified by ammonia IRMS-TPD method

[12], allowing the $[Al]_{Framework}$ and $[Al]_{Extra\text{-}framework}$ of zeolites to be calculated separately. In this study, the effect of Al concentration ($[Al]_{framework}$, $[Al]_{Extra\text{-}framework}$ and total [Al]) in Co/MFI on the catalytic activity and methylation selectivity for the direct methylation of benzene with methane was investigated.

5-2 Experimental

5-2-1 MFI zeolite

NH_4-MFI (SiO_2 / Al_2O_3 = 30 and 100 (values reported by manufacturer)), Na-MFI (SiO_2 / Al_2O_3 = 44, 47, 48, 51, 52 and 63) and H-MFI (SiO_2 / Al_2O_3 = 100) were provided by Mizusawa Industrial Chemicals, Ltd. NH_4-MFI ((SiO_2 / Al_2O_3 = 22) was purchased from Tosoh Corp. NH_4-MFI (SiO_2 / Al_2O_3 = 61) was obtained from Zeolyst International Corp. Na-MFI (SiO_2 / Al_2O_3 = 90) was supplied by Clariant Catalysts Ltd. All Na-MFIs were converted into NH_4 forms by the three times repetition of ion exchange with ammonium nitrate aqueous solution (NH_4/Al = 1000%) at 343 K for 4 h. H-MFI(22) was obtained by calcination of NH_4-MFI(22) at 823 K for 2 h in atmosphere. Since NH_4-MFI was also converted to H form by pretreatment during the catalytic reaction, NH_4-MFI is

Table 5-1. Parameters of MFI supports

MFI support	$[Al]_{maker}$ mol kg^{-1}	$[Al]_{Total}$ mol kg^{-1}	[Na] mol kg^{-1}	[Brønsted acid site] mol kg^{-1}	$[Al]_{Framework}$ mol kg^{-1}	$[Al]_{Extra\text{-}framework}$ mol kg^{-1}
NH_4-MFI(22)	1.35	1.33	0.04	1.25	1.29	0.04
H-MFI(22)	1.35	1.33	0.05	0.68	0.73	0.60
NH_4-MFI(30)	1.02	0.92	0.02	0.72	0.74	0.18
NH_4-MFI(44)	0.71	0.61	0.03	0.34	0.37	0.24
NH_4-MFI(47)	0.67	0.54	0.01	0.45	0.46	0.08
NH_4-MFI(48)	0.66	0.51	0.006	0.36	0.37	0.14
NH_4-MFI(51)	0.62	0.54	0.008	0.32	0.33	0.21
NH_4-MFI(52)	0.61	0.49	0.007	0.31	0.32	0.18
NH_4-MFI(61)	0.52	0.53	0.01	0.37	0.38	0.15
NH_4-MFI(63)	0.51	0.46	0.005	0.26	0.27	0.20
NH_4-MFI(90)	0.36	0.37	0.02	0.29	0.31	0.06
NH_4-MFI(100)	0.32	0.27	0.009	0.13	0.14	0.13
H-MFI(100)	0.32	0.26	0.009	0.15	0.16	0.10

referred to as in-situ H type, and H-MFI is marked as ex-situ H type in the reaction results for Si / Al_2 = 22 and 100. The Al and Na contents in all the above MFIs were measured with an aid of inductively coupled plasma optical emission spectroscopy (ICP-OES, Rigaku Spectro Ciros CCD and Agilent 5110 ICP-OES). Table 5-1 shows these values as $[Al]_{Total}$ and [Na], respectively. $[Al]_{maker}$ in Table 5-1 is concentration of Al reported by manufacturer. The amount of Brønsted acid site was analyzed by a method of ammonia IRMS-TPD in conditions described elsewhere [12]. The framework and extra-framework Al concentrations were calculated as in equations (3) and (4).

$$[Al]_{Framework} = [\text{Brønsted acid site}] + [Na] \quad (3)$$

$[Al]_{Extra\text{-}framework} = [Al]_{Total} - [Al]_{Framework}$ (4)

[Brønsted acid site], $[Al]_{Framework}$ and $[Al]_{Extra\text{-}framework}$ are also summarized in Table 5-1. Table 5-1 shows that the $[Al]_{framework}$ of H-form (ex situ H-form) MFI(22) was lower than that of NH_4-form (in situ H-form). This is because H-type zeolites with high Al concentration, such as those with SiO_2/Al_2O_3 ratio of 22, have been dealuminated by exposure to the atmosphere, as reported by our group in the past [13].

External surface area, micropore volume and mesopore volume were calculated by nitrogen adsorption-desorption isotherm using BELSORP MAX. The results are shown in Table 5-2.

5-2-2 Catalyst preparation

Table 5-2. Physicochemical properties of MFI support

MFI support	Micropore volume / $cm^3\ g^{-1}$	Mesopore volume / $cm^3\ g^{-1}$	External surface area / $m^2\ g^{-1}$
NH_4-MFI(22)	0.138	0.11	16.6
NH_4-MFI(30)	0.137	0.04	3.4
NH_4-MFI(44)	0.140	0.17	9.5
NH_4-MFI(51)	0.143	0.14	3.5
NH_4-MFI(52)	0.141	0.39	49.4
NH_4-MFI(63)	0.130	0.11	3.5
NH_4-MFI(90)	0.143	0.58	33.2
H-MFI(100)	0.148	0.21	1.7

Table 5-3. Chemical composition of Co/MFI prepared by ion exchange method

MFI support	$[Al]_{maker}$ / mol kg^{-1}	$[Al]_{Framework}$ / mol kg^{-1}	Amount in prepared solution			Amount in final solids	
			[Co] / mol kg^{-1}	$[Co]/[Al]_{maker}$	$[Co]/[Al]_{Framework}$	[Co] / mol kg^{-1}	$[Co]/[Al]_{Framework}$
NH_4-MFI(22)	1.35	1.29	0.27	0.2	0.21	0.23	0.18
			0.41	0.3	0.31	0.33	0.25
			0.54	0.4	0.42	0.41	0.32
			0.61	0.45	0.47	0.46	0.35
			0.81	0.6	0.63	0.49	0.38
			1.4	1	1.0	0.56	0.43
			2.7	2	2.1	0.55	0.42
			6.8	5	5.2	0.56	0.43
			14	10	10	0.62	0.48
			27	20	21	0.67	0.52
NH_4-MFI(30)	1.02	0.74	2.0	2	2.8	0.14	0.20
			102	100	138	0.12	0.17
NH_4-MFI(48)	0.66	0.37	0.13	0.2	0.36	0.08	0.21
			0.20	0.3	0.54	0.08	0.23
			0.26	0.4	0.71	0.08	0.23
			1.3	2	3.6	0.10	0.28
			66	100	178	0.15	0.41

Co/MFI were prepared by ion exchange and impregnation method. In the ion exchange method, powder of 1 g of NH_4-MFI zeolite with SiO_2/Al_2O_3 = 22, 30 and 48 was put into 100 mL of aqueous solution containing the desired amount of cobalt nitrate (Co / Al_{maker} molar ratio = 0.2 - 100) as shown in Table 5-3, and the mixture was stirred at 343 K for 4 h. The filtered solid was washed with ion exchanged water and filtered for three times, and dried at 383 K for 12 h in atmosphere. The Al and Co contents in the final solids of ion exchanged samples were measured with an aid of ICP-OES as shown in Table 5-3. In the impregnation method, powder of 1 g of NH_4- or H-MFI was put into 100 mL of aqueous solution containing the desired amount of cobalt nitrate (Co / Al_{maker} molar ratio = 0.15 - 1.8) as shown in Table 5-4, and the mixture was stirred at 343 K up

Table 5-4. Chemical composition of Co/MFI prepared by impregnation method

MFI support	$[Al]_{maker}$ / mol kg^{-1}	$[Al]_{Total}$ / mol kg^{-1}	$[Al]_{Framework}$ / mol kg^{-1}	$[Al]_{Extra-framework}$ / mol kg^{-1}	[Co] / mol kg^{-1}	$[Co]/[Al]_{maker}$	$[Co]/[Al]_{Total}$	$[Co]/[Al]_{Framework}$	$[Co]/[Al]_{Extra-framework}$
NH_4-MFI(22)	1.35	1.33	1.29	0.04	0.41	0.3	0.30	0.31	10.5
					0.54	0.4	0.41	0.42	14.0
					0.68	0.5	0.51	0.52	17.5
					0.81	0.6	0.61	0.63	21.1
					1.22	0.9	0.91	0.94	31.6
					2.43	1.8	1.83	1.88	63.2
H-MFI(22)	1.35	1.33	0.73	0.60	0.81	0.6	0.61	1.11	1.4
NH_4-MFI(30)	1.02	0.92	0.74	0.18	0.15	0.15	0.17	0.21	0.8
					0.20	0.2	0.22	0.28	1.1
					0.31	0.3	0.33	0.42	1.7
					0.41	0.4	0.44	0.55	2.2
					0.51	0.5	0.55	0.69	2.8
					0.61	0.6	0.67	0.83	3.3
					0.71	0.7	0.78	0.97	3.9
					0.92	0.9	1.00	1.25	5.0
					1.22	1.2	1.33	1.66	6.7
					1.84	1.8	2.00	2.49	10.0
NH_4-MFI(44)	0.71	0.61	0.37	0.24	0.11	0.15	0.17	0.29	0.4
					0.36	0.5	0.58	0.95	1.5
					0.43	0.6	0.70	1.14	1.8
NH_4-MFI(47)	0.67	0.54	0.46	0.08	0.40	0.6	0.74	0.87	5.0
NH_4-MFI(48)	0.66	0.51	0.37	0.14	0.10	0.15	0.19	0.27	0.7
					0.13	0.2	0.26	0.36	0.9
					0.20	0.3	0.39	0.54	1.4
					0.26	0.4	0.52	0.72	1.8
					0.33	0.5	0.65	0.90	2.3
					0.40	0.6	0.78	1.08	2.8
					0.46	0.7	0.91	1.26	3.2
					0.59	0.9	1.16	1.62	4.1
					0.79	1.2	1.55	2.16	5.5
					1.19	1.8	2.33	3.25	8.3
NH_4-MFI(51)	0.62	0.54	0.33	0.21	0.19	0.3	0.34	0.57	0.9
					0.37	0.6	0.69	1.13	1.8
NH_4-MFI(52)	0.61	0.49	0.32	0.17	0.09	0.15	0.19	0.29	0.5
					0.18	0.3	0.37	0.58	1.1
					0.37	0.6	0.75	1.15	2.1
					0.55	0.9	1.12	1.73	3.2
					1.10	1.8	2.24	3.46	6.3
NH_4-MFI(61)	0.52	0.53	0.38	0.15	0.08	0.15	0.15	0.21	0.5
					0.10	0.2	0.20	0.27	0.7
					0.16	0.3	0.29	0.41	1.0
					0.21	0.4	0.39	0.55	1.4
					0.26	0.5	0.49	0.68	1.7
					0.31	0.6	0.59	0.82	2.1
					0.36	0.7	0.69	0.96	2.4
					0.47	0.9	0.88	1.23	3.1
					0.62	1.2	1.18	1.64	4.2
					0.94	1.8	1.77	2.46	6.2
NH_4-MFI(63)	0.51	0.46	0.27	0.20	0.15	0.3	0.33	0.58	0.8
					0.26	0.5	0.55	0.96	1.3
					0.31	0.6	0.67	1.15	1.6
					0.92	1.8	2.00	3.46	4.7
NH_4-MFI(90)	0.36	0.37	0.31	0.06	0.05	0.15	0.15	0.17	0.9
					0.07	0.2	0.19	0.23	1.2
					0.11	0.3	0.29	0.35	1.8
					0.14	0.4	0.39	0.46	2.4
					0.18	0.5	0.49	0.58	3.0
					0.22	0.6	0.58	0.70	3.6
					0.32	0.9	0.88	1.05	5.4
					0.65	1.8	1.75	2.09	10.8
NH_4-MFI(100)	0.32	0.27	0.14	0.13	0.19	0.6	0.71	1.38	1.5
H-MFI(100)	0.32	0.26	0.16	0.10	0.10	0.3	0.37	0.60	1.0
					0.19	0.6	0.74	1.21	1.9

to most of the solvent (water) was removed by vaporization. The yielded solid was further

dried again at 383 K for 3 h in atmosphere.

5-2-3 Reaction tests

Catalytic methylation of benzene with methane was performed using a fixed-bed flow reactor shown in our previous report [3-5]. The catalyst (0.300 g) was placed in a Pyrex tube, and pretreated in a flow of N_2 (1.23 mmol min^{-1}) in the atmospheric pressure at 823 K for 1 h. Then, a mixture of CH_4 (99.9% from Iwatani Industrial Gases Corporation) and C_6H_6 vaporized from a liquid C_6H_6 (special grade, FUJIFILM Wako Pure Chemical Corporation) was fed to the catalyst bed (98.6 and 2.7 kPa, 1.2 and 0.033 mmol min^{-1}, respectively, corresponding to $W_{cat}/F_{benzene}$ = 147 g_{cat} h $mol_{benzene}^{-1}$) at 773 K. The outlet materials were trapped by hexane at 273 K with a known amount of 1,4-diisopropylbenzene as an internal standard compound and analyzed with a flame ionization detector-gas chromatograph (FID-GC, Shimadzu GC-2014).

Another set of conditions was applied to carry out the catalytic reaction at 813 K as shown in our previous report [9]. The catalyst (0.300 g) was pretreated in an oxygen flow with 1.23 mmol min^{-1} of the flow rate in atmospheric pressure at 823 K for 1 h, and then catalyst bed was cooled to 373 K. A mixture of CH_4, C_6H_6, and He (as internal standard, 99.9% from Taiyo Nippon Sanyo) with 1.10×10^3, 33.4 and 76.0 μmol min^{-1}, respectively,

was fed with recording the mass spectra continuously by using a mass spectrometer (Pfeiffer Vacuum, QMG250) connected to the outlet of reactor. After the ion currents were stabilized, the catalyst bed was heated again to 813 K at a ramp rate of 10 K min^{-1}. After reaching 813 K, the catalytic reaction was carried out for about 4 h. Benzene, toluene, and dihydrogen were quantitated from the ion currents.

The selectivity of methylation of benzene with methane was calculated by the following equation.

$$S_{\mathrm{Methyl}}\,(\%) = \frac{r_{\mathrm{Toluene}}}{r_{\mathrm{Toluene}} + \frac{r_{\mathrm{Dihydrrogen}} - r_{\mathrm{Toluene}}}{2}} \times 100 \qquad (5)$$

where, S_{Methyl}, r_{Toluene}, $r_{\mathrm{Dihydrogen}}$ are methylation selectivity, toluene formation rate, and dihydrogen formation rate, respectively. Here it is assumed that only the reactions (1) and (2) occurred.

5-3 Results and Discussion

Figure 5-1 shows the catalytic activity for methylation of benzene with methane at 773 K (yield of desired product, toluene, averaged over 0.5 - 3.75 h of the time on stream) plotted against Co / $Al_{Framework}$ molar ratio in Co/MFI (Si / Al_2 = 22 (in situ H form), 30,

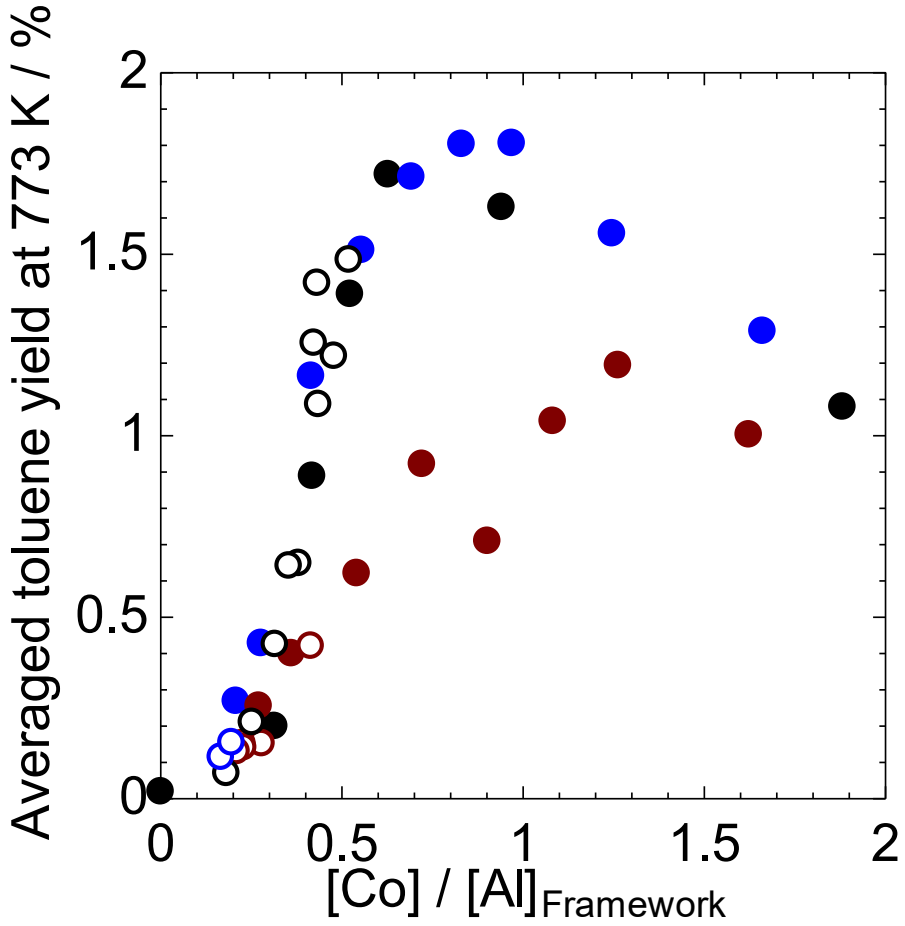

Figure 5-1. Catalytic activity for methylation of benzene with methane at 773 K plotted against [Co] on Co/MFI (Si / Al_2 = (●) 22 [in situ H type], (●) 30, (●) 48 prepared by (●)impregnation or (○) ion exchange method.

48) prepared by ion exchange or impregnation method. As shown in Chapter 4, when Co was loaded on MFI with high Al concentration (Si / Al_2 = 22) by ion exchange method, Co was easily ion exchanged as Co^{2+} on a pair of $Al_{Framework}$ atoms within a certain short distance on a zeolite, and the Co / $Al_{Framework}$ ratio in final solid reached about 0.5. The

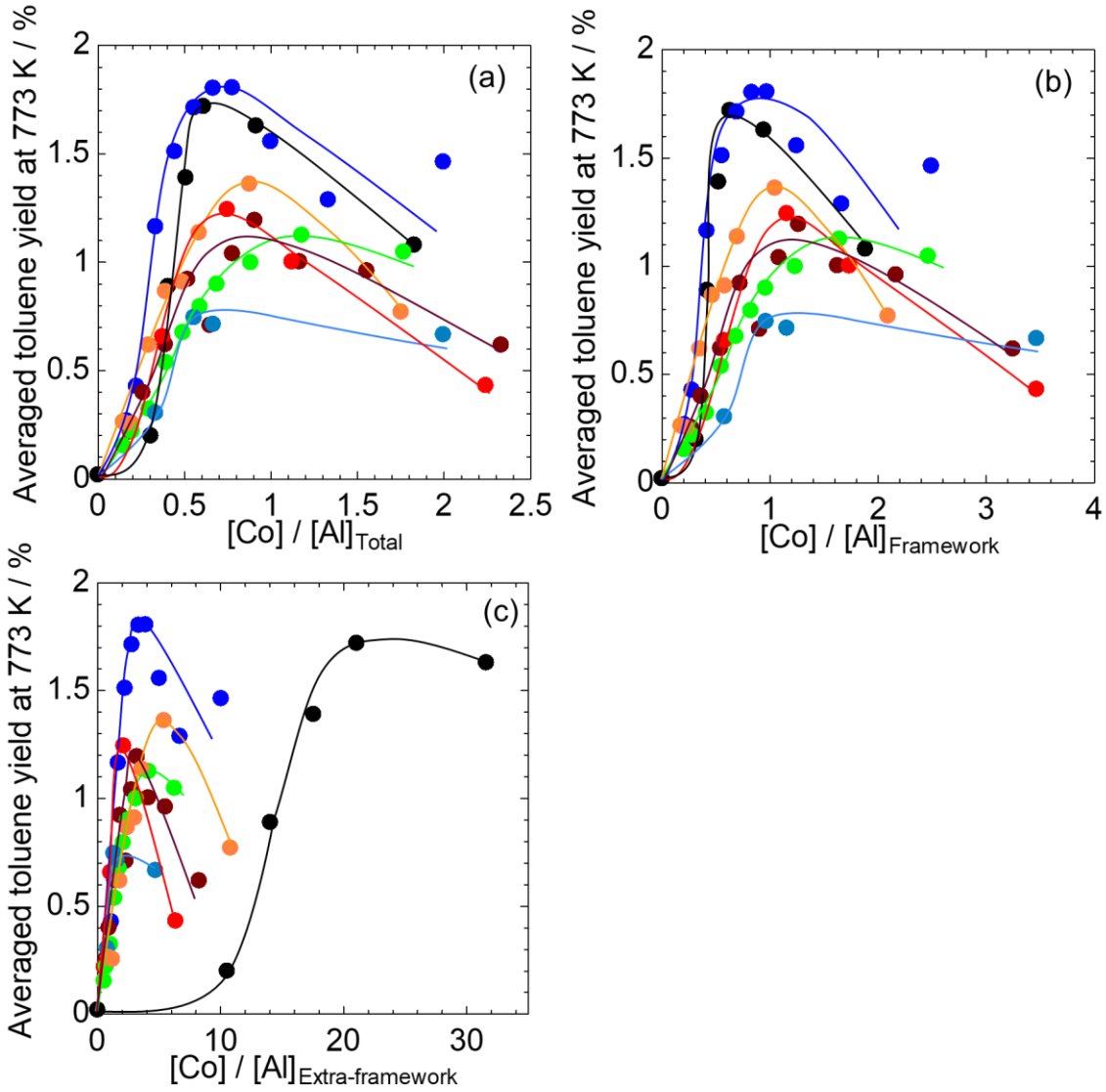

Figure 5-2. Catalytic activity for methylation of benzene with methane at 773 K plotted against (a) [Co] / $[Al]_{Total}$, (b) [Co] / $[Al]_{Framework}$ and (c) [Co] / $[Al]_{Extra\text{-}framework}$ ratio in Co/MFI (Si / Al_2 = (●) 22 [in situ H type], (●)30, (●) 48, (●) 52, (●) 61, (●) 63 and (●) 90) prepared by impregnation method.

active Co species was Co^{2+} on the α-site, which was not so different from the activity of

the impregnation method. On the other hand, at Si / Al_2 = 30, Co was loaded by the ion exchange method up to only Co/$Al_{Framework}$ in final solid = 0.17 which was obtained by using a large excess of Co contents in the preparation solution (Co / $Al_{Framework}$ = 138) (Table 5-3). This indicates that there were fewer paired Al sites at Si / Al_2 = 30 than at Si / Al_2 = 22. At Si / Al_2 = 30, the toluene yield was only about 0.15% in the case of the ion exchange method, whereas the activity increased significantly with increasing Co loading by impregnation, reaching 1.8% (Co / $Al_{Framework}$ = 1). In the case of Si / Al_2 = 48, when the amount of Co in the preparation solution for ion exchange was increased to a large excess (Co / $Al_{Framework}$ = c.a. 180), the Co / $Al_{Framework}$ in final solid was about 0.4, and the toluene yield was obtained up to about 0.4%. On the other hand, when Co was further loaded by impregnation, the yield reached about 1.2% (Co / $Al_{Framework}$ = 1.3). This suggests that not only Co^{2+} on MFI supported by ion exchange, but also Co species forcibly loaded by impregnation were active. As the Co loading was further increased by the impregnation method (e.g. Co / $Al_{Framework}$ > 1 for Si / Al_2 = 30), the average activity decreased. A similar result was observed for Si / Al_2 = 22 and 48. This may be due to the formation of inactive aggregated cobalt oxide species as we have reported in the past [3].

Figure 5-2 (a) shows the catalytic activity for methylation of benzene with methane at 773 K (yield of toluene, averaged over 0.5 - 3.75 h of the time on stream) plotted against

[Co] / $[Al]_{Total}$ molar ratio in Co/MFI (Si / Al_2 = 22 (in situ H type), 30, 48, 52, 61, 63 and 90) prepared by impregnation method. Maximum catalytic activity was obtained at [Co] / $[Al]_{Total}$ = 0.6 - 0.9 on MFI except for Si / Al_2 = 61. The activity of all MFIs reached a maximum with increasing Co loading and then decreased. This was attributed to the formation of aggregates of inactive cobalt oxide species, as described in Figure 5-1. A plot of the [Co] / $[Al]_{Framework}$ with the horizontal axis is shown in Figure 5-2 (b). Except for Si / Al_2 = 22 (in situ H type) and 61, the toluene yield was found to be maximum around [Co] / $[Al]_{Framework}$ = 1. This indicates that the $[Al]_{Framework}$, i.e., the concentration of ion exchange sites, was related to the toluene yield, and it is assumed that the Co species on the ion exchange sites ware active. The maximum activity was observed when one Co species was loaded on one ion exchange site, suggesting that the active Co species was a total monovalent species such as $[Co\text{-}OH]^+$ [14]. Dimeric species such as $[Co\text{-}O\text{-}Co]^{2+}$ [14-17] are also possible candidates for the active species, but it is expected that they are difficult to form on MFI with low Al concentration. On the other hand, in Si / Al_2 = 22 (in situ H type) with high Al concentration, Co species were stably ion exchanged as bare Co^{2+} due to the large number of paired Al sites, i.e., one Co was loaded per two ion exchange sites ($Al_{Framework}$) as shown in Chapter 4. Thus, for Si / Al_2 = 22 (in situ H-type), the activity was maximal at a [Co] / $[Al]_{Framework}$ ratio of 0.6. The toluene yield at

773 K (averaged over 0.5 − 3.75 h of the time on stream) plotted against the [Co] / $[Al]_{Extra\text{-}framework}$ ratio is shown in Figure 5-2 (c). For each concentration of MFI, the [Co] / $[Al]_{Extra\text{-}framework}$ ratio with maximum catalytic activity ranged from 2 - 20, indicating that the [Co] / $[Al]_{extra\text{-}framework}$ ratio was not correlated with catalytic activity.

Figure 5-3 shows the time course of toluene yield at 773 K over Co/MFI (Si / Al_2 = 22 (in situ H type), 30, 48, 52, 61, 63 and 90, [Co] / $[Al]_{maker}$ = 0.6) prepared by

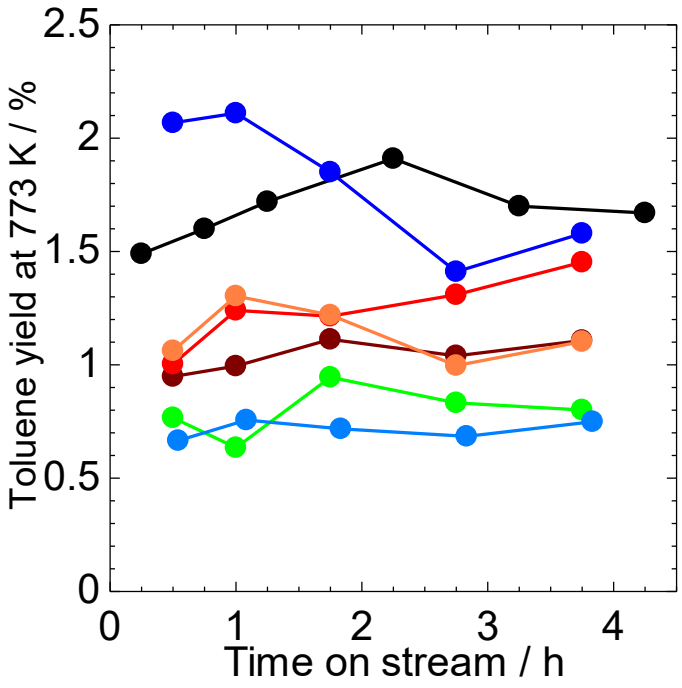

Figure 5-3. Time course of toluene yield at 773 K over Co/MFI (Si / Al_2 = (●) 22 [in situ H type], (●)30, (●) 48, (●) 52, (●) 61, (●) 63 and (●) 90)) prepared by impregnation method (Co / Al_{maker} = 0.6).

impregnation method. At Si / Al_2 = 30, the initial activity was the highest, around 2%, but catalyst degradation was observed. In the case of the other MFIs the catalytic activity was stable, and at the highest Al concentration, Si / Al_2 = 22, the activity was relatively high (c.a. 1.7%) and stable.

Figure 5-4 (a) shows the time course of toluene yield at 813 K over Co/MFI ([Co] / $[Al]_{maker}$ = 0.6) prepared by impregnation method. At Si / Al_2 = 22 (in situ H type) and 30,

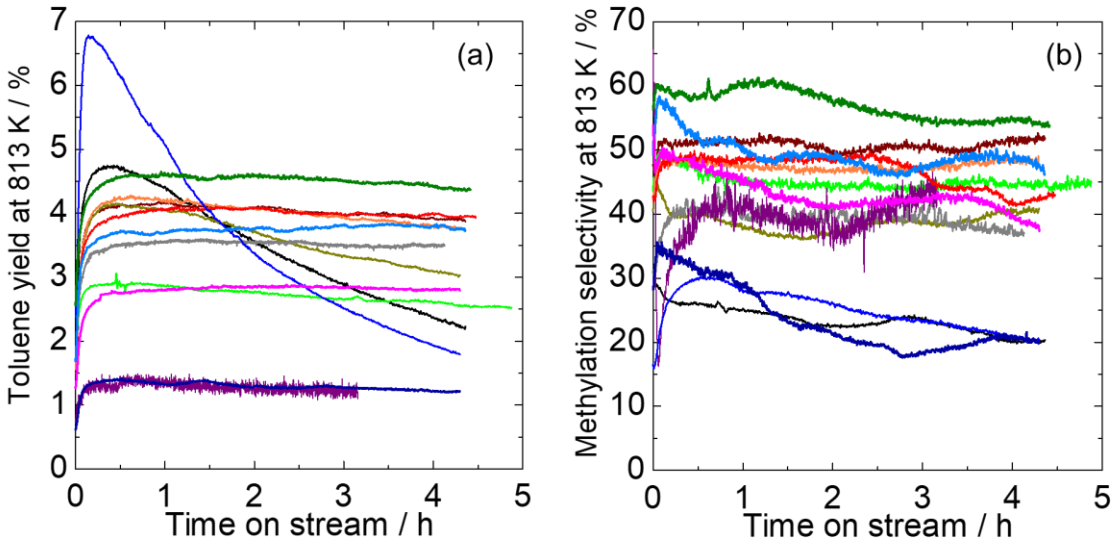

Figure 5-4. Time course of (a) toluene yield and (b) methylation selectivity at 813 K over Co/MFI (Si / Al_2 = (—) 22 [in situ H type], (—) 22 [ex situ H type], (—) 30, (—) 44, (—) 47, (—) 48, (—) 51, (—) 52, (—) 61, (—) 63, (—) 90, (—) 100 [in situ H type] and (—) 100 [ex situ H type]) prepared by impregnation method (Co / Al_{maker} = 0.6).

the toluene yield decreased significantly with time on stream, indicating catalyst deactivation. The ex situ H type conversion of MFI with Si / Al_2 = 22 suppressed the catalyst deactivation, although the initial activity decreased. Other Co/MFIs with high Si / Al_2 ratio showed stable catalytic activity. For Si/Al_2 = 100 (in situ and ex situ H type), the toluene yield was very low (about 1%). Figure 5-4 (b) shows the time course of methylation selectivity at 813 K over Co/MFI. At Si / Al_2 = 22 (in situ H type) and 30, the methylation selectivity was as low as 25%, indicating that the simple dehydrogenation of methane as side reaction proceeded. This is in good agreement with the progressive degradation of the catalyst as shown in Figure 5-4 (a). The simple dehydrogenation of methane produces coke, which leads to rapid catalyst deactivation. The ex situ H type conversion of MFI (Si / Al_2 = 22) increased the methylation selectivity to about 40%. This result is also consistent with the behavior of catalyst degradation in Figure 5-4 (a). For Si / Al_2 = 100 (ex situ H type), the methylation selectivity was as low as 25%. This is probably due to the low toluene yield of about 1%, as shown in Figure 5-4 (a). For Si / Al_2 = 48, 51, 52, 61, 63 and 90, high methylation selectivity was showed (≧45%).

Figure 5-5 (a) shows the relationship between toluene yield at 813 K (averaged in first 4 h of the time on stream) and $[Al]_{Framework}$ on Co/MFI with various Al concentrations ([Co] / $[Al]_{maker}$ = 0.3, 0.6 and 0.9). It can be seen catalytic activity was maximum at

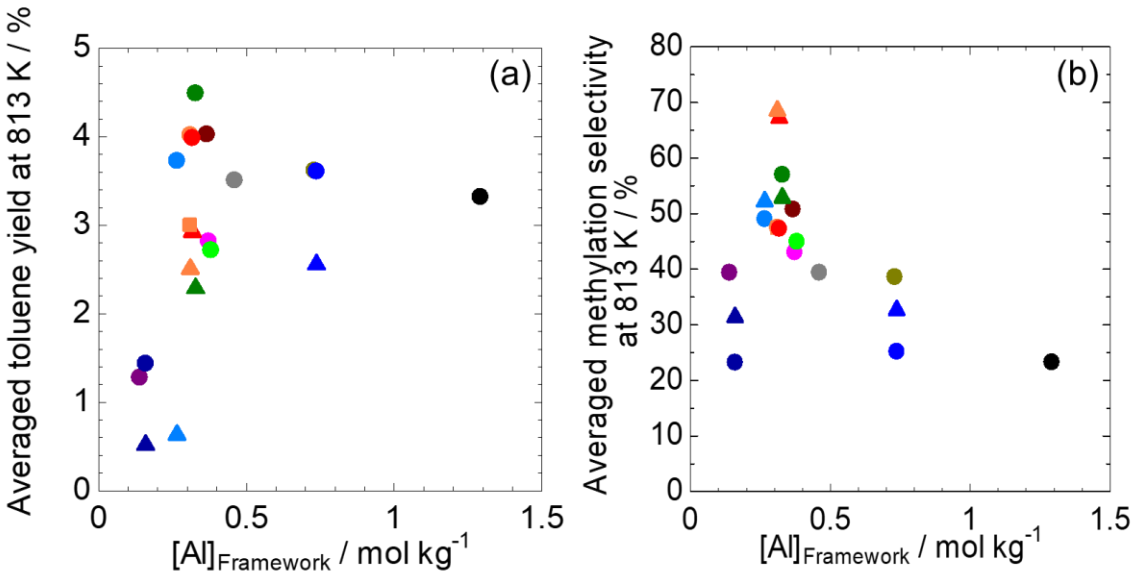

Figure 5-5. Relationship between (a) toluene yield or (b) methylation selectivity at 813 K and $[Al]_{Framework}$ on Co/MFI (Si / Al_2 = (●) 22 [in situ H type], (●) 22 [ex situ H type], (●) 30, (●) 44, (●) 47, (●) 48, (●) 51, (●) 52, (●) 61, (●) 63, (●) 90, (●) 100 [in situ H type] and (●) 100 [ex situ H type]) prepared by impregnation method (Co / Al_{maker} = (▲) 0.3, (●) 0.6 and (■) 0.9).

$[Al]_{Framework}$ = c.a. 0.3 mol kg^{-1}. The lack of increase in catalytic activity with increasing $[Al]_{Framework}$ is attributed to the significant deactivation of catalyst by coking as shown in Figure 5-4 (a). Figure 5-5 (b) shows the relationship between methylation selectivity at 813 K (averaged in first 4 h of the time on stream) and $[Al]_{Framework}$ on Co/MFI. The methylation selectivity was found to be maximal at $[Al]_{framework}$ = c.a. 0.3 mol kg^{-1},

indicating volcano-type correlation. Therefore, the active Co species were selectively generated on MFIs with $[Al]_{framework}$ = c.a. 0.3 mol kg^{-1} for methylation of benzene with methane. The low methylation selectivity at low $[Al]_{Framework}$ (< 0.2 mol kg^{-1}) may be due to too low catalytic activity. This is because a low $[Al]_{Framework}$ means that there are very few ion exchange sites ($Al_{Framework}$) that can support the active Co species.

Figure 5-6 shows the averaged methylation selectivity in first 4 h of the time on

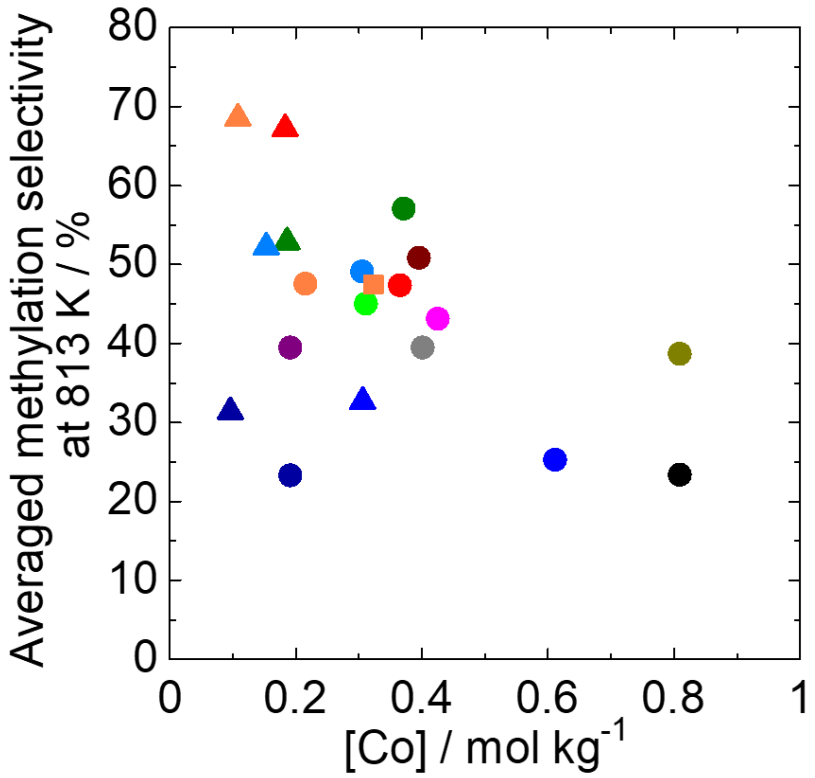

Figure 5-6. Relationship between methylation selectivity at 813 K and [Co] on Co/MFI (Si / Al_2 = (●) 22 [in situ H type], (●) 22 [ex situ H type], (●) 30, (●) 44, (●) 47, (●) 48, (●) 51, (●) 52, (●) 61, (●) 63, (●) 90, (●) 100 [in situ H type] and (●) 100 [ex situ H type]) prepared by impregnation method (Co / Al_{maker} = (▲) 0.3, (●) 0.6 and (■) 0.9).

stream at 813 K plotted against [Co] on Co/MFI. Except for the MFI with Si/Al_2 = 100 (in situ and ex situ H type), which had low catalytic activity, the methylation selectivity tended to increase with decreasing [Co]. We have previously found that the aggregation of cobalt oxide species on MFI tended to promote the side reaction (simple dehydrogenation of methane) [3]. Therefore, a smaller Co concentration may result in a higher selectivity because the formation of cobalt oxide species was suppressed. Alternatively, it is assumed that the higher the degree of dispersion of the active Co species on MFI, the higher the methylation selectivity.

Figure 5-7 (a, b) shows the (a) toluene yield and (b) methylation selectivity at 813 K (averaged in first 4 h of the time on stream) plotted against $[Al]_{Extra\text{-}framework}$ on Co/MFI. Figure 5-7 (c, d) shows the (c) toluene yield and (d) methylation selectivity at 813 K (averaged in first 4 h of the time on stream) plotted against external surface area of MFI support. Figure 5-7 (a)-(d) show that the $[Al]_{Extra\text{-}framework}$ and the external surface area of the MFI did not affect the catalytic activity or the methylation selectivity, since no correlation was found in all four figures.

All these results indicate that Co species supported on $Al_{Framework}$ were active, and impregnated Co on MFI with $[Al]_{Framework}$ = c.a. 0.3 mol kg^{-1} showed to high toluene yield and methylation selectivity at 813 K.

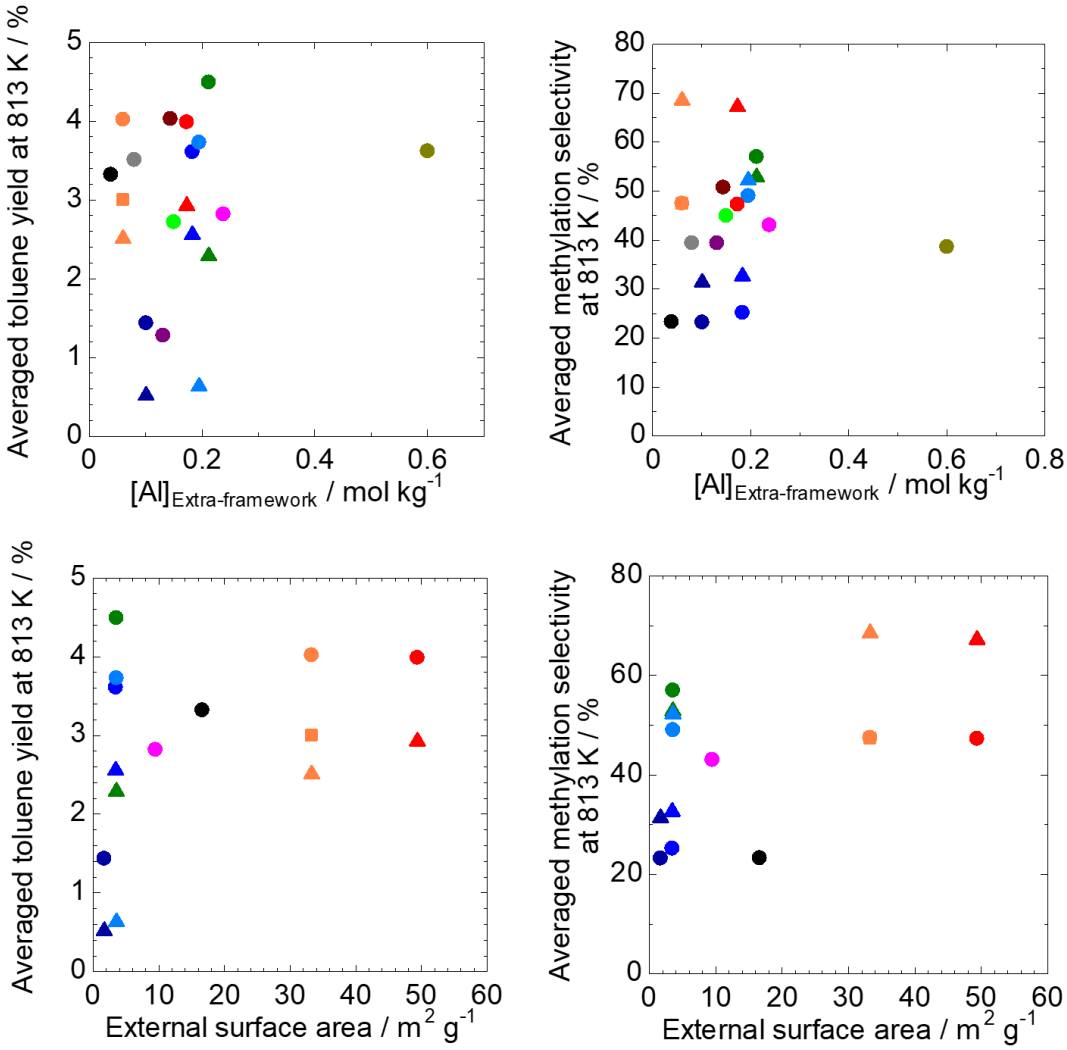

Figure 5-7. Relationship between (a) toluene yield or (b) methylation selectivity at 813 K and $[Al]_{Extra\text{-}framework}$ on Co/MFI. (c) toluene yield and (d) methylation selectivity at 813 K plotted against external surface in Co/MFI (Si / Al_2 = (●) 22 [in situ H type], (●) 22 [ex situ H type], (●) 30, (●) 44, (●) 47, (●) 48, (●) 51, (●) 52, (●) 61, (●) 63, (●) 90, (●) 100 [in situ H type] and (●) 100 [ex situ H type]) prepared by impregnation method (Co / Al_{maker} = (▲) 0.3, (●) 0.6 and (■) 0.9).

5-4. Conclusions

The $[Al]_{Framework}$ of MFI zeolite affected the catalytic performance for methylation of benzene with methane at 773 and 813 K. The Co species impregnated on MFI with $[Al]_{Framework}$ = 0.3 mol kg^{-1} shows high toluene yield and methylation selectivity at 813 K.

Acknowledgements

This study was partly supported by JST CREST Grant Number JPMJCR17P1, Japan, and JSPS KAKENHI Grant Number JP 19J15344.

References

[1] J.S. Beck, D.H. Olson, S.B. McCullen, U.S. Patent 5 367 099 (1994)

[2] D. Mitsuyoshi, K. Kuroiwa, Y. Kataoka, T. Nakagawa, M. Kosaka, K. Nakamura, S. Suganuma, Y. Araki, N. Katada, *Micropor. Mesopor. Mater.*, **242**, 118-126 (2017)

[3] K. Nakamura, A. Okuda, K. Ohta, H. Matsubara, K. Okumura, K. Yamamoto, R. Itagaki, S. Suganuma, E. Tsuji, N. Katada, *ChemCatChem*, **10**, 3806-3812 (2018)

[4] H. Matsubara, E. Tsuji, Y. Moriwaki, K. Okumura, K. Yamamoto, K. Nakamura, S. Suganuma, N. Katada, *Catal. Lett.*, **149**, 2627-2635 (2019)

[5] H. Matsubara, K. Yamamoto, E. Tsuji, K. Okumura, K. Nakamura, S. Suganuma, N.

Katada, *Micropor. Mesopor. Mater.*, **310**, 110649 (2021)

[6] J. Dědeček, D. Kaucký, B. Wichterlová, *Micropor. Mesopor. Mater*., **35**, 483-494 (2000)

[7] D. Kaucký, J. Dědeček, B. Wichterlová, *Micropor. Mesopor. Mater*., **31**, 75-87 (1999)

[8] T. Yokoi, H. Mochizuki, S. Namba, J. N. Kondo, T. Tatsumi, *J. Phys. Chem. C*, **119**, 15303-15315 (2015)

[9] K. Nakamura, K. Okumura, E. Tsuji, S. Suganuma, N. Katada, *ChemCatChem*, **12**, 2333-2340 (2020)

[10] P. Sazama, E. Tabor, P. Klein, B. Wichterlova, S. Sklenak, L. Mokrzycki, V. Pashkkova, M. Ogura, J. Dedecek, *J. Catal*., **333**, 102-114 (2016)

[11] P. Hu, K. Nakamura, H. Matsubara, K. Iyoki, Y. Yanaba, K. Okumura, T. Okubo, N. Katada, T. Wakihara, *Appl. Catal. A: Gen.,* **601**, 117661 (2020)

[12] M. Niwa, N. Katada, *Chem. Rec.*, **13**, 432-455 (2013)

[13] N. Katada, T. Kanai, M. NIwa, *Micropor. Mesopor. Mater*., **75**, 61-67 (2004)

[14] W. Li, S. Y. Yu, G. D. Meitzner, E. Iglesia, *J. Phys. Chem. B*, **105**, 1176-1184 (2001)

[15] P. Feng, X. Bu, G. D. Stucky, *J. Solid State Chem*., **129**, 328-333 (1997)

[16] L. Drozdová, R. Prins, J. Dědeček, Z. Sobalik, B. Wichterlova, *J. Phys. Chem. B*, **106**, 2240-2248 (2002)

[17] V. Indovina, M. C. Campa, D. Pietrogiacomi, *J. Phys. Chem. C*, **112**, 5093-5101 (2008)

Chapter 6 Conclusions

The author studied active Co species on MFI zeolite for methylation of benzene with methane. The knowledges from this study are desirable to provide the precise preparation of active catalysts for various reactions.

Concluding remarks are shown below.

Chapter 2

The active and inactive Co species for methylation of benzene with methane were found at Co/Al > 0.2 and Co/Al < 0.2, respectively. Furthermore, even in the low Co/Al region, co-presence of typical divalent elements such as Mg, Zn, Pb and Ca during the Co loading process was found to enhance the catalytic activity.

Chapter 3

In situ IR spectra showed that benzene was adsorbed on the Co species on MFI zeolite. The electronic environment of benzene was changed by adsorption to Co species. It was speculated that the benzene adsorbed on the Co species caused the methylation of benzene by methane.

Chapter 4

The active species for direct methylation of benzene with methane was identified to be the Co^{2+} on α site with strong base-stabilizing and electron-withdrawing nature (L1S type).

Chapter 5

The Co species supported on MFI with higher $[Al]_{Framework}$ ($[Al] > 0.7$ mol kg^{-1}) tended to occur side reaction. Co species impregnated on MFI with $[Al]_{Framework}$ of about 0.3 mol kg^{-1} showed the high toluene yield and methylation selectivity for reaction of methane and benzene.

List of publications

[1] Selective Formation of Active Cobalt Species for Direct Methylation of Benzene with Methane on MFI Zeolite by Co-presence of Secondary Elements

Hitoshi Matsubara, Etsushi Tsuji, Yasumi Moriwaki, Kazu Okumura, Kana Yamamoto, Koshiro Nakamura, Satoshi Suganuma, Naonobu Katada

Catalysis Letters, **149**, 2627-2635 (2019)

[2] Position and Lewis Acidic Property of Active Cobalt Species on MFI Zeolite for Catalytic Methylation of Benzene with Methane

Hitoshi Matsubara, Kana Yamamoto, Etsushi Tsuji, Kazu Okumura, Koshiro Nakamura, Satoshi Suganuma, Naonobu Katada

Microporous and Mesoporous Materials, **310**, 110649 (2021)

Supplementary publications

[1] Direct Methylation of Benzene with Methane Catalyzed by Co/MFI Zeolite

Koshiro Nakamura, Akihito Okuda, Kiyotaka Ohta, Hitoshi Matsubara, Kazu Okumura, Kana Yamamoto, Ryosuke Itagaki, Satoshi Suganuma, Etsushi Tsuji, Naonobu Katada

ChemCatChem, **10**, 3806-3812 (2018)

[2] Comparative Study of Direct Methylation of Benzene with Methane on Cobalt-exchanged ZSM-5 and ZSM-11 Zeolites

Peidong Hu, Koshiro Nakamura, Hitoshi Matsubara, Kenta Iyoki, Yutaka Yanaba, Kazu Okumura, Tatsuya Okubo, Naonobu Katada, Toru Wakihara

Applied Catalysis A: General, **601**, 117661 (2020)

Acknowledgements

The author is deeply grateful to Professor Naonobu Katada, Professor Toshiyuki Masui, Associate Professor Etsushi Tsuji and Associate Professor Satoshi Suganuma for their careful supports in the studies for this thesis.

The author is deeply grateful to Professor Kazu Okumura, Department of Applied Chemistry, Kogakuin University, for XAS and UV-vis experiments.